

Investigating the Role of Mini Viral RNAs in Influenza A Virus Pathogenesis

Student: Annika Ranta

Supervisors: Hollie French, Dr Aartjan te Velthuis

Introduction

Influenza A virus (IAV) is the causative agent of flu. Various strains of IAV exist, but it is chiefly the interplay between the virus and the host innate immune system that determines pathogenesis and disease outcome. The Spanish Flu of 1918, which infected approximately 500 million people and resulted in an estimated 50 million deaths, was caused by the highly pathogenic 1918 H1N1 strain.(1) 1918 H1N1 has been shown to induce a strong, dysregulated stimulation of the innate immune system, which contributes to disease pathogenicity. The stimulation is mediated via dsRNA agonists that bind to a pathogen recognition receptor called RIG-I.(2) The segmented (-)ssRNA IAV genome is replicated in the host cell nucleus by the heterotrimeric viral RNA dependent RNA polymerase (RdRp), which consists of polymerase basic protein 1 (PB1), polymerase basic protein 2 (PB2), and polymerase acidic protein (PA). Erroneous RdRp activity results in the production of aberrant mini viral RNAs (mvRNAs), which contain dsRNA elements that RIG-I binds preferentially. Abundant mvRNA production by 1918 H1N1 implies that mvRNAs may play a key role in pathogenesis.(3) mvRNAs of different lengths elicit immune responses of varying degrees *in vivo*, but it is unclear how RIG-I gains access to them and if some are preferentially bound and replicated by the viral RdRp.(3) The latter may be an important factor in disease severity.

Aims

This project aimed to investigate IAV mechanisms of pathogenesis in regard to mvRNAs by:

- Studying the binding affinities mvRNAs to the RdRp (replication deficient mutant)
- Generating fluorescent RIG-I constructs for *in vivo* localization studies, and studying binding affinities of mvRNAs to RIG-I

Methods

Maintenance of HEK293T Cells and Transfections

HEK293T cells were maintained at 37 °C, 5% CO₂ in high glucose DMEM (Cat. No. D6546) supplemented with 2 mM glutamine and 10% FCS. To study the binding affinities of mvRNAs to the RdRp, cells were transfected using PEI (GENEFLOW LIMITED) with plasmids: pcDNA3-PB1a, pcDNA3-PB2-STREP-TAP, pcDNA3-PA, pcDNA3-NP, and a segment 5-based mvRNA construct (NP47, NP76, GC33, GC50.1, or GC50.2), previously described.(3) For verification of expression of pEGFPΔ-RIG-I, cells were transfected with pEGFPΔ-RIG-I and/or empty pcDNA3, for a total amount of 1 µg DNA per transfection, using Lipofectamine2000 (Cat. No. 11668-019).

PB2 Pull-Down and RNA Extraction

Transfected cells were harvested 24 h post-transfection and lysed with a high-salt lysis buffer (50 mM Hepes pH 8, 200 mM NaCl, 25% glycerol, 0.5% igepal [NP40], 1 mM B-mercaptoethanol, 1x PMSF, 1x EDTA-free protease inhibitor). Lysed cells were centrifuged at 13000 rpm at 4 °C for 5 minutes, and crude lysates were collected. Crude lysate aliquots were retained for downstream protein analysis by western blot, and primer extension of extracted RNA. Pull-down purification of PB2-STREP-TAP was performed on using anti-TAP IgG sepharose beads (Cat. No. 17-0969-01), equilibrated with wash buffer (10 mM Hepes pH 8, 15 mM NaCl, 0.1% Igepal [NP40], 10% glycerol, 1x PMSF). Purified RdRp was aliquoted for western blotting, and the remainder was dissolved in TRIzol (Cat. No. T3934). RNA was isolated according to the manufacturer's instructions. Crude lysate aliquots and purified samples were western blotted and probed with primary antibodies: 1:3000 Rb a-GAPDH (Cat. No. GTX100118), 1:1000 Rb a-PB2 (Cat. No. GTX125926), 1:1000 Rb a-NP (Cat. No. GTX125989). After incubation with secondary antibody, 1:8000 D-a-Rb (Cat. No. 926-32213), blots were imaged using an Odyssey CLx Imaging System (Li-Cor).

Primer Extension and Quantitation

Isolated RNA from PB2-TAP pull-down was converted to cDNA by 50 U SuperScript III Reverse Transcriptase (Cat. No. 18080044), 1 h at 50 °C, using a ³²P radioactively labelled primer which specifically binds segment 5-based mvRNAs. 5S100 RNA was also radioactively labelled as a loading control. Samples were mixed with loading buffer (90% formamide, 10 mM EDTA, xylene cyanol, bromophenol blue) and run on 6% 7 M urea PAGE gel. Phosphorimaging was conducted using a Typhoon FLA 7000 Phosphorimager (GE Healthcare Life Sciences). Quantitation of RNA data was performed using ImageJ. mvRNA signal was normalized to 5S100 to determine input. Output was determined by normalizing mvRNA signal to PB2 from the western blot, quantified with ImageStudioLite.

Cloning of RIG-I into pEGFP

PCR primers were used to amplify RIG-I and introduce restriction sites for *NheI* and *HindIII*. pEF-RIG-I was acquired from a collaborator. The PCR product was purified by gel extraction using EconoSpin All-in-One Mini Spin Columns (Cat. No. 1940-250) following manufacturer's protocol. Restriction digest of RIG-I was performed overnight at 37 °C with *NheI* (Cat. No. R0131S) and *HindIII* (Cat. No. R0104S) in 1x CutSmart Buffer (Cat. No. B7204S). Subsequent cleanup of RIG-I was done with an Oligo Clean & Concentrator Kit (Cat. No. D4061) following manufacturer's protocol. The pEGFP vector was digested with *NheI* and *HindIII* for 2 h at 37 °C, with a subsequent cleanup. Ligation of RIG-I and pEGFP (3:1) was done using T4 DNA ligase (Cat. No. M0202L) in T4 DNA ligase buffer (Cat. No. B0202S) for 1 h at RT, followed by a 10 min heat inactivation at 65 °C. The ligation replaced EGFP with RIG-I, generating pEGFPΔ-RIG-I. DH5a cells (New England Biolabs) were transformed with the ligation mix, inoculated onto 2TY agar plates with 25 ug/ml kanamycin, and grown overnight at 37 °C. Colonies were picked and grown in 2TY with 25 ug/ml kanamycin at 37 °C for 16 h. The construct was purified using EconoSpin All-in-One Mini Spin Columns and verified by Sanger sequencing. pEGFPΔ-RIG-I-transfected cells were lysed in Laemmli buffer 24 h post-transfection to verify construct expression. Western blot was performed using primary antibodies: 1:1000 Rb a-RIG-I (Cat. No. PA5-11726) and 1:3000 Rb a-GAPDH. Following incubation with secondary antibody, 1:8000 D-a-Rb, the blot was imaged as above.

Results and Discussion

PB2-mvRNA Binding Affinity

Primer extension following purification of the RdRp showed a reduction in the 5S rRNA band and an increase in the mvRNA signal relative to the crude samples (Fig. 1A), indicative of successful purification and enrichment for RdRp-bound mvRNAs. The efficiencies of the various experimental stages leading up to primer extension were assessed by western blotting for PB2, NP, and, GAPDH. GAPDH levels were comparable between the crude samples, and negligible in the purified samples. However, levels of PB2 varied between the purified samples (Fig. 1B). Additionally, remnant NP persisted in purified samples, with more distinct levels in the NP47, NP76 and GC33 samples. Quantitation revealed variation in binding affinities of RdRp and mvRNA constructs (Fig. 1C). The previously observed dissimilarities in immunogenicity and replication exhibited by the mvRNAs may be partially attributable to their inherent differences in RdRp binding. (3) Further experiments are required to confirm the presented results.

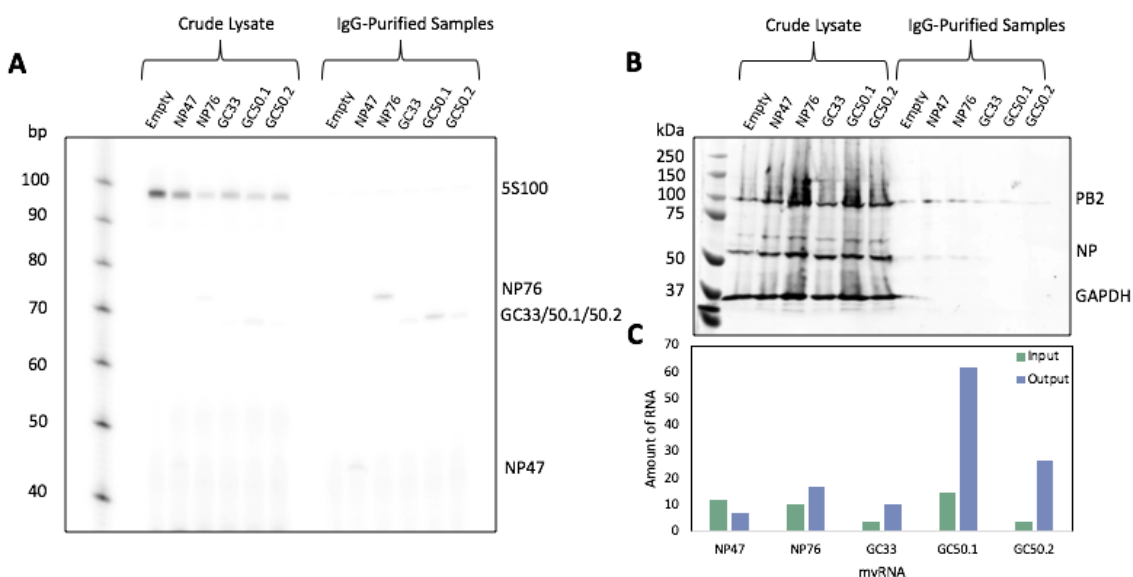
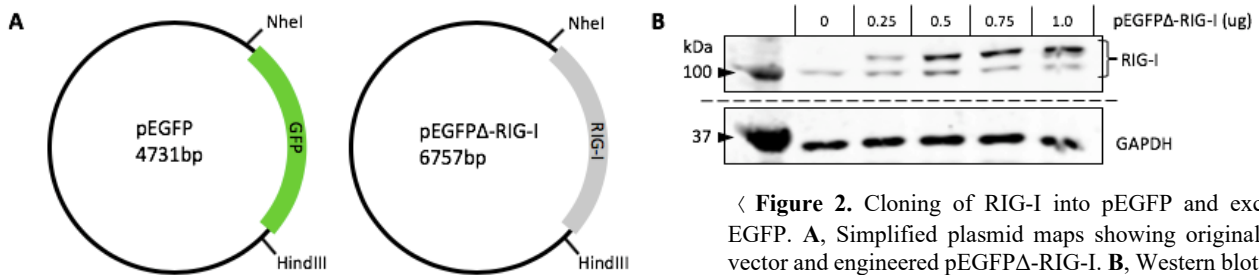


Figure 1. PB2-mvRNA binding affinity. A, Primer extension of crude lysate and affinity-purified PB2-bound mvRNAs. B, Western blot analysis of crude lysate and affinity-purified samples. C, Quantitation of primer extension gel showing normalized mvRNA amounts.

Cloning of RIG-I into pEGFP

pEGFP Δ -RIG-I was generated as shown in figure 2A. Alignments (not shown) of the pEGFP backbone to sequencing data, and of the sequencing data to RIG-I, confirmed successful cloning of RIG-I into the pEGFP backbone. Levels of RIG-I expression are correlated to amount of RIG-I transfected, with an increase in transfected plasmid RIG-I resulting in concomitant increase in expression (Fig. 2B). The transfected RIG-I runs higher than endogenous RIG-I, which may be due to ubiquitination, an essential modification in RIG-I signalling.(4,5) As RIG-I is placed under a constitutively expressed CMV promoter in the pEGFP backbone, this was the expected outcome. The cellular protein GAPDH serves as the loading control and shows comparable loading of samples.



< **Figure 2.** Cloning of RIG-I into pEGFP and excision of EGFP. **A**, Simplified plasmid maps showing original pEGFP vector and engineered pEGFP Δ -RIG-I. **B**, Western blot analysis to verify *in vivo* expression of pEGFP Δ -RIG-I construct.

Future Work and Departures from the Original Project

The initial project proposal consisted of cloning multiple EGFP-RIG-I constructs, including mutated RIG-I variants, to study the colocalization of mvRNAs and RIG-I using fluorescence microscopy. The initial proposal also included studying the binding affinities of RIG-I and different mvRNAs by an EGFP pull-down, RNA extraction, and primer extension. Efforts were made to optimize cloning, but owing to the limited time frame, this proved unsuccessful for all but the pEGFP Δ -RIG-I, which was intended to be the negative control in the initial project proposal. Future work may involve studying the colocalization of mvRNAs and RIG-I using fluorescence microscopy, following the generation of the remaining constructs. Additionally, repeats will need to be performed to study the PB2-mvRNA binding affinities.

Value of Studentship

Student: During my educationally enriching time at the te Velthuis lab, I got to practice a plethora of scientific techniques, and expand upon transferable skills, such as communication of results. I have gained both confidence and independence in a laboratory setting, and am eagerly anticipating to undertake my bachelor's thesis in biomedicine. I would like to thank everybody in the te Velthuis lab for the thoroughly enjoyable experience, and the Biochemical Society for making this internship possible.

Supervisor: Annika's project was to design and construct reporter constructs to better understand where different influenza virus RNA species are detected by an infected cell. During her time in the lab, Annika has gained experience in construct design, molecular cloning, cell culture, transfection, western blot, and luciferase reporter assays. She was well-organised, sensible, and actively contributed to lab meetings and discussions, gaining confidence throughout her internship. In all aspects of her project, Annika has shown great enthusiasm and an excellent work ethic and she was, simply put, a pleasure to supervise.

References

- (1) Johnson P, Mueller J. Updating the accounts: global mortality of the 1918–1920 “Spanish” influenza pandemic. *Bull. Hist. Med.* 2002;76(1): 105-115.
- (2) Kash, JC. et al. Genomic analysis of increased host immune and cell death responses induced by 1918 influenza virus. *Nature* 443, 578–581 (2006).
- (3) te Velthuis AJ, Long JC, Bauer DLV, Fan RLY, Yen HL, Sharps J, et al. Mini viral RNAs act as innate immune agonists during influenza virus infection. *Nat. Microbiol.* 2018;3:1234-1242.
- (4) Loo YM, Gale M. Immune signaling by RIG-I-like receptors. *Immunity.* 2011;34(5):680-692.
- (5) Jiang Z, Kinch LS, Brautigam CA, Chen X, Du F, Grishin NV, Chen ZJ. Ubiquitin-Induced Oligomerization of the RNA Sensors RIG-I and MDA5 Activates Antiviral Innate Immune Response. *Immunity.* 2012;36(6):959-973.

Rescuing functional decline in a rat model of doxorubicin-induced cardiotoxicity via administration of 5- aminoimidazole-4-carboxamide ribonucleotide (AICAR).

Ben Thackray, Corpus Christi College, University of Oxford.

Supervised by Dr Kerstin Timm and Prof. Damian Tyler, Department of Physiology, Anatomy & Genetics, University of Oxford.

Experimental background:

The prototypical anthracycline medication doxorubicin (DOX) has been used extensively in the treatment of a wide array of different cancers over the past 40 years, demonstrating broad spectrum efficacy both in isolation and as part a combination chemotherapy regimen. Despite its widespread usage, patients treated with DOX have a high likelihood (around 5% - Moslehi, J.J. (2016)) of developing congestive heart failure as a consequence of DOX-induced cardiotoxicity (DIC). Our lack of understanding of the molecular and cellular mechanisms underpinning DIC not only precludes effective therapeutic intervention, but also prevents diagnosis of DIC until irreversible functional decline. The molecular mechanisms underpinning DOX-induced cardiotoxicity are manifold and highly interconnected, complicating the identification of major cause-and-effect relationships, but seem largely to converge upon broad mitochondrial dysfunction (Tokarska-Schlattner, M. et al. (2006)) , which is perhaps unsurprising given the intimate relationship between contractile function and energy homeostasis in the myocardium.

Previous work in the Tyler group identified aberrations in cardiomyocyte respiratory substrate oxidation in hearts from DOX treated rats which were linked to functional decline, characterised by dysfunctional carbohydrate oxidation independent of glycolysis. This metabolic dysfunction was conclusively established to act independently of ROS production, as several markers of oxidative stress were found to be absent in our rat model of DOX-induced cardiotoxicity and treatment with the mitochondrial-targeted antioxidant MitoQ could not rescue cardiac failure (as yet unpublished data). My research builds upon this previous work, examining the effect of the direct AMPK activator 5-aminoimidazole-4-carboxamide ribonucleotide (AICAR) upon cardiomyocyte metabolism and declining cardiac function, assessed using a combination of CINE imaging to monitor cardiac function, and hyperpolarised [$1-^{13}\text{C}$] and [$2-^{13}\text{C}$] pyruvate metabolite imaging (Apps, A. et al. (2018)) to assess myocardial carbohydrate oxidation *in vivo*. As AMPK is the master regulator of cellular energy homeostasis, we hypothesised that its activation would relieve the inhibition of CPT1 (via AMPK mediated inhibition of ACC, in turn lowering cytosolic [malonyl-CoA]) and thus boosting mitochondrial oxidation of long-chain fatty acids, as well as increasing mitochondrial number by stimulating mitochondrial biogenesis through PGC-1 α signalling.

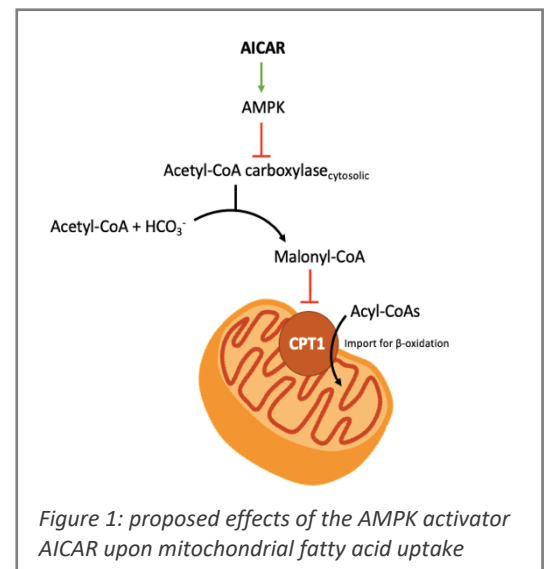


Figure 1: proposed effects of the AMPK activator AICAR upon mitochondrial fatty acid uptake

Materials and methods:*

Treatment regime: 18 juvenile male Wistar rats were age-matched and divided between a control group (n=6; received weekly IV saline injections over 5 weeks), a DOX + saline group (n=6; received weekly IV DOX injections (3mg/kg) and daily subcutaneous saline injections), and a DOX + AICAR group (n=6; received both weekly IV doxorubicin and daily sc AICAR (0.5g/kg) injections). Body weight and food intake were monitored over the course of the study, to assess whether AICAR mitigated DOX-induced weight loss.

Hyperpolarised MRS and CINE imaging: At weeks 1, 3, and 6, cardiac function and myocardial metabolism were assessed in a 7T vertical bore MR spectrometer (Varian) using a CINE-FLASH sequence (to monitor any deterioration in LV ejection fraction) and both [$1-^{13}\text{C}$] and [$2-^{13}\text{C}$] pyruvate hyperpolarised MRS respectively using a ^{13}C -receive surface coil (Rapid Biomedical). The summed signal peaks over the first 30s of signal appearance can be integrated, and the relative abundance of bicarbonate/pyruvate or glutamate/pyruvate (for C1 and C2 pyruvate respectively) used as a surrogate measure of flux through PDH and the TCA-cycle. On the day of scanning, blood samples were taken and the plasma analysed for concentrations of non-esterified fatty acids, in order to assess impaired lipid handling in DOX-treated rats.

Assessing mitochondrial number and function using qPCR and OC measurements: After week 6 scans, all rats were sacrificed, their hearts excised, and both the subsarcolemmal and interfibrillar mitochondria isolated. Isolated mitochondria were then used for O₂ consumption measurements, monitoring state 3 respiratory rate when provided with different substrates (glutamate, pyruvate + malate, palmitoyl-CoA + carnitine, and TMPD – a potent e⁻ donor to cytochrome c), as a means of assessing mitochondrial respiratory substrate preference and ETC functionality. A small piece of heart tissue was excised from the heart before mitochondrial extraction and freeze clamped, and its genomic and mitochondrial DNA isolated using a commercial extraction kit (Qiagen). qPCR was performed

* My methodology did not deviate significantly from the original project proposal.

on the DNA extract using primers for GAPDH and cytochrome b to determine the relative abundance of nuclear DNA and mtDNA in the samples and thus the mtDNA copy number, which serves as a measure of mitochondrial loss.

Results and discussion:

In accordance with previous results, treatment with DOX markedly decreased PDH flux and flux through the TCA cycle from pyruvate, as indicated by the decreased C1 Bicarb/Pyr and C2 Glu/Pyr ratios of the DOX + saline population relative to the saline control, demonstrating a reduced carbohydrate oxidative capacity (Fig. 2). Treatment with AICAR did not significantly lower PDH flux compared to the DOX + saline population, nor has it changed the C2 glutamate/pyruvate ratio (Fig 2). Despite not affecting the myocardial metabolic phenotype of DOX-treated rats *in vivo*, AICAR administration preserved myocardial ejection fraction, and ameliorated both DOX-induced weight loss and dyslipidaemia (Figures 3 and 4), indicating that it exhibits a cardioprotective effect independent of its hypothesised role as an exogenous modulator of metabolism.

The isolated mitochondria from DOX-treated rats exhibited generally lower respiratory rates than the controls regardless of substrate, as is shown for isolated IFMs supplied with palmitoyl-CoA and carnitine in figure 5. Treatment with AICAR did not seem to increase the respiratory rate of isolated mitochondria when supplied with palmitoyl-CoA, indicating that AICAR administration did not significantly upregulate mitochondrial lipid import and β -oxidation as expected. qPCR results were analysed using the comparative C_T method (Schmittgen, T.D., and Livak, K.J. (2008)), revealing that the cardiomyocytes of the DOX treated rats had 50% fewer mitochondria than the control population. This mitochondrial loss did not seem to be offset by treatment with AICAR, again supporting a cardioprotective role for AICAR other than its hypothesised role as an activator of mitochondrial biogenesis.

In summary, this study identifies AICAR as a promising therapeutic tool for rescuing cardiac function in DOX-induced cardiotoxicity in rats, that could potentially be scalable for future clinical use, but suggests that its cardioprotective effect is independent of AICAR's established roles both as an activator of mitochondrial biogenesis and as an upregulator of fatty-acid oxidation. Further work is necessary to dissect the true basis for AICAR-mediated cardioprotection in DOX-treated rats, to investigate the systemic effects of AICAR administration, particularly in rescuing hyperlipidaemia, and thus also to better define the purported mechanisms of DOX-induced cardiotoxicity (e.g. reactivation of the foetal gene programme, $IFN\gamma$ signalling) that may constitute AICAR's true targets.

Acknowledgements and student experience:



I have really enjoyed my time in the Tyler group, and would like to thank my supervisor Dr Kerstin Timm, along with Prof. Damian Tyler, Vicky Ball, and the rest of the Tyler group, for making me feel so supported and welcome. One of the major benefits of joining the Tyler group and the CMRG as a whole has been being exposed to a truly multidisciplinary research environment, which helped me to appreciate the intricate engineering behind hyperpolarised MR

experiments, and the wider physiological implications of myocardial metabolic dysfunction. In addition to my own research, I have been able to observe diverse experiments beyond the practical limitations of an undergraduate biochemistry degree while nurturing my own interest in ^{13}C MFA/FBA, and intend to pursue a PhD in the field of metabolism and bioenergetics.

References:

1. Apps, A., Lau, J., Peterzan, M., Neubauer, S., Tyler, D., & Rider, O. (2018). Hyperpolarised magnetic resonance for in vivo real-time metabolic imaging. *Heart*, 104(18), 1484–1491.
2. Moslehi, J. J. (2016). Cardiovascular Toxic Effects of Targeted Cancer Therapies. *New England Journal of Medicine*, 375(15), 1457–1467.
3. Schmittgen, T. D., & Livak, K. J. (2008). Analyzing real-time PCR data by the comparative C_T method. *Nature Protocols*, 3(6), 1101–1108.
4. Tokarska-Schlattner, M., Zaugg, M., Zuppinger, C., Wallimann, T., & Schlattner, U. (2006). New insights into doxorubicin-induced cardiotoxicity: The critical role of cellular energetics. *Journal of Molecular and Cellular Cardiology*, 41(3), 389–405.

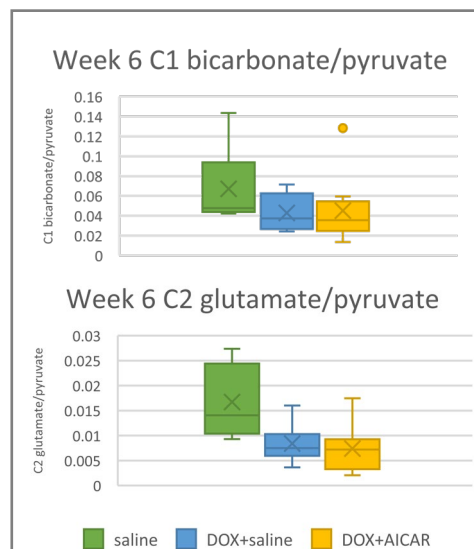


Figure 2: comparative signal ratios from $[1-^{13}C]$ and $[2-^{13}C]$ pyruvate hyperpolarised MRS scans

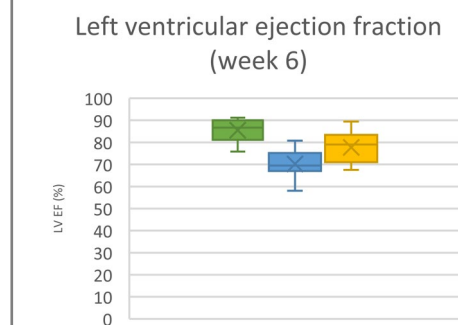


Figure 3: left ventricular ejection fraction values derived from week 6 CINE-MRI images

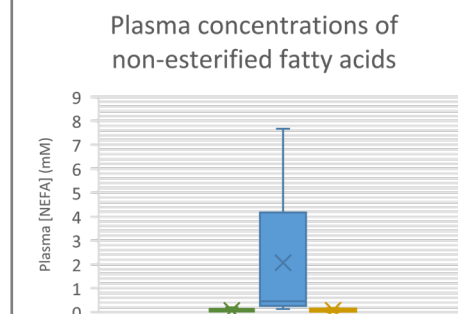


Figure 4: plasma [NEFA] from blood samples taken at week 6

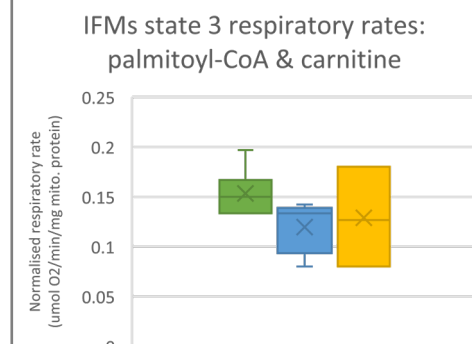


Figure 5: state 3 respiratory rates of isolated IFMs supplied with palmitoyl-CoA

Biochemical links between DNA damage, inflammation and cell fate in the human lens

Biochemical Society Summer Student: Holly Cooper; Supervisors: Dr Richard Bowater & Prof Michael Wormstone, School of Biological Sciences, University of East Anglia, Norwich

Background

DNA in cells codes for all of its functions, however damage to DNA often occurs, leading to mutations and in some cases cell death. Damage to the DNA can be from internal or external factors, with examples including: chemicals generated during cellular processes or ultraviolet radiation. For example H_2O_2 damages DNA by inducing oxidative stress. To counter damage, cells have many repair pathways that increase chances of survival. Although much is known about the variety of different mechanisms in humans, experimental models of DNA damage are under-developed under physiologically relevant conditions.

One molecule associated with DNA repair is PARP1 (PARP = poly-ADP-ribose polymerase), which is often involved in base excision repair and for the repair of single stranded breaks in DNA¹. Poly-ADP-ribosylation (PARylation) describes a post-translational modification² where ADP-ribose units are added to proteins, which is catalysed by a family of enzymes known as PARPs: poly-ADP-ribose polymerases³. PARP1 is the most common type of PARP and its inhibition leads to increased levels of DNA damage in cells exposed to oxidative stress and to reduced levels of cell death, demonstrating how PARP1 can have many, seemingly conflicting cellular roles.

Aims

This project aimed to examine links between DNA damage and cellular function using the human lens cell line, FHL124, studying biochemical activities of PARP1 in physiological responses to cellular damage. The project aimed to identify the amount of DNA damage under different cellular conditions, correlating this with levels of PARP1, thereby improving understanding of PARP regulation and the potential of PARP inhibitors in therapeutic settings.

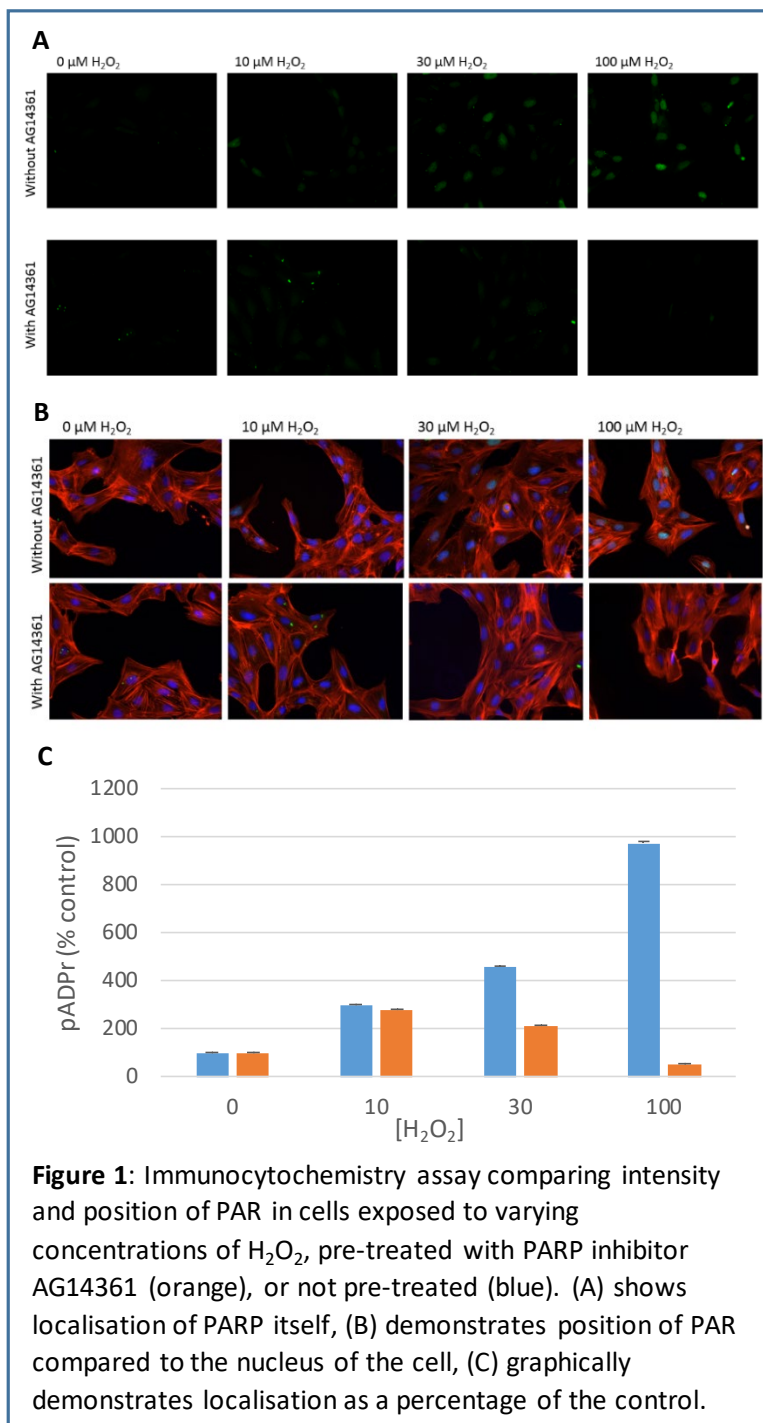
Description of work

Cells from the human lens cell line FHL124 were cultured in medium and set on coverslips, dishes and 96 well plates and DNA damage was induced using H_2O_2 at varying concentrations³: 0, 10, 30 and 100 μM . H_2O_2 treatments were for 30 minutes on the coverslips and for 24 hours on the dishes and 96 well plates. Following this, the severity of DNA damage was investigated using the alkaline comet assay and the CellTiter-Glo (CTG) assay that assesses cell viability. Proteins were extracted from cells and analysed using a western blot procedure. Localisation of PARP was then carried out using an immunocytochemistry procedure, where PARP acts as a marker of DNA damage. This protocol was then repeated using a sample of FHL124 cells treated with the PARP inhibitor AG14361, compared to a control sample that was not treated with PARP inhibitor. These samples were treated with the varying H_2O_2 concentrations and analysed using the CTG procedure for cell viability (data not shown), and the immunocytochemistry protocol to localise PARP.

Results and outcomes

The alkaline comet assay showed levels of DNA damage in the nucleus of cells where cells that has been subjected to more DNA damage gave bigger tails of DNA extending from the nucleus, while undamaged cells has much shorter tails or no tails at all (data not shown). Cells treated with 100 μM H_2O_2 gave the largest percentage of DNA seen in the tail while those not exposed to any H_2O_2 had smaller tails. Samples treated with 10 μM H_2O_2 gave higher levels of damage than those treated with 30 μM H_2O_2 , this does not correlate with what we would expect to see and also goes against previous findings seen in other papers. Furthermore a higher than expected amount of DNA damage was seen even in the 0 μM H_2O_2 control which should only display low levels of DNA damage, however this experiment was only carried out once due to time constraints and would benefit from being refined and repeated in order to eliminate the background noise seen.

Preliminary experiments using extracted proteins from the cells tested the antibodies against PAR and PARP using western blots (data not shown). Further experiments using antibodies to determine presence of PAR and PARP in cells were then carried out. With PARP uninhibited this showed that increasing the concentration of H_2O_2 correlated with an increased intensity and a greater concentration of PAR, but when PARP was inhibited the intensity did not increase with H_2O_2 concentration (Fig. 1A). Full immunocytochemistry images give context of where PARP was localised, showing it was seen predominantly in the nucleus, in line with what we would expect due to the fact that PARP is recruited to damaged nuclear DNA (Fig. 1B). This is also shown graphically, demonstrating that PARP is recruited to DNA damage as PARylation occurred (Fig. 1C).



Future directions

In this project we investigated the relationship between PARP and oxidative stress. It has been found that PARP protects against cell death and, in the context of the lens, this suppresses lens opacification seen in cataract development. Further studies could delve into the biochemical mechanisms by which PARP does this. Further repeats would also help refine the comet procedure and understand why damage was seen in some of the controls.

Departures from original proposal

The proposal suggested using the ApoTox-Glo triplex assay to analyse cell viability, apoptosis and damage, however the procedure used was the CellTiter-Glo assay, which is a different approach to measuring cell viability. Also, the proposal suggested investigation into localisation of H2AX to visualise double strand breaks, but this was not covered due to time constraints.

How the grant contributed to/shaped career aspirations

The grant has massively helped confirm my previous interest in working in a laboratory setting and, in particular, on human cells and tissues. Furthermore, the laboratory work has helped realise my interest in pursuing a PhD after graduation, and I hope to build on the knowledge and networks developed during this studentship.

Value of the studentship to the student and research group

This studentship has helped develop my awareness of a laboratory environment. It has given me opportunities for training in multiple

methods, such as cell culturing, analysis of DNA damage using alkaline comet assays, use of immunocytochemical approaches to localise DNA damage, knowledge of cell viability assays, such as the CTG assay, and western blotting. This has been helpful to the research group because it has further developed and optimised a range of assays that will be used in future research. Alongside learning of the laboratory techniques, the studentship has helped me acquire skills such as networking and communicating with academics at the departmental colloquium and has helped develop my writing skills for laboratory journals and report, and has improved my ability to self-reflect.

References

1. Morales J., Ji L., Fattah F., et al., Review of pol (ADP-ribose) polymerase (PARP) mechanisms of action and rationale for targeting in cancer and other diseases, *Crit Rev Eukaryot Gene Expr.*, 2014, **24**, 15-28
2. Alemasova E, Lavrik O., Poly(ADP-ribosyl)ation by PARP1: reaction mechanism and regulatory proteins, *Nucleic Acids Research*, 2019, **47**, 3811-3827
3. Smith A., Ball S., Bowater R., Wormstone I., PARP-1 inhibition influences the oxidative stress response of the human lens, *Redox Biol*, 2016, **8**, 354-362



Development of a novel biosensor of MAPK pathway activation status for use in single cell expression analysis.

Kathryn Temple

Introduction

The MAP kinase pathway regulates transcriptional outputs that control important processes such as the cell cycle and differentiation. As these are essential processes, it is not unexpected that dysregulation of the pathway results in a variety of diseases including oncogenesis (Rauen & Tidyman, 2009). The involvement of the pathway in disease highlights the importance of having an ability to measure MAPK activity. Traditionally, this is done using western blotting which measures phosphorylation of MAPK which is indicative of activity. However, the activity of the MAPK pathway can be quantified by measuring gene expression induced by activation of growth receptors. Growth factors present in serum activate the MAPK pathway and lead to gene expression due to a common regulatory motif, known as the serum response element (SRE), present in the gene's promoter region (Treisman, 1992). The SRE can be attached to a reporter such as luciferase which will then generate a luminescent output when the gene is activated.

The half-life of mRNA can be highly variable, ranging from 1 to 40 hours (Selbach, 2011). Therefore, it can remain in the cell for a long time after activation of the gene. However, as cell signalling is very dynamic, a reporter with a short-lived product would be required to see the rapid changes in gene expression.

The aim for the project was to combine different mRNA instability factors to create a short-lived reporter. Variations of this sequence included rare codons and an mRNA destabilising motif to enhance degradation rate of the mRNA (Presnyak et al, 2012). Other destabilising motifs included AU-rich elements in the 3' untranslated region (3'UTR) to destabilise the mRNA through deadenylation (Zubiaga et al, 1995).

Aims

The aim of the project was to create a short-lived reporter that would define any recent activity of the MAP kinase pathway in cells.

Methods

Insertion of oligonucleotides into plasmid

Oligonucleotides designed by AddGene based at the University of Liverpool (see supplementary material) were ligated into 1 µg of *Ascl*/*FseI* digested serum response element (SRE) vector before the plasmid was transformed into DH5α cells to amplify the amount of DNA. The plasmid was extracted from the cells and restriction digests using *NheI* and *EcoRI* were performed to ensure the correct

product was inserted. PCR was carried out using primers to amplify the oligonucleotides, this confirmed that the plasmid contained the desired inserts.

Testing half-life of mRNA

1 µg of the plasmid was transfected into 6 wells on a plate containing 5×10^5 HEK293T cells per well. After 6 hours of incubation, 5 µg/mL actinomycin D was added to the 24hour time point well, this was repeated for 7 hour, 4 hour, 2 hour and 1 hour time points. The cells were then treated with 1 mL of TRIzol and the mRNA extracted. Reverse transcription was used to transcribe mRNA to cDNA which would consequently be used in qPCR to observe the degradation of mRNA at these different time points. This was repeated for each of the constructs.

qPCR

A two-step amplification and melt qPCR was conducted on the resulting cDNA. The method was optimised for a 95°C denaturation temperature and 52.5°C annealing temperature for 39 cycles. The melt data ranged from 65°C to 95°C with 0.5°C intervals.

Results

PCR

PCR was used to confirm the oligonucleotides had been successfully ligated into the SRE vector. Three constructs were designed by ligating into the SRE vector a parent sequence (tH), a variation using rare codons (tH rare) and a sequence with an additional 3SHE destabilising motif (tH 3SHE).

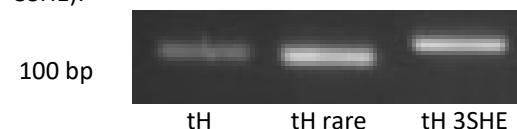


Figure 1. Agarose gel containing PCR amplified oligonucleotides inserted into SRE vector.

Expected insert sizes: tH = 93 bp, tH rare = 93 bp, tH 3SHE = 120bp

The agarose gel shows the fragment sizes are correct for tH, tH rare and tH 3SHE, suggesting ligation of the oligonucleotides into the vector was successful (Figure 1).

Serum Response

In order to determine if the reporter was responsive to serum, two conditions were applied to the cells. Treatment

of cells with fetal bovine serum (FBS) and cells starved of FBS for 24 hours.

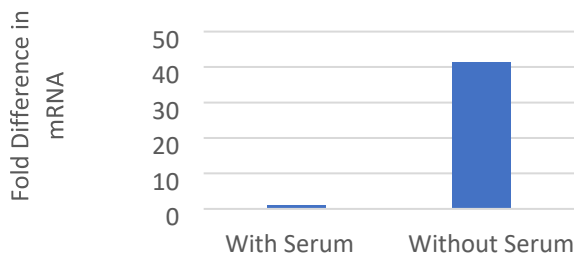


Figure 2. Fold difference in mRNA from qPCR amplification of tH insert in cells treated with media containing fetal bovine serum (FBS) and cells starved of FBS for 24 hours.

When comparing the mRNA expression of the reporter in the two different conditions, a 41-fold difference was apparent (Figure 2).

mRNA degradation

A range of time points between addition of actinomycin D to HEK293T cells and lysis of cells using TRIzol were used to observe the degradation of the mRNA produced from the reporter.

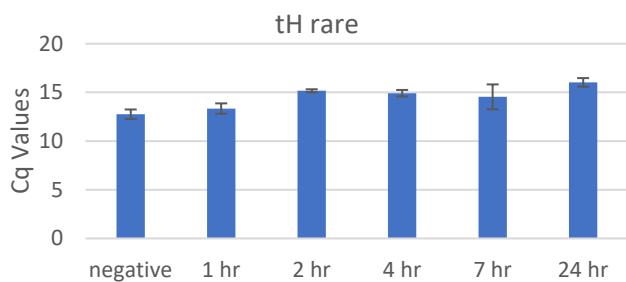


Figure 3. qPCR amplification Cq values for mRNA degradation over 24-hour time period for reporter containing tH rare.

An increase in the Cq values over time suggests a decrease in transcription of the reporter sequence (figure 3). Similar Cq values were also obtained for tH and tH 3SHE.

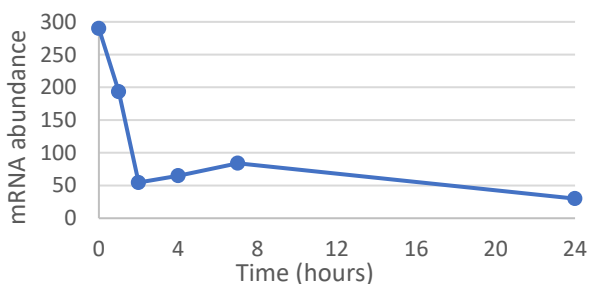


Figure 4. mRNA abundance decrease over a 24-hour time period for reporter containing tH rare.

mRNA abundance was calculated from Cq values. An exponential decrease in mRNA abundance occurs during the first 2 - 4 hours (figure 4).

Discussion

Ligation of oligonucleotides

Ligation of the tH oligonucleotides into the SRE vector was successful with PCR confirming the expected fragment sizes. If the mRNA degradation had been successful, ligation of the 3'UTRs into the vectors would have been the next step.

Serum response

Growth factors present in serum activate the MAPK pathway leading to expression of genes. Serum inducible transcription of the reporter is dependent on the SRE present in the vector as this is the motif present in the promoter region of genes that are targeted by the MAPK pathway (Norman et al, 1988). The 41-fold difference in gene expression displays the dependence of the SRE on serum.

mRNA degradation

The Cq values increase over time showing that the amount of mRNA is decreasing due to degradation (figure 3). Degradation is also apparent by a rapid decrease in mRNA abundance during the first 4 hours (figure 4). The mRNA abundance is 1/4 of the control in 2-4 hours, this is consistent with a half-life of 2 hours, a relatively short half-life (Selbach, 2011). Further work with more biological replicates would be required to confirm an exact half-life value.

The reporter was more unstable than expected and therefore shorter time periods needed to be tested to determine a more precise half-life. The differences in values seen at the longer time periods may be due to toxic effects of actinomycin D. If the drug prevented the cells from proliferating, it could result in differences in the numbers of cells.

Future Directions

In future, it would be advisable to try shorter time periods, e.g. 30 min, as it appears that the reporter is shorter lived than we expected it to be. By exposing the cells to actinomycin D for a shorter period, it may reduce the toxic effects of the drug on the cells therefore creating less variation.

Value of the studentship

I thoroughly enjoyed the 8 weeks I spent working in a professional laboratory. I gained valuable scientific techniques as well as vital analytical skills. The project had its challenges, I was expected to carry out experiments that I had not encountered before, and they were often unsuccessful. This taught me that the aim isn't always achieved in the first instance. However, creating improvements to get experiments to work taught me the valuable skill of problem solving. The experience has better prepared me to take on my final year project as well as instilling in me the desire to pursue a PhD following my degree.

References

- Norman, C., Runswick, M., Pollock, R. and Treisman, R. (1988). *Cell* 55(6), pp.989-1003.
- Rauen, K. and Tidyman, W. (2009). *Current opinion in Genetics & Development*, 19(3), pp. 230-236.
- Selbach, M., Schwanhausser, B., Busse, D., Dittmar, G., Schuchhardt, J., Wolf, J., Chen, W. (2011). *Nature*, 473, pp. 337-342.
- Treisman, R. (1992). *Trends in Biochemical Sciences*, 17(10), pp. 423-426.
- Vladimir, P., Alhusaini, N., Chen, Y., Martin, S., Morris, N., Kline, N., Olson, S., Weinberg, D., Baker, K., Graveley, B., Collier, J. (2012). *Cell*, 160(6), pp.1111-1124.
- Zubiaga, A., Belasco, J., Greenberg, M. (1995). *Molecular and cellular biology*, 15(4), pp. 2219-2230.

Supplementary Material

Oligonucleotides

tH

GGCGGCCACCACCATGCATCACCATCACCATCACCCGGCTGCATGAGCTGCA
AGTGTGTGCTCTCCTGAGAATTCGGCCGGCC

tH_rare

GGCGGCCACCACCATGCATCACCATCACCATCACCCAGGATGTATGAGTTGTA
AATGTATTAAAGTTGAGAATTCGGCCGGCC

tH-3SHE_rare

GGCGGCCACCACCATGCATCACCATCACCATCACAGTCATGAAAGTCATGAAA
GTCATGAACCAGGATGTATGAGTTGTAATGTATTAAAGTTGAGAATTCGGCC
GGCC

1. Aims of the project-

P2X purinoceptors form a family of ionotropic receptors, that are ligand gated ion channels. P2X receptors have three structural domains – (i) extracellular, (ii) transmembrane helices and (iii) intracellular. These receptors comprise a distinct family of ion channels which are activated upon extracellular binding of ATP. ATP is an extracellular transmitter which is stored in vesicles. These transmitters release ATP in a regulated manner in a variety of ways (i) through hemichannels, (ii) followed by shear stress or (iii) following membrane damage. This ATP released into the cell binds to the extracellular domain and causes a conformational change and a major rearrangement of the TM helices, leading to opening of the channel. P2X subunits assemble as homo- and hetero-trimeric ion channels which after binding of ATP and channel opening allow the unspecific influx of small cations. Aims of this project specifically included-

- (i) Study structural aspects of the receptor;
- (ii) Understand the molecular basis of the channel properties and their functions in its activation;
- (iii) Propose a model of how ATP binds to the P2X3 receptor and how it might induces opening of the channel using molecular dynamic techniques.

2. A description of the work carried out-

In order to achieve the aims of the project a variety of softwares were used. The molecular dynamics simulations were set up and run using the qwikmd simulation feature of vmd. A pdb version of the crystal structure of closed, apo state of P2X3 (RCSB code: 5SVJ) was downloaded and visualised in pymol.

The functional homo trimer was generated via the pymol feature symmetry mates (FIGURE 1).

The simulation of the apo state of P2X3 without ATP was performed as reference run. In the pymol structure an ATP molecule was introduced. Various orientations were created by moving the ATP molecule around the extracellular domain of the P2X3R to run an individual simulation of each of these.

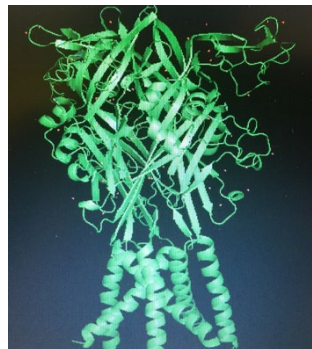


Figure 1c: Functional homotrimer



Figure 1a: Non-functional monomer of P2X3R



Figure 1b: Symmetrical mates for the monodimer

3. An assessment of the results and outcome of the studentship-

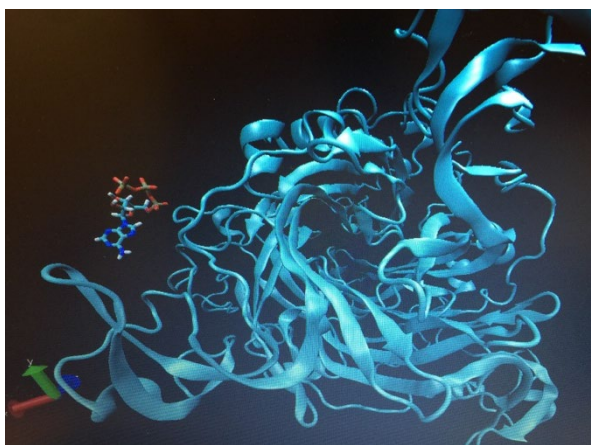


Figure 2(a) Starting point of simulation (before)

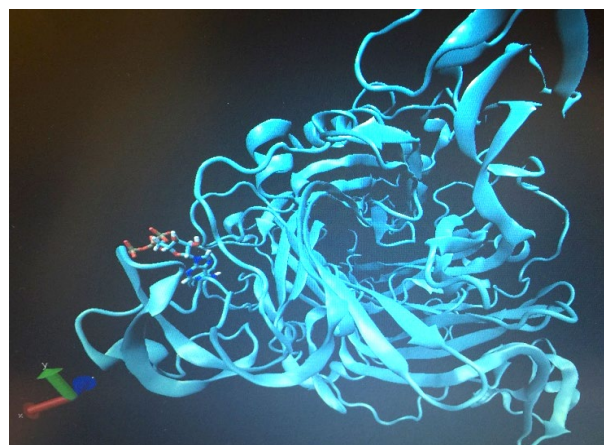


Figure 2(b) End point of simulation (After)

The project successfully modelled how ATP is pulled towards the receptor by the positive charges on the surface of the ATP binding site as shown in figure 2(a) and 2(b).

4. Future directions in which the project can be taken

It would be good to replicate the simulations from different starting positions to see how this affects the first steps of ATP binding. Also extending the simulations would be useful so to maybe cover the next steps of binding and channel opening. It would also be very interesting to analyse how the simulation works with other such agonists and antagonists.

5. Any departures from the original proposal:

The plan initially proposed to model how N-methyl-d-glucamine (NMDG) accesses extracellular lateral portal of P2X receptors and the how it may pass through the pore. Using a coding language and performing molecular dynamics were completely new methods for me. Other than performing supervised practicals as part of the coursework for a module, I have never used these analytical research tools before. So we decided to focus on ATP binding to the extracellular domain which was easier to approach as parameters for ATP were already calculated.

Please also include details of how the grant has contributed to or shaped your career aspirations.

Studying the molecular aspects of bioscience and performing research to analyse development of diseases, is what I see as a possible future career for myself. Over the course of the summer vacations, I gained eminent experience in the field of computational biology to enhance my knowledge of molecular modelling techniques and enhance my analytical skills. Under the guidance of my supervisor I learnt the use of coding language. I received rather a lot of training in using softwares and programs such as 'vmd', 'qwikmd' and 'namd'. I performed tutorials for the molecular dynamic simulation program called 'amber'. Along with this I enhanced my knowledge on ligand docking techniques and analysing protein structure supplementing evaluative and data analysis skills. Working under my supervisor, Dr Ralf Schmid, I discovered the lifestyle of a research scientist. This experience has led me to take a very definitive decision of choosing the field of research as a future career prospect. I express immense humble gratitude towards Dr Schmid for giving me this opportunity and The Biochemical Society for making this possible with the help of the grant.

Please also add a short paragraph highlighting the value of the studentship, both to yourself and to the lab. You may want your supervisor to write this.

"Nishtha's project contributed to our ongoing research on binding of agonists and antagonists to P2X receptors by generating preliminary data for the binding of ATP to the human P2X3 receptor. Her project also allowed us to trial the "qwikmd" set-up tool for this type of simulation. Nishtha picked up required computational skills and background knowledge quickly, and I believe she developed a good understanding how we test hypotheses, how we design controls, and how to troubleshoot and solve problems in general." (RS)

The chance of receiving a yearlong membership with the biochemical society is much appreciated as it will help me stay in touch with all the recent scientific discoveries and ongoing researches. This will eventually help me chose a topic for a PhD at an esteemed institute in the UK. (Contact details mentioned below)

Name- Nishtha Singh

Phone number – 07827340123

UK address- 40C Ratby Lane, Markfield, Leicester| LE67 9RJ

Email Address- ns477@student.le.ac.uk

The characterisation of G-protein coupled receptor CLR in human endothelial cells

Student: Oktawia Anna Ryskiewicz, **Supervisor:** Dr Leonid Nikitenko,
Department of Biomedical Sciences, Faculty of Health Sciences, University of Hull.

Background and hypothesis

The G-protein-coupled receptor (GPCR) calcitonin receptor-like receptor (CLR) mediates signalling pathways upon stimulation with agonists, such as adrenomedullin (AM), calcitonin gene-related peptide (CGRP) and intermedin (IMD/AM-2), as shown in ectopic expression and animal models. These molecules have implications in cardiovascular disease, migraine, lymphoedema and cancer [1]. However, CLR properties in human cells are not fully understood [2]. Recently, Dr Leonid Nikitenko's group has discovered that CGRP and IMD/AM-2 play a role in primary human dermal lymphatic endothelial cell (HDLEC) by promoting proliferation and p42/44 MAPK phosphorylation, but induce very distinct transcriptional responses and CLR internalisation profiles (Hasan, et al. unpublished).

Aims and objectives

The aim of this project was to further compare and contrast molecular mechanisms underlying the effects of three putative CLR agonists in HDLECs, including:

1. Agonist-induced activation of signalling pathways by using qRT-PCR and immunoblotting.
2. Agonist-induced CLR internalisation by using immunofluorescence.
3. Confirm that these effects are CLR-mediated by using antagonists and RNAi methods.

Materials and methods

HDLEC were cultured accordingly to established protocol [3]. Western Blotting was used to characterise the phosphorylation of p44/42 MAPK upon the agonist stimulation (AM, IMD and CGRP). PBS was used as a control. The cells were stimulated with the agonists at 10^{-6} M at different time points ranging from 0 to 30 minutes. The experiment was repeated three times. Immunofluorescence was used to analyse CLR internalisation. Antibodies raised against human CD107 (lysosome marker) and EEA1 (early endosomes marker) were used for co-localisation with CLR. Appropriate secondary antibodies conjugated with Alexa Fluor 488 and Alexa Fluor 594 were used. The experiment was repeated two times. Statistical analysis was done to quantify the Western Blotting results using Two-way ANOVA and GraphPad Prism. Two-way ANOVA is a non-parametric test, which compares multiple groups of two factors (time and relative p42/44 MAPK intensity). P-values less than 0.05 were considered as significant.

Results

Firstly, I have analysed the p42/44 MAPK signalling pathway activation in HDLEC upon agonist stimulation (Fig. 1A,1B). All agonists phosphorylate p42/44 MAPK at 5-15 minutes, de-phosphorylation is observed at 30 minutes. Next, I have analysed CLR internalisation (Fig. 1C). Immunofluorescence results show the co-localization of CLR. As indicated on the images CLR overlaps with the CD107, which can be seen as yellow colour. The data suggests receptor internalisation upon stimulation with AM only.

Discussion and future perspectives

Further research will be carried out as final year undergraduate 40-credit project to confirm whether observed effects are CLR-mediated. Dissecting the molecular basis of CLR function in human endothelial cells would help in understanding potential application for this GPCR as a target for future functional studies and development of drugs with fewer side effects.

Departures from original proposal

Initially, I was aiming to complete all of my objectives during the 8-weeks period of the internship. However, I wanted to obtain the most reliable results, therefore I have repeated Immunoblotting experiments three times and Immunofluorescence two times. Hence two objectives were achieved, the third one will be performed during my undergraduate project.

Value of studentship

Summer studentship has been a beneficial and thoroughly enjoyable experience, which has confirmed my desire to pursue a career in research. It has provided experience with laboratory techniques that would have not been possible to gain in an undergraduate lab in time for my 40-credit project. An internship allowed me to gain first experience of designing and carrying out research on my own in an established laboratory. It has also improved my confidence and skills such as problem solving, team work and data analysis. The chance to work alongside my supervisor and his MSc and PhD students at such an early stage in my academic career has been immensely rewarding.

References

- [1] Hay, D., et al. (2018). *IUPHAR Review 25*.
- [2] Nikitenko, L., et al. (2006). *Journal of Cell Science*, 119(5), pp.910-922.
- [3] Nikitenko, L., et al. (2013). *Journal of Investigative Dermatology*, 133(7), pp.1768-1776.

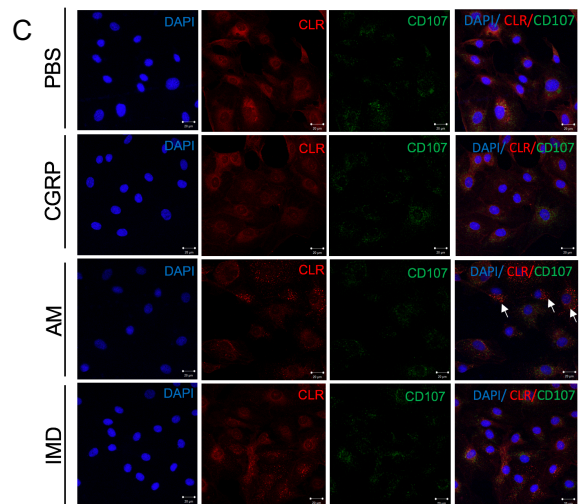
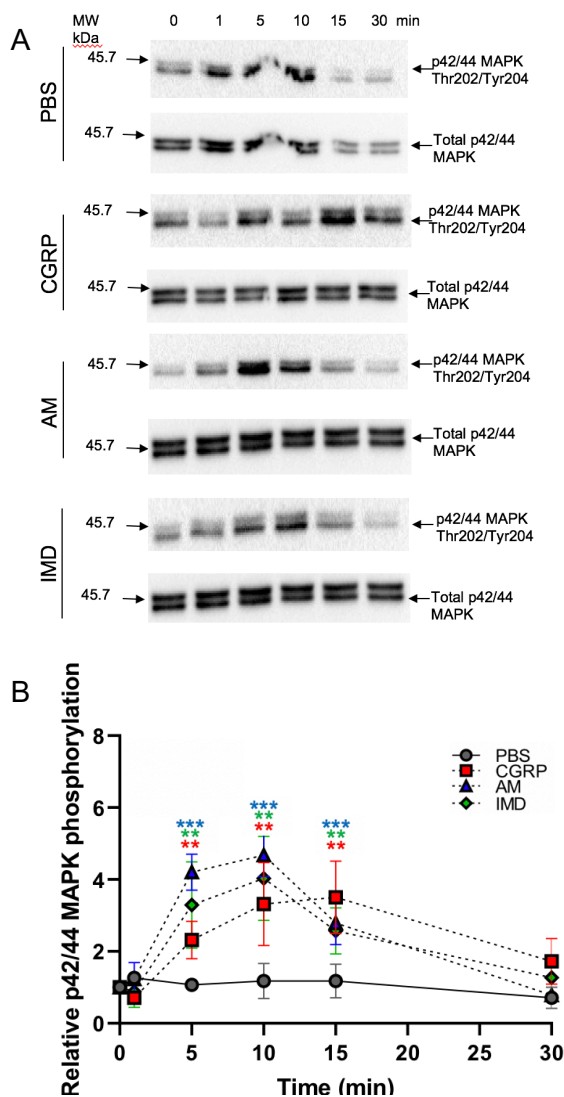


Figure 1. p42/44 MAPK phosphorylation and CLR internalisation in HDLEC upon agonist stimulation. The cells were stimulated with agonists (AM, IMD, CGRP and PBS as a control) at different time phases ranging from 0 to (A,B) 30 or (C) 45 min. (A) Western blotting was used to detect the signalling of p42/44 MAPK pathways. All agonists were stimulated at the same time (0, 1, 5, 10, 15, 30 minutes). (B) The graph generated using the GraphPad Prism based on Two-way ANOVA relative phospho- to total p42/44 MAPK intensity. n=3, data represents +/- SEM; *-p<0.05, **-p<0.01, ***-p<0.001; Two-way ANOVA. (C) Representative results showing CLR internalisation dynamics after colocalization with CD107. PBS was used as a control. Arrows indicate internalisation in form of speckles.

Acknowledgements

Firstly, I would like to thank the Biochemical Society for giving me this opportunity to pursue my interest in research. I want to specifically thank all other members of Dr Nikitenko's lab – with special thanks to Shirin Hasan and Dimitrios Manolis for their help, support and all of the knowledge they have shared with me (Figure 2). Finally, I would like to show my heartfelt appreciation for Dr Leonid Nikitenko's contribution to my research project for his unwavering support during this studentship and his continued mentorship.

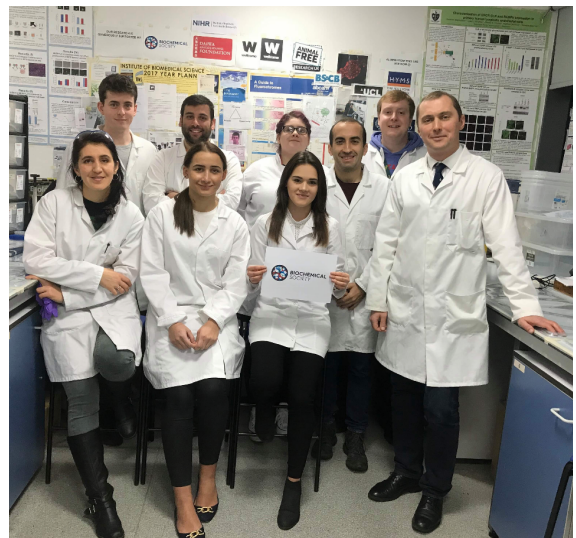


Figure 2. Right to left: Front - Dr Leonid Nikitenko (supervisor) and students: Oktawia Ryskiewicz (3rd year undergraduate), Karolina Jagielka (3rd year undergraduate), Shirin Hasan (2nd year PhD), Back - Eamon Faulkner (MRes), Dimitrios Manolis (3rd year undergraduate), Amelia Gamble (MRes), Paulo Saldanha (2nd year PhD), Matthew Morfitt (2nd year PhD).

Creating designer polymers for 3D cell culture and regenerative medicine

Student: Victoria Burge Supervisor: Professor Jeremy Lakey

Introduction

Key to the virulence of the plague-causing bacterium *Yersinia pestis*, the chaperone-usher (CU) protein Caf1, forms long polymers that protect the bacteria from phagocytosis [1]. However, these strong, non-covalent Caf1 polymers can also form 3D scaffolds for use in drug discovery and wound healing, and could replace animal experiments. Natural Caf1 polymers are biologically inert; however, with the introduction of bioactive motifs this phenotype can be reversed, enabling them to form artificial extracellular matrices [2].

Caf1 polymers form from 15 kDa subunits through donor strand complementation (DSC), where the N-terminal strand of one subunit completes the Ig-like fold of the next one in the polymer chain (**Fig. 1A**) [3]. Another CU protein from *Salmonella*, SafA, forms nearly identical polymers via DSC [4]. However the N-terminal strands are unique, meaning that only Caf1-Caf1 and Saf-Saf links are formed. Designing chimeric Caf1/SafA constructs would allow for specific ordered heteropolymers to be designed. Caf1 polymers can reform following monomerisation by thermal denaturation (**Fig. 1B**) [5], enabling the mixed polymers to be easily formed at a high yield in the test tube (**Fig. 1C**) [6].

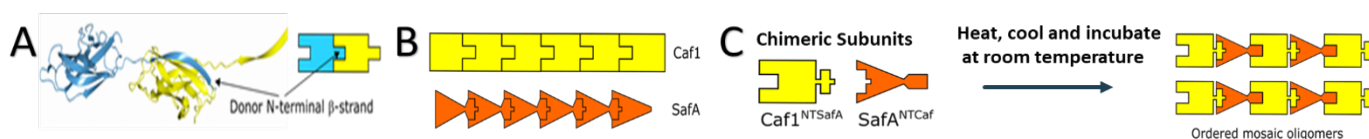


Figure 1: The formation of oligomers by DSC after heating and cooling. (A) Diagram of two Caf1 subunits undergoing DSC where the yellow subunit has an acceptor cleft that binds the N-terminal β -strand of the blue subunit. (B) Schematic showing the reassembly of the Caf1 (yellow) and SafA (orange) monomers to form separate homo-oligomers. (C) Schematic showing novel chimeric subunits by swapping the N-terminal β -strands of SafA and Caf1, the subunits can no longer form an oligomer with themselves but should form an alternating pattern when mixed.

Project Aims

(1) Determine whether Caf1 and SafA subunits can be expressed in the cytoplasm. (2) Design and purify chimeric Caf1/SafA CU subunits and test whether patterned hetero-oligomers are formed. (3) Characterise the resulting oligomers using biophysical techniques.

Results

By removing the periplasmic localisation sequence, each protein construct could be produced in the cytoplasm as insoluble inclusion bodies. Purification resulted in good yields (SafA= 7.74 mg/L, Caf1= 10.57 mg/L, Caf1^{NTSafA}= 4.62 mg/L and SafA^{NTCaf1}= 2.21 mg/L).

All samples were heat denatured and cooled to cause *in vitro* polymerisation. To determine whether the chimeric proteins bound to their partner protein, SDS-PAGE, native PAGE, tryptophan fluorescence and CD were used, with non-chimeric SafA and Caf1 as controls. SDS-PAGE (**Fig. 2A**) analysis shows that the individual chimeric protein samples only have a single monomer band, as expected. However, only a monomer band was clearly visible when the chimeras were mixed, except for the presence of a faint band \sim 35 kDa potentially corresponding to a dimer. Moreover, oligomers were not detected in pure SafA samples, suggesting that SafA is not as stable as Caf1 and is not resistant to incubation with SDS. This was verified by a CD thermal melt assay, where SafA had a melting temperature of 51.4°C compared to the 83°C displayed by Caf1 [7].

CD spectra (**Fig. 2B**) show that, like Caf1 polymers, the Caf1^{NTSafA}:SafA^{NTCaf1} mixture has some tertiary structure which can be unfolded by heating to 90°C and refolded at RT for 24 h. However, it was difficult to see whether the chimeras were interacting as SafA alone produces a strong signal at 293 nm, whereas the Caf1 signal is much weaker at 290 nm. The thermal renaturation supports the hetero-oligomer formation hypothesis, as the fraction folded is above 1.0, suggesting that a new structure is forming. The tryptophan fluorescence shows a red shift when heated returning to the initial folded value after the chimeric mixture was left to refold over 24 h. However, this was also the case for SafA^{NTCaf1} and Caf1^{NTSafA} alone and therefore these results do not demonstrate an interaction between the protein chimeras.

Native PAGE analysis provides the clearest evidence for hetero-oligomer formation (**Fig. 2C**). WT Caf1, which oligomerises after heating, forms a ladder with distinct bands corresponding to the formation of the dimer, trimer etc. The SafA^{NTCaf1}, which has a high pI produces a smear at the top of the gel with no distinct bands present, as it cannot oligomerise alone. This is also the case for Caf1^{NTSafA}, but this construct has a low pI and so travels further down the gel. Finally, the Caf1^{NTSafA}:SafA^{NTCaf1} equimolar chimeric mix produces a distinct ladder which is likely due to hetero-oligomer formation, the low pI Caf1^{NTSafA} allowing the high pI SafA^{NTCaf1} to migrate further into the gel.

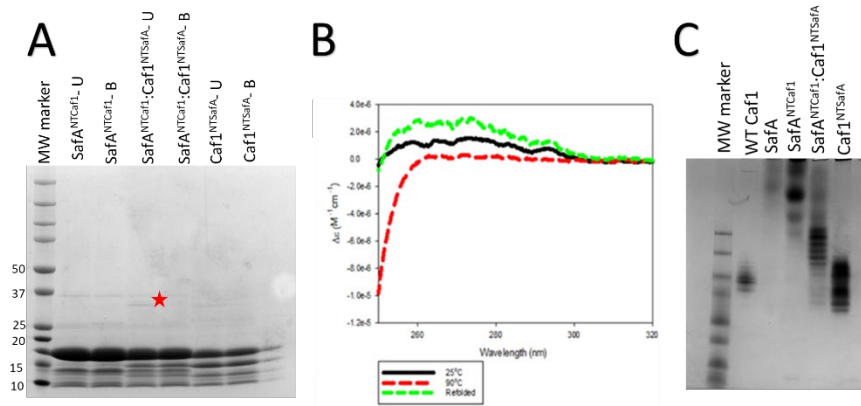


Figure 2: Caf1^{NTSafA} and SafA^{NTCaf1} subunits can form patterned hetero-oligomers. (A) SDS-PAGE of Caf1^{NTSafA}: SafA^{NTCaf1} hetero-oligomer formation. Where U= not heated and B= heated, in SDS sample buffer for 5 min at 95°C. An equimolar mixture of Caf1^{NTSafA}: SafA^{NTCaf1} was run alongside the individual chimeric protein constructs. A potential dimer band at ~35 kDa is highlighted by the red star. (B) Near UV spectra of Caf1^{NTSafA}: SafA^{NTCaf1} equimolar mixture at 25°C, 90°C and after allowing to refold for 24 h at 25°C showing increased structure compared to homo-oligomers. (C) Native-PAGE analysis of hetero-oligomer formation of WT Caf1, SafA, Caf1^{NTSafA}: SafA^{NTCaf1}. pH 8.3 Running Buffer was used. Caf1 WT pI- 4.56, SafA pI-8.08, Caf1^{NTSafA} pI- 5.84, SafA^{NTCaf1} pI- 8.11.

Conclusion

In this project, we have successfully purified each protein chimera and shown them to interact to form patterned hetero-oligomers via several techniques. These data suggest that the protein chimeras interact, but further characterisation is needed to provide a definitive answer.

Future Work

To further determine whether patterned hetero-oligomers are forming, a long cross-linker should be used to try visualise the resulting oligomers more clearly on SDS. A cross-linker assay was done using formaldehyde, however this experiment was not successful due to the short length of the crosslinker. Also, co-expressing the SafA chaperone, SafB, may encourage the DSC of the SafA N-terminal β -strand from Caf1^{NTSafA} with the acceptor cleft of SafA^{NTCaf1}.

Deviations from the Original Proposal

Firstly, labelling assays e.g. FRET were not undertaken as other assays seemed more appropriate, such as native PAGE and cross-linker assays. This was done to try and obtain conclusive evidence whether Caf1^{NTSafA} and SafA^{NTCaf1} could form patterned hetero-oligomers. Also, cloning was done prior to my placement starting to allow more time for purification and characterisation using a range of biophysical techniques.

Value of the Studentship

Personally, I was able to apply the knowledge about protein structures and biophysics taught in lectures to help me understand my results and why each test was carried out. It was very rewarding to gather new knowledge about the previously uncharacterised SafA, discover its unexpected behaviour and work out how that relates to its fine structure. I gained confidence working independently and was able to troubleshoot and optimise a purification protocol which the Lakey Group will continue to use. The group and I have gained a lot of unexpected knowledge in regard to how SafA works, and with future characterisation of whether hetero-oligomers can form, my research will direct the lab's future projects. This opportunity has been invaluable and has enhanced my future ambitions to do a Research Masters and PhD following my Undergraduate Biochemistry Degree, to then pursue a career in Biomolecular Research.

References

- [1] Du Y, Rosqvist R, Forsberg A. Role of Fraction 1 Antigen of *Yersinia pestis* in Inhibition of Phagocytosis. *Infection and Immunity*. 2002;70(3):1453-1460
- [2] Roque AI, Soliakov MA, Phillips SR, Shah DSH, Lakey JH. Reversible Non-Stick Behaviour of a Bacterial Protein Polymer Provides a Tuneable Molecular Mimic for Cell and Tissue Engineering. *Advanced Materials*. 2014;26:2704-2709
- [3] Zavalov AV, Berglund J, Pudney AF, Fooks LJ, Ibrahim TM, MacIntyre S, Knight SD. Structure and biogenesis of the capsular F1 antigen from *Yersinia pestis*: preserved folding energy drives fibre formation. *Cell*. 2003;113(50):587-596.
- [4] Zeng L, Zhang L, Wang P, Meng G. Structural basis of host recognition and biofilm formation by *Salmonella* Saf pili. *Elife*. 2017;6:e28619
- [5] Dura, Peters et. al., unpublished data.
- [6] Rose RJ, Verger D, Daviter T, Remaut H, Paci E, Waksman G, Ashcroft AE, Radford SE. Unraveling the molecular basis of subunit specificity in P pilus assembly by mass spectrometry. *Proceedings of the National Academy of Sciences of the United States of America*. 2008;105(35):12873-8
- [7] Chalton DA, Musson JA, Flick-Smith H, Walker N, McGregor A, Lamb HK, Williamson ED, Miller J, Robinson JH, Lakey JH. Immunogenicity of a *Yersinia pestis* vaccine antigen monomerized by circular permutation. *Infection and Immunity*. 2006;74(12):6624-31.

Biochemical Society Report

Aims of the project

This Summer, I have been looking at Neuroinflammation in Down Syndrome (DS). DS occurs in humans when there is triplication of chromosome 21 (Hsa21). Results from Dr. Wiseman's Lab have revealed that people with DS are at an increased risk of developing Alzheimer's Disease (AD), known as AD in DS (AD-DS; [Wiseman et al., 2015](#)). In AD, the activation of microglia by amyloid beta (A β) accumulation triggers inflammation in the brain, known as neuroinflammation ([Heneka et al., 2015](#)). Hence, the main aim of my research was to investigate whether neuroinflammation, and its associated effects in AD, is the same in DS and AD-DS.

Work Conducted

This research involved me looking at male and female 12-month-old mice from the Dp1Tyb mouse model of DS. Dp1Tyb mice contain an additional copy of a 148-coding gene-long region of mouse chromosome 16. This area shares genes with a significant proportion of Hsa21 that is known to cause phenotypes specific to DS when triplicated ([Lana-Elola et al., 2016](#)). My work involved assessing microglial activation on tissue that had already been stained for microglia, using Iba1, by one of my colleagues at the lab. This involved manual microglial number and branch counting by splitting the hippocampus into three regions – CA1, CA2/3 and the Dentate Gyrus (**Figure 1**). Following this, I stained tissue sections from the same mice for astrocytes using the GFAP immunofluorescence stain, and analysed the area and intensity of this staining, using an ImageJ software script written by another one of my colleagues at the lab. This was to assess the extent of astrocyte presence within the different hippocampal regions of the mouse brain sections.

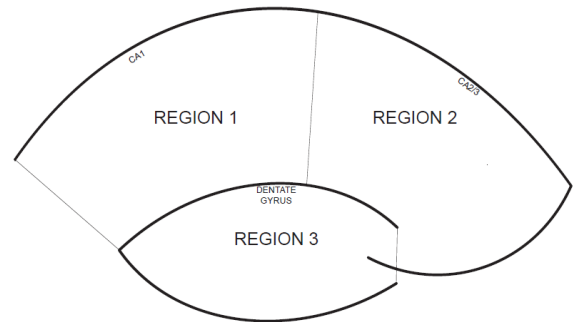


Figure 1 – Mouse hippocampal region divisions

Investigating neuroinflammation by looking at astrocytes, as well as microglia, is beneficial because these two cells are known to communicate with one another in a reciprocal way. For example, microglia help to regulate the innate immune functions of astrocytes, whilst astrocytes regulate microglial phenotypes ([Jha et al., 2019](#)). Furthermore, the cross-talk between microglia and astrocytes has been found to alter both A β pathology and neuroinflammation in mouse models of AD ([Lian et al., 2016](#)).

Microglial Activation Results

With regards to total microglial number per hippocampus, we found that the presence of trisomy significantly increased the total number of microglia ($p=0.019$), and that hippocampal region also significantly affected microglial quantity ($p<0.001$). Furthermore, sex had a significant effect ($p=0.003$), with male wild type (WT) and Dp1Tyb mice having more microglia than female mice. In contrast, there was no significant effect of trisomy ($p=0.589$), hippocampal region ($p=0.062$) or sex ($p=0.378$) on mean microglial branching.

Astrocyte Staining Results

The astrocyte staining revealed that trisomy had no effect on mean area ($p=0.695$) or mean intensity ($p=0.523$) of GFAP staining. Sex had a significant effect on mean area of staining ($p=0.048$) but not mean intensity of staining ($p=0.087$), with male WT and Dp1Tyb mice having a greater area of GFAP staining than female mice.

Future Directions

In light of the microglial activation results, the next step is to work towards conducting a co-stain of Iba1 with CD68, a lysosomal activation marker, in Dp1Tyb brain sections. Whilst Iba1 highlights the presence of microglia, CD68 can be used to highlight activated microglia by looking at lysosomes ([Bodea et al., 2014](#)).

This will give further insight into the extent of microglial activation, and hence neuroinflammation, within these mice.

Departures from Original Project Proposal

We originally proposed to look at both DS and AD-DS mouse models. However, I have only conducted work on DS mouse models during this studentship. This is purely because upon beginning the studentship, the key research focus of those I've been working with and assisting at the lab has been in specific DS mouse models. We also proposed to detect and quantify cytokine release using cytokine ELISA assays. This was not done because the immunofluorescence study took longer than originally anticipated.

How the Grant has shaped Career Aspirations

This grant has been of huge benefit to my planned future endeavours. I am working towards applying for the MBPhD programme at my university, which gives me the opportunity to complete a 3-4 year PhD during Medical degree. The grant has given me the opportunity to obtain valuable research experience, which has further fuelled my desire to undertake a PhD. Furthermore, it has helped me deepen my appreciation for the key role of scientific research in advancing medicine and the way we treat certain diseases.

Value of the Studentship

The studentship has not only allowed me to gain increased confidence with using statistical analysis programmes like SPSS, but it has also exposed me to new techniques, such as Western Blotting. Furthermore, it allowed me to build on my limited experience in presenting scientific data, which has pushed me to becoming less reliant on notes when presenting.

Comments from Dr. Frances Wiseman

Debbie's work over the summer contributed to the discovery of a novel phenotype in one of our group's mouse models of DS; increased microglial numbers. This finding has been recently submitted as part of preliminary data for an onward grant application for the study of neuroinflammation in AD-AD (Alzheimer's Society PhD application). Debbie also worked hard to develop staining protocols for markers of microglial activation states which have been useful for several other members of our group.

REFERENCES

- Bodea L-G., Wang Y., Linnartz-Gerlach B., Kopatz J., Sinkkonen L., Musgrove R., Kaoma T., Muller A., Vallar L., Di Monte DA., Balling R. & Neumann H. (2014) Neurodegeneration by activation of the microglial complement-phagosome pathway. *The Journal of neuroscience: the official journal of the Society for Neuroscience*. 34(25) p.8546-8556. Available from: DOI: 10.1523/JNEUROSCI.5002-13.2014
- Heneka MT., Carson MJ., El Khoury J. et al. (2015) Neuroinflammation in Alzheimer's disease. *The Lancet Neurology*. 14(4) p.388-405 Available from: DOI: 10.1016/S1474-4422(15)70016-5
- Lana-Elola E., Watson-Scales S., Slender A., Gibbins D., Martineau A., Douglas C., Mohun T., Fisher EMC. & Tybulewicz VLJ. (2016) Genetic dissection of Down syndrome-associated congenital heart defects using a new mouse mapping panel. *eLife*. 5 (e11614). Available from: DOI: 10.7554/eLife.11614
- Jha MK., Jo M., Kim J-H. & Suk K. (2019) Microglia-Astrocyte Crosstalk: An Intimate Molecular Conversation. *The Neuroscientist*. 25(3). p. 227-240. Available from: DOI: 10.1177/1073858418783959
- Lian H., Litvinchuk A., Chiang AC., Aithmitti N., Jankowsky JL. & Zheng H. (2016) Astrocyte-microglia cross talk through complement activation modulates amyloid pathology in mouse models of Alzheimer's disease. *The Journal of neuroscience: the official journal of the Society for Neuroscience*. 36(2). p.577-589. Available from: DOI: 10.1523/JNEUROSCI.2117-15.2016
- Wiseman FK., Al-Janabi T., Hardy J. et al. (2015) A genetic cause of Alzheimer disease: mechanistic insights from Down Syndrome. *Nature Reviews Neuroscience*.16(9) p.564-574 Available from: DOI: 10.1038/nrn3983

I was the recipient of a Biochemical Society Summer Studentship award in the summer of 2019 to work with Dr Anna Barnard at Imperial College, London on the design and synthesis of mimetic molecules to target protein-protein interactions (PPI).

Traditional enzymatic drugs target active sites, which are structurally well-defined pockets of 300-500 Å². Typically, these will contain key catalytic residues, and protein engineering can reveal those residues necessary for substrate binding, enabling them to be targeted through structure-based design of inhibitors.

However, the majority of the human genome encodes for non-enzymatic proteins, and the interaction between these proteins is often implicated in human disease thus making them attractive medicinal targets. Drugging PPI's can be significantly more challenging than enzymatic targets, as the protein landscape is often significantly larger than an enzyme active site pocket (1000-2000 Å²) and topographically featureless, regularly presenting as a hydrophobic surface. The interactions are often multi-dimensional, taking place across many faces of helices simultaneously, and can involve very many residues in binding. This makes structure-guided small molecule inhibitor design very difficult, and many molecules developed in this way display very weak binding.

One method has been to make use of native peptides, truncating binding proteins down to the structural elements necessary for binding only. However, these tend to be conformationally promiscuous when in isolation from the rest of the protein, and are rapidly degraded by the proteasome.

Previous research in the Barnard Group has led to the development of a new class of multi-facial helix mimetic. These allow the introduction of sidechain functionality at two faces of an unnatural amino acid, each of which mimics one turn of an α -helix. These unnatural helix mimetics are then inserted into the peptide sequence of interest, replacing the binding helix. This chimeric molecule should then be conformationally reliable and stable towards degradation.

My project was to use these principles to design an inhibitor of the Bcl-xL/Bak PPI. Bcl-xL is an anti-apoptotic protein implicated in cancer cell survival through inhibition of the tumour suppressor gene p53, the so-called 'guardian of the genome'. When complexed to Bak, Bcl-xL's ability to promote cell survival is inactivated, leading to cell death. A drug that would permanently inactivate Bcl-xL in tumour cells could therefore show potential as an anti-cancer treatment.

X-ray crystal structures of the interaction exist, and previous research has revealed 'hot spot' residues, which make important energetic contributions to binding. I designed three amino-acid monomers that mimicked the sidechains of these hotspot residues in the binding helix. The aim was to synthesise these monomers, incorporate them into the Bak peptide sequence using solid-phase peptide synthesis and then assay the binding activity of the chimeras using a previously optimised assay.

Initially the synthesis went to plan, however each of the monomers contained a carboxylic acid group which lead to difficulties in purifying the compounds. Several strategies were tried, but difficulties were encountered at each stage. By the end of my

time in the group, I had successfully synthesised one of the three monomers, but was unable to proceed beyond intermediates for the other two. Although frustrating, this has taught me a lot about the process of research chemistry and the problems that can be encountered when making new reactions and molecules. It was an enjoyable and satisfying challenge to try and find solutions and negotiate these issues.

There is a lot of opportunity for future work on this project, as the synthesis of the remaining monomers will have to be completed, the chimeras constructed and then assayed for activity. Several suggestions for new synthetic routes were made when I presented the work I had done at a group meeting which could avoid the problems I ran into. If the activity of the chimeras proves to be sufficiently good then this opens up a pathway for several physiologically important PPI's to be targeted in the future, and I would be excited to see it tested against some more challenging PPI's.

I learned an enormous amount during my studentship, and enjoyed it tremendously. The practical skills and experience that I gained from working day to day in a research laboratory has provided me with invaluable insight and techniques that have been very useful to me in my project so far this year. Taking part in research has convinced me that I want to continue my studies further through a PhD, and then look to pursue a career in research. I am incredibly grateful for the opportunity that I was able to take part in through my studentship award, and to Anna and her incredibly friendly and hospitable group for welcoming me so warmly and giving me so interesting a project to work on.

Cryo-EM of CCDC61^{cc} in complex with microtubules

Introduction

Centrosomes are the main microtubule-organising centre and, hence, are important for correct cell division (Nigg & Raff, 2009). The core structure of the centrosome is a pair of centrioles, each of which is mainly comprised of nine copies of microtubule triplets (Breslow & Holland, 2019). One of the pair has appendage structures that are crucial for generating a cilium (Kobayashi & Dynlacht, 2011). Cilia are hair-like structures that play key roles in cell signalling (Pala et al. 2017) and motility. During ciliogenesis, centrioles attach to cell membrane and become basal bodies (Breslow & Holland, 2019). Therefore, centrosomes and cilia share a set of proteins that localises at both of them.

CCDC61 is one of these proteins. It has been previously shown in green algae that the protein is essential for the correct synthesis of basal bodies (Wright et al., 1983), probably via helping the assembly of the sub-structures of the organelles. Recently, the host laboratory of my summer intern found that the coiled-coil domain of CCDC61 binds to microtubules, and this binding is important for a ciliary function of the protein (unpublished). However, the molecular mechanism of how this microtubule binding plays a role in the protein function is unclear. Toward filling this knowledge gap, as the first step, my project focused on determining the structure of the coiled-coil domain of CCDC61 (CCDC61^{cc}) in complex with microtubules using cryo-electron microscopy (cryo-EM). I optimised the CCDC61/microtubule complex so that microtubules are fully decorated with CCDC61, prepared cryo-EM grids and collected data using a Titan Krios equipped with a Falcon III direct electron detector.

Aims

The primary aim of my project is to optimise the sample and grid of the CCDC61/microtubule complex in order to determine the structure of the complex and understand how CCDC61 binds to microtubules.

Methods

Expression of CCDC61^{cc}

C41(DE3) competent cells were transformed with plasmids encoding the coiled-coil domain of human CCDC61 fused with a DNA-repair protein PAXX (Ochi et al., 2015) by heat shock. 1 µl of plasmid was added to 50 µl of *E. coli* cells. The competent cell/DNA mixture had been kept on ice for 30 minutes before put at 42 °C water bath for 45 seconds. After recovering on ice for 2 minutes, cells were inoculated into 100ml 2×YT containing 100 µg/ml ampicillin at 37 °C overnight. 10ml starting culture was transfer into 1L 2×YT. Cells grew at 37 °C until the OD reached 0.6. Then IPTG was added to induce expression at 16 °C. The cell culture was centrifuged at 4,000 g to harvest cells. Cells were washed with PBS and snap frozen. Frozen cells were thawed on ice and resuspended in binding buffer (50 mM Tris pH 8.0, 500 mM NaCl, 10 mM imidazole, 2mM β-mercaptoethanol). Cells were sonicated at 80% amplitude for one and a half minutes. The lysate was then centrifuged at 35,000 g.

Affinity Chromatography

A gravity flow column packed with 5ml Ni Sepharose 6 Fast Flow was used to purify the protein. After mixing the clarified lysate with Ni²⁺ beads for 1 hour, the resin was washed by washing buffer (50 mM Tris pH 8.0, 500 mM NaCl, 30 mM imidazole, 2mM β -mercaptoethanol). Flow-through was collected for analysis. Target protein was eluted by elution buffer (50 mM Tris pH 8.0, 500 mM NaCl, 300 mM imidazole, 2mM β -mercaptoethanol). The eluate was dialysed against the dialysate (20 mM HEPES pH 7.5, 300 mM NaCl, 2 mM DTT) overnight to remove imidazole.

Ion Exchange Chromatography

5 ml HiTrap Q HP had been equilibrated with start buffer (20 mM HEPES pH 7.5, 300 mM NaCl, 2 mM DTT) before the sample was applied to it by syringe. Elution is performed using a linear gradient volume of 20 column volume with an increasing salt concentration up to 80% elution buffer (20 mM HEPES pH 7.5, 1 M NaCl, 2 mM DTT). Eluate with significant Ultraviolet absorbance (280 nm) was collected and concentrated by Vivaspin 20 (10K MWKO) and Vivaspin 2 (10K MWKO). The concentration of CCDC61 was quantitated by spectrophotometer at 280 nm.

Microtubule pelleting assay

Microtubule pelleting assays were performed as described (https://hymanlab.mpi-cbg.de/hyman_lab/wp-content/uploads/2012/08/Tubulin-Protocols-Mitchison.pdf).

Briefly, CCDC61 was incubated with microtubules in BRB80 buffer at room temperature for 15 minutes. The mixture was then overlaid onto BRB80 cushion buffer (BRB80 buffer with 40%(v/v) glycerol). The mixture was spun at 189,000 g for pelleting. Both supernatant and pellet were collected for SDS-PAGE analysis. In addition to the mixture, CCDC61 solution and microtubule suspension were also spun and analysed.

Negative staining EM

Glow discharge was performed on 400 mesh copper EM grids just before use. 3.5 μ l of the sample was placed on the EM grid and left for 1 min. After the excessive sample had been absorbed away, the grid was washed with 5 μ l of water twice. The sample was stained with 2% (w/v) uranyl acetate for 30 seconds. The pellets were imaged under Tecnai T12 at a magnification of 68,000 \times at the Asbury BioStructure Laboratory.

Cryo-EM grid preparation & data collection

3.5 μ l of resuspended pellet was deposited onto Quantifoil R1.2/1.3 400 mesh copper grids. FEI Vitrobot Mark IV blotted the grids with -5 blotting force for 3 seconds at 4 $^{\circ}$ C and 100% humidity and flash-froze them in liquid ethane. The data was collected on an FEI Titan Krios transmission electron microscope working at 300 kV and equipped with a Falcon III. The magnification was set to 75,000 \times , corresponding to 1.065 \AA per pixel. The detector was operated in linear mode with a total dose of 93.24 e-/ \AA^2 fractionated over 60 frames for 2 seconds. The defocus ranged from 0.7 μ m to 2.5 μ m.

Assessment of the results

Purification of CCDC61^{cc}

Using an established protocol of CCDC61^{cc} fused to PAXX (PAXX-CCDC61^{cc}). I successfully purify the protein at the final concentration of 2.04 mM (Figure 1A and B).

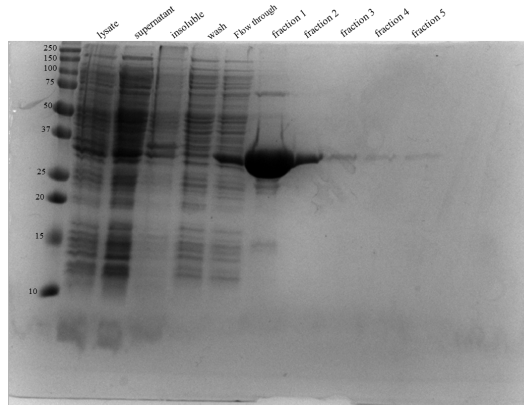


Figure 1A. SDS-PAGE showing the expression of CCDC61^{cc} fused with PAXX and the fractions of the eluate of the affinity chromatography

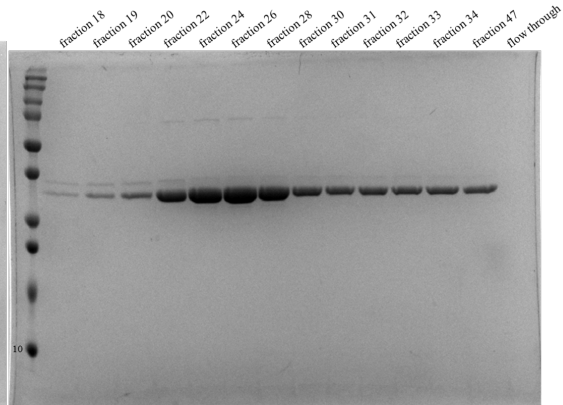


Figure 1B. SDS-PAGE showing the fractions of the eluate of the ion exchange chromatography

Microtubule pelleting assay

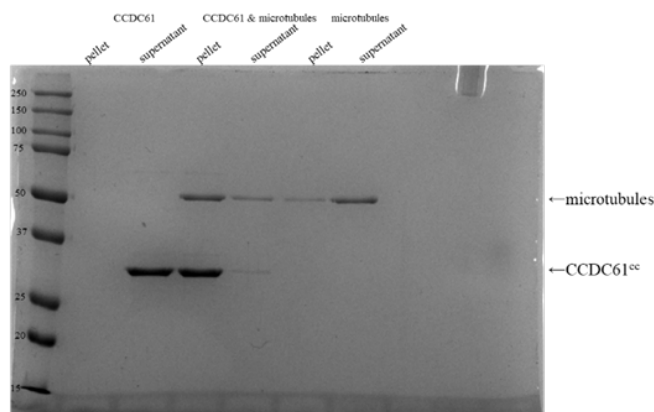


Figure 2. SDS-PAGE image of microtubule pelleting assay

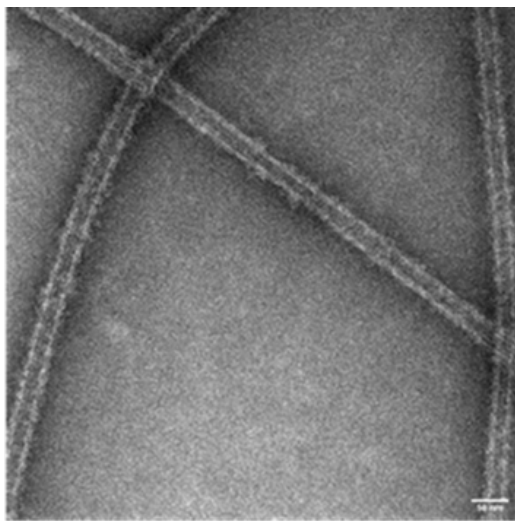


Figure 3. The image of negatively stained CCDC61^{cc}/microtubule complexes

The result of the microtubule pelleting assay is shown in Figures 2 and 3. The image of SDS-PAGE (Figure 2) displayed two bands in the lane loaded with the pellet. One band marks the molecular weight is around 50 kDa which corresponds to the molecular weight of tubulin. The other band indicates the molecular mass is between 25 kDa and 37 kDa which corresponds to the molecular weight of CCDC61^{cc}. Compared with the lane only contained CCDC61^{cc}, a significant amount of the protein was pelleted together with microtubules, illustrating that CCDC61^{cc} binds to microtubules.

Negative staining EM of CCDC61^{cc} in complex with microtubules

It is clear that the edge of the microtubule is fuzzy, suggesting that CCDC61^{cc} binds to the microtubule. In addition, microtubules seem wider after incubation

with CCDC61 (24 nm versus 30 nm). The electron micrographs are satisfactory, i.e. microtubules are densely coated with CCDC61^{cc}, the complex is stable, and the number of microtubules is reasonable in a given field. Nevertheless, the resolution of those electron micrographs is too low to study the structure of CCDC61 coiled-coil domain. Therefore, it is necessary and feasible to prepare grids for cryo-EM.

Cryo-EM of CCDC61^{cc} in complex with microtubules

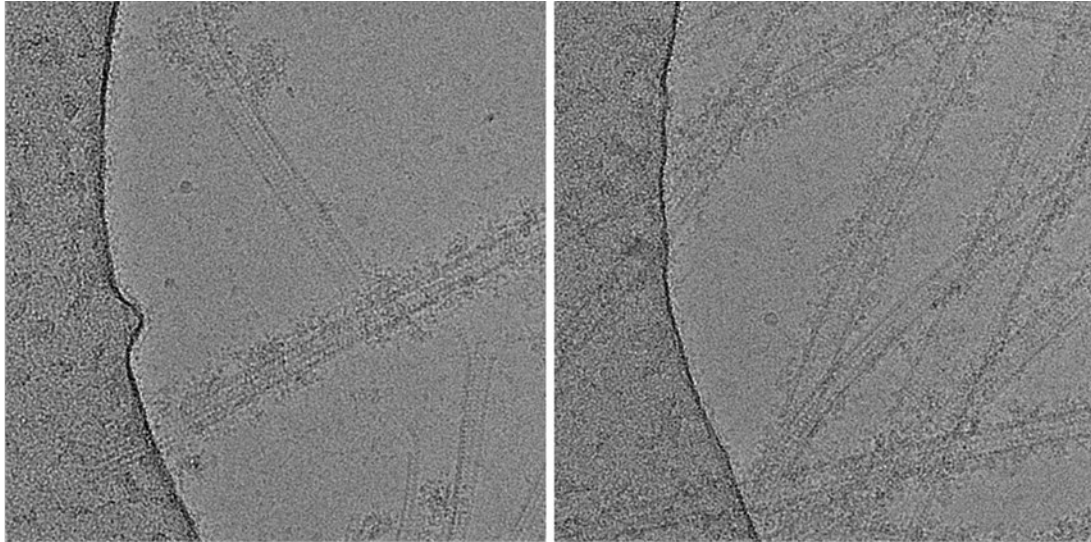


Figure 4. Cryo-electron micrograph of CCDC61^{cc}/microtubule complexes

Cryo-EM micrographs of CCDC61^{cc}/microtubule showed that microtubules were clearly decorated with CCDC61^{cc} (Figure 4). However, the regular alignment of CCDC61^{cc} on microtubules was not clear from the micrographs. Also, microtubules were not completely decorated with CCDC61^{cc} as observed in negative-stained micrographs (Figure 3). Therefore, these cryo-EM micrographs need to be processed to understand the microtubule-binding mode of CCDC61, and also cryo-EM grids of the complex should be further optimised.

Future directions

The micrographs collected from cryo-EM can then be processed to reconstruct microtubules in complex with CCDC61. The helical reconstruction will illustrate the interaction mode of microtubules with CCDC61, which may reveal the function of CCDC61. Ultimately, understanding the function of CCDC61 will shed light on a process that governs the assemblies of basal bodies.

The value of the studentship to the lab

The summer vacation studentship provided by the Biochemical Society was an excellent opportunity for my lab particularly because I just set up my own group and did not have anyone who could support me to do experiments. Steven took up an on-going project that required sample optimisation for cryo-EM data collection. Since he is knowledgeable, enthusiastic and quickly absorbed what I taught him, he managed to push the project forward and made significant contributions to my lab. It was a valuable

experience for me to have Steven in my lab.

Reference

Breslow, D.K. and Holland, A.J. 2019. Mechanism and Regulation of Centriole and Cilium Biogenesis. *Annual Review of Biochemistry*. 88, pp.691-724

Kobayashi, T. and Dynlacht, B.D. 2011. Regulating the transition from centriole to basal body. *The Journal of Cell Biology*. 193(3), pp.435–444

Nigg, E.A. and Raff, J.W. 2009. Centrioles, Centrosomes, and Cilia in Health and Disease. *Cell*. 139(4), pp.663–678

Ochi, T., Blackford, A.N., Coates, J., Jhujh, S., Mehmood, S., Tamura, N., Travers, J., Wu, Q., Draviam, V.M., Robinson, C.V., Blundell, T.L. and Jackson, S.P. 2015. PAXX, a paralog of XRCC4 and XLF, interacts with Ku to promote DNA double-strand break repair. *Science*. 347(6218), pp.185-188

Pala R., Alomari N. and Nauli S.M. 2017. Primary cilium-dependent signaling mechanisms. *International journal of molecular sciences*. 18(11), [no pagination]

Wright, R.L., Chojnacki, B. and Jarvik, J.W. 1983. Abnormal basal-body number, location, and orientation in a striated fiber-defective mutant of *Chlamydomonas reinhardtii*. *Journal of Cell Biology*. 96(6), pp.1697–1707

Acknowledgement

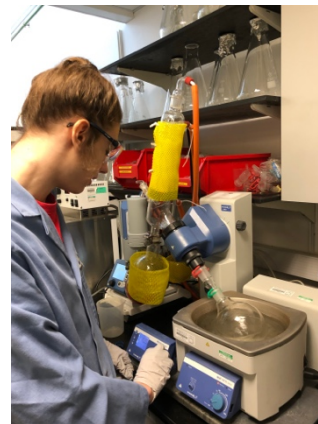
I would like to thank Dr Emma Hesketh for the cryo-EM data collecting using a Titan Krios.

Student: Vukan Milovanović

Supervisor: Dr. JL Kiappes
Department of Glycobiology, University of Oxford

Synthesis of potential small molecule inhibitors of alpha-glucosidase II

There are a number of viruses which utilise an envelope to protect their capsid and genetic material from being detected as foreign by the host's immune system and to allow easier entry into host cells by membrane fusion. The envelope is made out of host cell membranes (upon release of viral particles from the host cell), however it also contains a number of viral glycoproteins which are used to bind to host cell receptors and mediate viral entry. These proteins are synthesised by the host cell, after the virus hijacks the cellular machinery. Thus, successful replication of the virus relies on the host cell's endoplasmic reticulum protein folding machinery. As part of this machinery, there exists a quality control check which ensures that produced glycoproteins are folded correctly. This is known as the endoplasmic reticulum quality control (ERQC). ERQC contains the calnexin cycle, where the folding of glycoproteins is ordered and assessed by a series of lectins. The synthesised, not-yet-folded glycoprotein is N-glycosylated at the beginning of the cycle. The glycan has three terminal glucose residues. Alpha glucosidase I and II trim these glucose residues until only one is left. The monoglucosylated glycan is then a substrate for the calnexin cycle machinery and is aided by chaperones to fold. Alpha glucosidase II also trims off the final glucose residue after the folding process is completed in the cycle. If the protein fails to fold it may undergo the cycle once again, being reglucosylated by UDP-glucose glycoprotein glucosyltransferase (UGGT). However, after multiple unsuccessful attempts it will be targeted for ER associated degradation.



The project was to focus on developing small molecule inhibitors of Alpha glucosidase II, with the idea that this would prevent glycoproteins from folding correctly and put high ER stress on infected cells. This is because virally infected cells have higher rates of glycoprotein synthesis than normal cells. As a result, they are more prone to being affected by calnexin cycle inhibition. In addition, by inhibiting glycoprotein synthesis, the viral envelope would not be properly formed, lowering the number of infectious viral particles released from infected cells.

The work I performed involved attempting to optimise a known inhibitor of Alpha glucosidase II so that it would bind tighter to the enzyme and hopefully induce higher levels of inhibition. The work thus focused on organic synthesis together with my supervisor. We used 3-hydroxybenzaldehyde and 4-hydroxybenzaldehyde as the two compounds from which inhibitors were to be synthesised. Our goal was to add a carbon tail ending with an OH group onto the OH group of the hydroxybenzaldehydes, and to add various heterocycles as a substituent. Different lengths of carbon chains were to be used for the first reaction, to try and get the optimal inhibitor. Initially we wanted to do the tail addition reaction first by utilising a Mitsunobu reaction. Reaction

progress was monitored by thin layer chromatography, and products purified by column chromatography. Afterwards proton NMR was performed to confirm the identity of the product.



Later we decided to form the heterocycles first, and set out to achieve this by first creating the unoxidised ring, before adding iodine and base to aromatise it. The first step was easily achieved but the second proved elusive, as the OH group seemed to be interfering with the reaction. As a result, some protection group reactions were also performed on the OH group before attempting to form the ring again.

As the compounds being synthesised had never been made before, my work mostly involved optimising the reaction conditions used to obtain the wanted products as easily and efficiently as possible. Much vacuum evaporation, chromatography, and NMR was performed during this time, and I learned how to perform these techniques / operate the devices.

In the end, a sequence of three reactions resulting in the unoxidised ring and the carbon tail being added to the hydroxybenzaldehydes was found that worked well. These compounds were not the final target inhibitors, and there is still work to be done. This is where the lab will now continue the project, finishing up the synthesis optimisation, before testing the created inhibitors for potency. The binding to Alpha glucosidase II will be tested by STD NMR. If tightly binding efficient inhibitors are discovered they may enter drug trials to deem whether they could actually be applied to treat infections caused by Hepatitis C or dengue viruses.

As a result of the studentship, I was able to confirm my interest in organic chemistry and its application to medicine, now certain that this is the field I want to work more in. I have gained invaluable experience in the laboratory which will certainly be of great use when it comes to my Part II project at Oxford next year. I hope to use this experience as a base from which to stride further into the field.



References:

- Alonzi, D., Scott, K., Dwek, R. and Zitzmann, N. (2017). Iminosugar antivirals: the therapeutic sweet spot. *Biochemical Society Transactions*, 45(2), pp.571-582.
- Caputo, A., Alonzi, D., Marti, L., Reza, I., Kiappes, J., Struwe, W., Cross, A., Basu, S., Lowe, E., Darlot, B., Santino, A., Roversi, P. and Zitzmann, N. (2016). Structures of mammalian ER α -glucosidase II capture the binding modes of broad-spectrum iminosugar antivirals. *Proceedings of the National Academy of Sciences*, 113(32), pp.E4630-E4638.
- Kiappes, J., Hill, M., Alonzi, D., Miller, J., Iwaki, R., Sayce, A., Caputo, A., Kato, A. and Zitzmann, N. (2017). ToP-DNJ, a Selective Inhibitor of Endoplasmic Reticulum α -Glucosidase II Exhibiting Antiflaviviral Activity. *ACS Chemical Biology*, 13(1), pp.60-65.

Tom Trainer

Supervisors: Dr Eva Kevei and Dr Patrick Lewis

Lysosomal dysfunction as determinant of Parkinson's disease: investigating the potential role of novel risk genes

Introduction

Parkinson's Disease (PD), the second most common neurodegenerative disorder is characterised by the progressive loss of dopaminergic neurons in the Substantia Nigra. PD is genetically heterogenous, and only around 10% of PD cases has been assigned to a genetic cause. A cellular process becoming seen as central to PD pathology is the lysosomal degradation pathway. Dysfunction of lysosomal degradation impairs cellular homeostasis through decreased removal of damaged cellular content and it is thought that a dysregulation in these pathways enable progression of PD pathology. Interestingly, recent genome wide studies identified numerous risk genes with potential lysosomal function that could contribute to the development of PD (Table 1). To date, however, we have little information on how and whether the affected genes could contribute to PD. Therefore studying genes governing the lysosomal degradation pathway would benefit the understanding of PD progression and revealing novel therapeutic targets.

Aims

The purpose of this study was to investigate the potential pathogenic role of candidate PD risk genes involved in the lysosomal degradation pathway, that have been nominated by Genome Wide Association studies as potential cause of PD. To do this, the powerful model organism *Caenorhabditis elegans* has been used with genetic knockout models for these genes. I have studied dopamine-dependent physiology and lysosomal degradation pathway to identify the dysfunction of which candidate gene leads to PD pathology in *C. elegans*.

Techniques used

Behavioural analysis of dopaminergic function in *C. elegans*: Basal Slowing Assay: Dopamine is a conserved neurotransmitter between humans and *C. elegans*. In *C. elegans* it drives specific behavioural responses that can be used to assess the functionality of dopaminergic neurons. I have used the 'Basal Slowing' assay, which measures a slowing response of the worms when reaching their food source (*E. coli* OP50), a behaviour that is entirely dependent on dopaminergic neuronal signalling in well-fed worms.

Detecting steady-state levels of p62, an autophagy receptor protein that degrades via autophagy: Total protein lysates were used for detecting the steady state levels of the p62 orthologue protein (SQST-1) in *C. elegans* upon deletion of candidate lysosomal genes, the orthologues of which have been nominated as potential PD risk factors. p62 (SQST-1) is an autophagy receptor protein that recognizes and targets proteins to autophagy and being bound to the target p62 is also degraded in the autophagosome-lysosome degradation pathways. Therefore, increased level of p62 signals dysfunction of the lysosomal degradation pathway. I have used Western-blotting technique with *C. elegans* specific anti-p62 antibody (1:4000 dilution) to monitor p62 (SQST-1) protein level and mouse specific anti-Actin antibody (1:5000 dilution) as loading control.

Results and Outcomes

This study has identified ASAH1 (*asah-1* in *C. elegans*) as a strong candidate risk factor for developing PD. A dopamine-dependent behavioural assay, called basal slowing, has been performed on 11 deletion mutant worm strains of lysosomal genes along with the wild-type (N2(WT)) and *cat-2* mutant strains. *cat-2* mutants do not express dopamine as they lack tyrosine-hydroxylase, an enzyme involved in dopamine synthesis (Table 1). Wild-type worms (WT) decrease their speed when reaching food (bacteria) on the maintenance plates as food acts as mechanical signal that is sensed by dopaminergic neurons in the worms. The mean speed decreased in WT worms with 49.16% while the *cat-2* mutant showed no basal slowing response (negative control). *ser-1* mutant lacking serotonin neurotransmitter have normal basal slowing response (positive control). Interestingly, it has been found that *asah-1* knockout mutant worms showed a severely impaired slowing response, indicating that this gene is important for dopamine-driven behaviours even at an early adult stage, and therefore its human orthologue ASAH1 could be implicated in PD. *asp-4* knockouts show a 75.24% average decrease in speed, which is peculiar as it is expected that lysosomal knockouts would hinder this response. More testing would be required to determine the nature that this knockout has on

Human gene	<i>C. elegans</i> gene	knockout mutant
GBA	F11E6.1 (<i>gba-3</i>)	F11E6.1(gk3287)
ATP13A2	W08D2.5 (<i>catp-6</i>)	W08D2.5(ok3473)
NAGLU	K09E4.4	K09E4.4(gk161202)
GUSB	Y105E8B.9	Y105E8B.9(ok3031)
SLC17A5	C38C10.2 (<i>slc-17.2</i>)	<i>slc-17.2</i> (gk821665)
CTSD	R12H7.2 (<i>asp-4</i>)	<i>asp-4</i> (ok2693)
ASAH1	K11D2.2 (<i>asah-1</i>)	<i>asah-1</i> (gk738376)
	F27E5.1 (<i>asah-2</i>)	F27E5.1(ok564)
SCARB2	Y49E10.20 (<i>scav-3</i>)	Y49E10.20(ok1286)
	Y76A2B.6 (<i>scav-2</i>)	Y76A2B.6(ok877)
ATP6AP2	T14B4.3	-
	R03E1.2 (<i>vha-20</i>)	-
SMPD1	ZK455.4 (<i>asm-2</i>)	<i>asm-2</i> (gk293929)
	W03G1.7 (<i>asm-3</i>)	<i>asm-3</i> (ok1744)
	B0252.2 (<i>asm-1</i>)	<i>asm-1</i> (gk832037)
GALC	C29E4.10	C29E4.10(ok2752)

Table 1. List of genes for the mutants of which have been investigated for dopaminergic and lysosomal function in this study.

Tom Trainer

Supervisors: Dr Eva Kevei and Dr Patrick Lewis

other neuronal systems that might cause this response. The *lrrk-1* mutant used in this study has increased kinase activity, which mutation in the human LRRK2 orthologue is associated with PD. In this assay, which was performed in adult, but young worms (day 1 of reproductive maturity) *lrrk-1* mutation did not show impaired basal slowing response which is in agreement of previous observations, suggesting an age-dependent loss of dopaminergic function in this genetic PD model. Future experiments will include the analysis of this behavioural response in aged worms as many risk factors contribute to development of PD in old age.

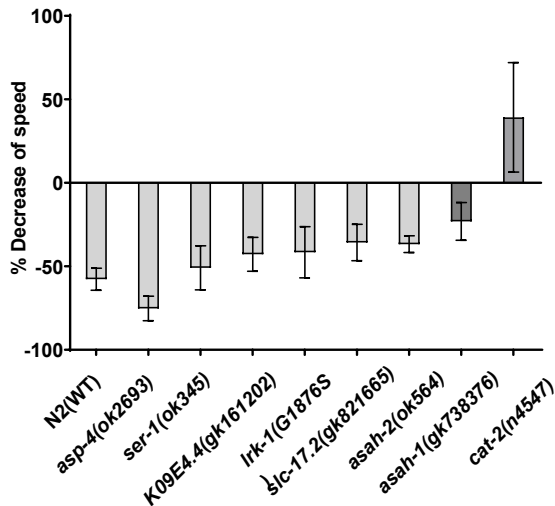


Figure 1. Basal slowing response in the mutant worm strains. Graphs shows mean change (difference of mean with +SEM) in crawling speed of worms on media without food and with food at the early stage of reproductive adulthood (day 1 adult).

Western blot analysis of p62 protein levels in the knockout mutant strains have showed increased levels of p62 autophagy receptor protein in most *C. elegans* mutant worms examined (Figure 2), indicating that lysosomal degradation is impaired even in basal conditions upon deletion of these genes. This observation has suggested the the selected lysosomal gene orthologues of PD risk factor candidates indeed are involved in lysosomal clearing mechanisms of *C. elegans*. It has been noted that deletion of these genes caused abnormal growth, with delayed development in most knockout mutant strains

analysed, which limited this investigation to the use of then strains shown on Figure 2. The strongest accumulation of p62 is observed in *gba-3*, *catp-6* and *asm-2* knockout mutants. Both GBA and ATP13A2 are established risk factors for PD, while SMPD1 (*asm-2* orthologue) is a novel candidate risk factor

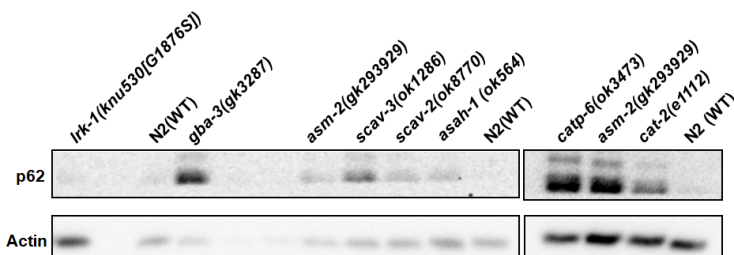


Figure 2. Western blot analysis of p62 protein levels. p62 protein has been detected in early adulthood (same day as basal slowing assay performed, day 1 adulthood) under basal conditions.

Future directions:

Due to observed developmental delay and growth defects in multiple mutant worm strains some of the assays have been limited to the use of a subgroup of lysosomal mutants. The planned lysosome visualization by microscopy has not been performed due to the same limitation, as growing and maintenance of these mutant strains took more time learn. Experiments in the host lab is now underway to analyse lysosome structure, distribution and function via fluorescent microscopy. Furthermore, the investigation of the selected lysosomal risk factors for their involvement in age-dependent disease pathology is planned. The next step of this research will involve the visualisation of dopaminergic neurodegeneration upon RNAi depletion of those genes which show defective dopamine-behaviour, including the *asah-1* candidate.

Value of the studentship:

Working in this lab has been one of the most valuable learning experiences in research I have ever received, and I believe it has given me a great advantage on further projects I may choose to undertake. I have learned not only molecular biology techniques, but management and organisational skills with handling my large number of worm strains, large amounts of data analysis and communication skills within a group of scientific peers. I have already begun applying for PhD programmes as a result of the enthusiasm for research these two months have given me. This project will contribute to future projects in the host lab in investigating oligogenic inheritance of PD. Lysosomal genes are in the centre of attention, as deep genome analysis of large PD patient cohorts indicated that Mendelian inherited PD mutations are often associated with mutations in lysosomal genes such as ATP13A2 or GBA. Therefore this study strongly contributed to the development of *C. elegans* models of oligogenic PD inheritance.



Imaging the mitochondrial TIM lateral sort complex by electron microscopy

Student: Cassie Hopton, Supervisors: Dan Watkins; Ian Collinson, University of Bristol.

Introduction

99% of mitochondrial proteins are produced within the cytosol and imported into mitochondria via one of five import pathways. One such pathway involves the outer membrane (TOM) and inner membrane (TIM) translocases. Cytosolic proteins containing a cleavable amino acid presequence are recognised by TOM and imported via the TOM channel into the intermembrane space. Presequence proteins are then bound by the TIM receptor TIM50 which activates the transmembrane TIM channel, TIM23, within the inner membrane that may mediate presequence protein sorting to the matrix or lateral insertion into the inner membrane¹.

Ten subunits form a complex around the TIM23 channel, the TIM23 complex, with subunits TIM50, TIM23 and TIM17 forming the core TIM complex. While this is known, no high-resolution structures of the complex currently exist. Subsequently, the functionality of each subunit is still not well defined. TIM17 is homologous in structure to TIM23 and interacts with the channel - it has shown to regulate TIM23 voltage gating², but the precise function of this subunit is not clear. Subunit Mgr2 also interacts closely with the TIM23 channel and has shown to regulate lateral insertion³ as well as bind TIM21 to TIM23⁴, and likewise TIM21 is also believed to facilitate lateral insertion by mediating an association between the TIM23 complex and proton-pumping respiratory chain complexes. However, precise functionalities of both subunits are not yet reported. Defects in import may affect homeostasis and metabolism; given that human TIM17 and TIM50 have been implicated in breast cancer⁵ and deletion of TIM23 in mice has shown to be fatal⁶, structural and functional knowledge of the TIM23 complex is key to understanding mitochondrial-mediated disease development and treatment.

Project aims

My project aimed to clone *mgr2* into a plasmid for transformation into yeast along with previously developed plasmids containing *tim50/tim21* and *tim23/tim17*. Yeast transformed with core TIM (TIM50, TIM23 and TIM21) (T1) and core TIM with TIM21 (T2) were established prior to my arrival, while I aimed to transform competent yeast cells with core TIM, TIM21 and Mgr2 (T3). It was then my aim to stimulate protein overexpression of all three forms of complexes, purify the proteins and image the resulting complexes by transmission electron microscopy (TEM).

Methods

Cloning and isolation of *mgr2*. *mgr2* was yielded by restriction digest and cloned into the pBEVY-GL plasmid with ampicillin resistance by T4 DNA ligase. Competent α -select *E. coli* cells were transformed with the recombinant pBEVY-GL-*mgr2* vector and incubated for 37 °C/200 RPM/1 hour. Cells were grown selectively on LB agar with ampicillin at 37 °C. Selected colonies were cultured in 2×YT media and pBEVY-GL-*mgr2* isolated using the QIAprep Spin Miniprep Kit (Qiagen) according to the manufacturer's protocol, with the following exceptions: (i) 750 μ L PB buffer used; (ii) two washes performed with PE buffer. pBEVY-GL-*mgr2* concentrations were determined by Nanodrop (Denovix).

Transformation of competent yeast with T3 complex. TE/LiAc and plate mix solutions were prepared using 10 × Tris-EDTA and 1 M lithium acetate added with sterilised water or 50% PEG 3000, respectively. YPH499 yeast were made competent and suspended in TE/LiAc supplemented with plate mix, boiled salmon testes DNA (Sigma, D9156) and 1 μ g pBEVY-GU-*tim23/tim17*, pBEVY-GT-*tim50/tim21* and pBEVY-GL-*mgr2* recombinant plasmids encoding uracil (U), tryptophan (T), and leucine (L), respectively. Cells were incubated at 30 °C/800 RPM/30 minutes followed by a 15-minute incubation at 42 °C, pelleted and resuspended in 2×YPD and incubated at 30 °C/200 RPM/2-3 hours. Following sufficient recovery, cells were plated on agar with 20% glucose, T, U and L drop-out and incubated at 30 °C for two days.

Overexpression of TIM complexes. Precultures of nitrogen base media, amino acid supplements with the required drop-out, glucose and 1 × penicillin and streptomycin were inoculated with yeast colonies transformed with either T1, T2 or T3. Cultures were incubated overnight at 30 °C/200 RPM. Large-scale 10 L cultures containing the aforementioned components in addition to 50% glycerol were inoculated with yeast cultures to give an OD of 0.15 and incubated at 30 °C/200 RPM overnight. At OD 2.0, expression was induced with 0.4% galactose for three hours.

Isolation of mitochondria and purification of TIM complexes. Mitochondria were isolated as described by Gregg *et al*⁷, with alterations: 200 RPM utilised for incubation; incubation with zymolyase for 40 minutes; low- and high-speed centrifugation at 1500 and 20,000 RCF for 10 minutes, respectively; pellets after homogenisation resuspended in sorbitol/mannitol buffer. Mitochondria were homogenised in Tris buffer. 5% Digitonin and cardiolipin were added to solubilise membrane-embedded TIM complexes. TIM23 was N-terminally 6×His-tagged and complexes purified by nickel affinity chromatography using His analog imidazole. Desired fractions were pooled and underwent broad-ranged Superose 6 size exclusion chromatography (SEC) followed by narrow-ranged Superdex 200 SEC if necessary.

Results

Cloning, isolation and subsequent transformation and overexpression of *mgr2* into yeast along with two additional plasmids was successful as shown by elution of all five proteins, including Mgr2 in the loading well (LW) at 12 kDa (Fig. 1B). Likewise, yeast *tim23/tim17* and *tim50/tim21* overexpression was also successful as elution of these subunits is similarly exhibited in Fig. A and B at ~25, 17, 21 and 50 kDa, respectively. TIM23

elutes at a larger weight than 23 kDa however this is expected. Elution of TIM17 appears poor compared to the other subunits and Fig 1B shows unclear elution of all subunits, but presence was confirmed by western blot. Presence of Mgr2 will need to be assayed once the Collinson lab purchases a suitable antibody. SDS-PAGE shows elution of degraded TIM50 at 50 kDa but also an unknown protein below 37 kDa that indicate issues in purity. But, given these bands appear on both SDS-PAGE gels suggests a protein not yet characterised that is strongly interacting with TIM23. Comparison between the SDS-PAGE and western blots in Fig. 1A shows the desired T1 subunits eluted optimally in both purity and quantity between fractions 38-42. Western blot shows T3 subunits eluted optimally between fractions 23-27 (Fig 1B).

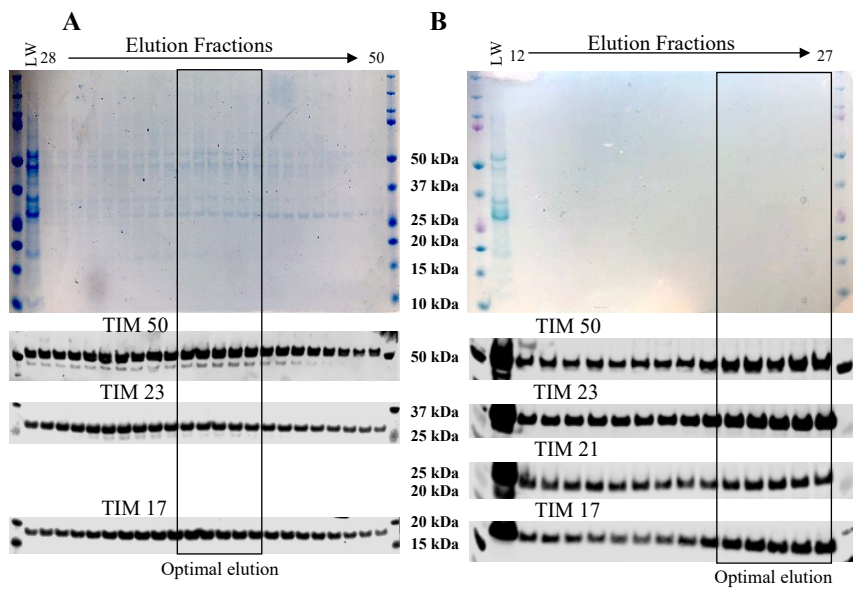


Figure 1 | (A) SDS-PAGE (top) of fractions from final SEC and western blots (bottom) of fraction samples labelled with fluorescent secondary antibody. Both show successful elution of TIM50, TIM23 and TIM17. Fractions with optimal elution are indicated. (B) SDS-PAGE and western blot showing elution of core TIM as in (A) but with Mgr2 and 21 also. T2 analysis has been omitted for clarity; the TIM21 band clarity was poor as in Fig. 1B but presence confirmed by western blot.

Selected fractions were utilised for TEM analysis (Fig. 2). Imaging with TEM revealed that while not all grids were successful due to over- or under-staining; heterogeneous protein size; or physical defects in grids, those in Fig. 2 yielded homogenous protein sizes and adequate protein distribution, in particular Fig. 2C. Protein distribution could be improved with higher dilutions of fractions. These qualities are necessary for single particle analysis as this process involves automatic collation and averaging of the protein complexes within the micrographs to create a single structure that is representative of all the purified T1, T2 or T3 complexes collected on the grid. The complexes prepared are therefore suitable for further analysis and the outcome of the project has been a success.

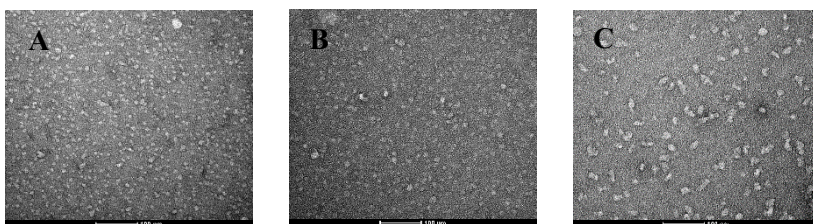


Figure 2 | TEM analysis of complexes (A) T1, (B) T2 and (C) T3. Optimal fractions were diluted 1/6, applied to glow-discharged carbon mesh grids and negatively stained with 2% uranyl acetate. Micrographs depict T1, T2 and T3 complexes at $\times 68,000$ imaged on a Tecnai Spirit microscope (Fei). Scale bar, 100 nm

Future directions

The TEM micrographs will undergo single particle analysis to produce a crude image of the complexes that will facilitate cryo-EM by the Collinson lab in the future. If successful, the high-resolution images will allow structural comparison between the subunits in varying states of complex assembly, which may elucidate greater Mgr2, TIM50, TIM17 and TIM21 functional insights. Such insights may not only direct future research in the Collinson lab but may also benefit our current understanding between TIM dysfunction and disease development; knowledge of TIM subunit functions may allow the development of appropriate treatments if such known functionalities become deficient.

Departure from original proposal

It was originally proposed I would be joining postdoc Will Allen in optimising the current techniques of trapping proteins in mitochondrial import for cryo-EM. However, I alternatively joined postdoc Dan Watkins and therefore the focus of the project changed to that reported here.

Value of studentship

The opportunity to experience a research lab has been invaluable. I have not only gained insights into life as a research scientist but have also produced tangible results that will hopefully contribute to the current understanding of the TIM complex. The variety of essential techniques and procedures I have now learned, from cloning and culturing to microscopy, will be applicable and advantageous whether as a PhD student or research scientist as I hope to study structural biology. While I was before apprehensive to enter the lab for my final year research project, I now feel confident as I have gained skills in experimental time management and enhanced my understanding of principles learned in my degree by using them in a practical setting. My experience has further inspired me to pursue a career in membrane protein research, and it has been a pleasure to work with everyone in the lab.

References

1. Wiedemann, N. and Pfanner, N. Mitochondrial machineries for protein import and assembly. *Annu. Rev. Biochem.* **86**, 685-714 (2017).
2. Martinez-Caballero, S. *et al.* Tim17p regulates the twin pore structure and voltage gating of the mitochondrial import complex TIM23. *J. Biol. Chem.* **282**, 3584-3593 (2007).
3. Schrempf, S.G. *et al.* Mgr2 functions as lateral gatekeeper for preprotein sorting in the mitochondrial inner membrane. *Mol. Cell.* **56**, 641-652 (2014).
4. Gebert, M. *et al.* Mgr2 promotes coupling of the mitochondrial presequence translocase to partner complexes. *J. Cell. Biol.* **197**, 595-604 (2012).
5. Salhab, M. *et al.* High TIMM17A expression is associated with adverse pathological and clinical outcomes in human breast cancer. *Breast Cancer.* **19**, 153-160 (2012).
6. Ahting, U. *et al.* Neurological phenotype and reduced lifespan in heterozygous Tim23 knockout mice, the first mouse model of defective mitochondrial import. *Biochim. Biophys. Acta.* **1787**, 371-376 (2009).
7. Gregg, C., Kyryakov, P. and Titorenko, V.I. Purification of mitochondria from yeast cells. *J. Vis. Exp.* **30**, 1417 (2009)

Investigating the control of bile duct cancer cell proliferation and migration by PRH/HHEX

Student: Esme Fowkes, Supervisor: Prof. Kevin Gaston, Cancer Biology, University of Nottingham

Background

PRH (proline rich homeodomain) is an essential transcription factor expressed in a range of human cell types in the embryo and in the adult, whose misregulation is involved in the development of cholangiocarcinoma (cancer of the bile duct) [1]. The PRH protein is expressed at high levels in cholangiocarcinoma cells in tissue samples from patients and weakly expressed or not expressed at all in normal bile duct epithelial cells. RNA sequencing and chromatin immunoprecipitation sequencing have identified putative PRH regulated genes in cholangiocarcinoma cells, many of which are involved in the control of cell proliferation and/or the control of cell migration.

Aims

The aim of the project was to investigate the role of PRH in cholangiocarcinoma cells by observing the behaviour of PRH knockdown cholangiocarcinoma cells *in vitro* and by measuring the expression levels of selected genes hypothesised to be regulated by PRH on the basis of RNA sequencing data.

Methods

Cell culture: CCLP1 SVC (scrambled vector control) cholangiocarcinoma cells stably expressing a control shRNA and CCLP1 PRH KD (PRH knockdown) cells stably expressing a PRH shRNA were cultured in Dulbecco's Modified Eagle's Medium - high glucose, 10% FBS and NEAA (non-essential amino acids) at 37°C and 5% CO₂.

RNA extraction and reverse transcription: Cells were harvested by centrifugation following 5 minutes incubation with trypsin/EDTA and RNA extracted from the cell pellets using a Qiagen RNeasy Mini Kit. RNA concentration was determined using a NanoDrop spectrophotometer and both samples were adjusted to the same concentration with RNase-free water. RNA was reverse transcribed to make cDNA using a QuantiNova Reverse Transcription Kit.

qPCR: Reagents were CCLP1 SVC and CCLP1 PRH KD cDNA samples, primer pairs, SYBR green and RNase-free water. Fluorescence level was quantified in real time using a Rotor Gene Q thermocycler. Primers were optimised using serially diluted CCLP1 cDNA samples (from the cell line in which higher expression is expected) to calculate the threshold value and to

evaluate whether primer dimers had formed. After optimisation, RT-qPCR was performed with CCLP1 SVC and CCLP1 PRH KD cDNA samples and a single primer pair alongside the cDNA samples and GAPDH primer pairs as a reference. cDNA level reflects the mRNA level and therefore the expression levels of genes regulated by PRH can be quantified.

EdU proliferation assay: Cell proliferation was measured using an Invitrogen Click-It EdU Microplate Assay following the manufacturer's protocol.

Migration assay: 80 x 10³ cells in 100 µl were seeded on ThinCert tissue culture inserts containing 100 µl 2% FBS DMEM and hydroxyurea to block cell proliferation (375 µM final concentration). Inserts were placed in wells containing 800 µl 10% FBS DMEM and hydroxyurea (250 µM final concentration) and incubated for 24 hours at 37°C in a humidified atmosphere. Inserts were transferred to wells containing calcein AM (5mM diluted 1:1000 in SFM) and incubated for 1 hour then transferred to wells containing trypsin. After 1 hour incubation the level of fluorescence was measured at 495 nm excitation and 515 nm emission.

Results

To confirm that PRH knockdown decreases cell proliferation and cell migration I performed EdU incorporation assays and Boyden chamber chemotaxis assays. EdU incorporation assays showed that CCLP1 SVC cells have a higher proliferation rate than CCLP1 PRH KD cells, suggesting that PRH has a role in increasing cell proliferation and therefore contributing to tumour growth (Fig.1). Three biological repeats each with three technical repeats showed the same trend. Cell migration assays showed that CCLP1 SVC cells have a higher migration rate, suggesting that PRH has a role in increasing cell migration (Fig.2). This could contribute to the metastasis of cholangiocarcinoma. The same trend was seen in three biological replicates each with two technical replicates.

RNA sequencing has identified several genes that are reciprocally differentially expressed in PRH KD cells and PRH over-expressing cells. 10 pairs of primers for genes hypothesised to be regulated by PRH were optimised for qPCR, however some produced primer dimers or did not amplify the correct product. Primer pairs for PPP1R14A and MGAT3 optimised well and following $\Delta\Delta C_t$ analysis showed higher expression levels of the genes in the CCLP1 PRH KD cell line suggesting PRH has a role in the transcriptional

repression of these genes (Fig.3 and Fig. 4). In three independent experiments PRH KD cells had higher expression levels for both genes. The combined results were not statistically significant, but the 3 biological repeats showed the same trend. PPP1R14A, a phosphatase, and MGAT3, a glycosyltransferase, have been shown to have tumour suppressor roles in colorectal cancers [2][3]. Therefore downregulation of these two genes by PRH may contribute to tumourigenesis in bile duct cells.

PRRX2 and LRRC4B primer optimisations produced good standard curves (Fig.5 and Fig.6) but did not amplify the correct product with SVC and PRH KD cDNA samples. It is possible that repeated freezing and thawing decreased the stability of these primers. New primers pairs could be investigated further.

Fig. 1 Edu proliferation assay

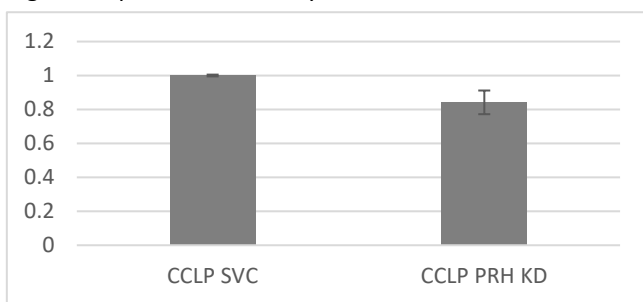


Fig. 2 Migration assay

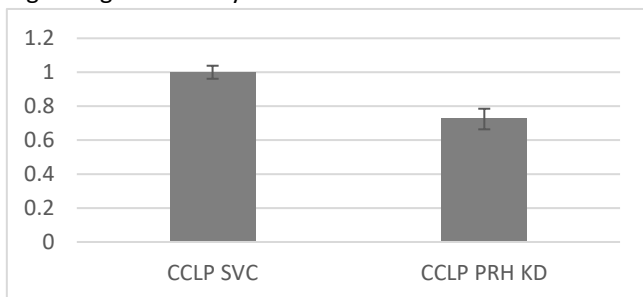


Fig. 3 RT-qPCR of MGAT3 and GAPDH

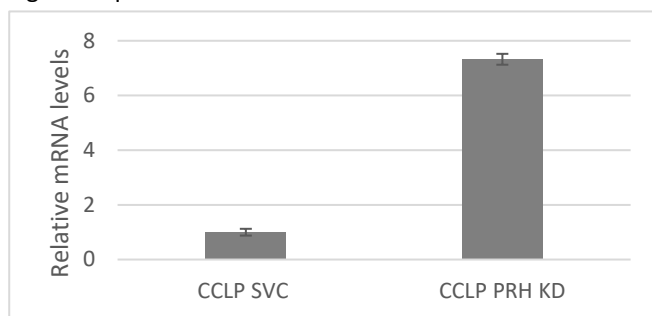


Fig. 4 RT-qPCR of PPP1R14A and GAPDH

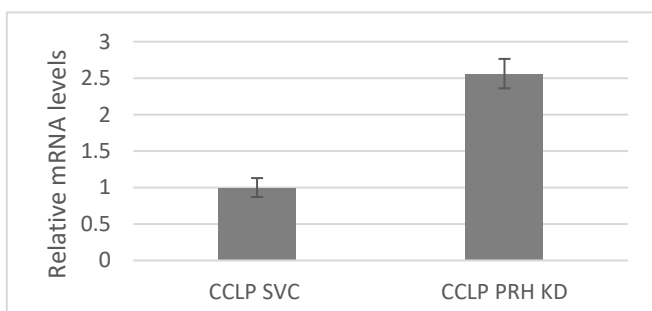
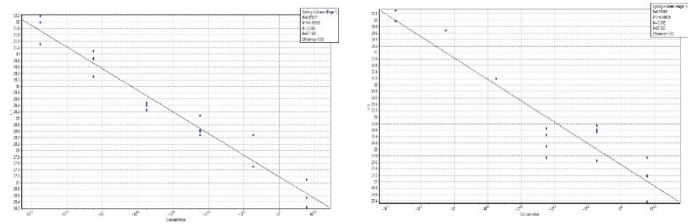


Fig. 5 (left) PRRX2 optimisation, efficiency = 0.98
Fig. 6 (right) LRRC4B optimisation, efficiency = 1.00



Further directions

For the primer pairs which dimerised, temperature gradient PCR followed by gel electrophoresis could be carried out to determine whether a different annealing temperature would prevent dimer formation. If unsuccessful, new primers could be designed which are less likely to dimerise. Western blotting could be used to assess changes in PPP1R14A and MGAT3 protein expression levels in these cells. Further characterisation of changes in the expression of these proteins in cholangiocarcinoma tissues could identify biomarkers to assist in diagnosis as well identify new drug targets for the treatment of the disease.

Deviations from original

The original plan included generating PRH knockdown and overexpression CCLP1 cell lines but instead previously prepared cell lines were used meaning there was time available to perform RT-qPCR which had not been included in the original plan.

Value of studentship

Student: I have greatly improved my practical lab skills and enjoyed building on what I have already learned about cancer and cell biology. I became much more confident in the use of laboratory equipment and working with cell culture, which will be extremely helpful for my further studies and career in science. I found being in an academic research lab an insightful and rewarding experience which has confirmed by ambition to pursue a PhD and career in biochemistry.

Supervisor: Esme has confirmed that PRH increases the proliferation and migration of cholangiocarcinoma cells in vitro. She has also shown for the first time that two genes reported to encode tumour suppressor proteins in colorectal cancers are repressed by PRH in cholangiocarcinoma cells. Future work will investigate the importance of these genes in cholangiocarcinoma cancer cells.

References

Gaston K, Tsitsilianos MA, Wadey K, Jayaraman PS. Misregulation of the proline rich homeodomain (PRH/HHEX) protein in cancer cells and its consequences for tumour growth and invasion. *Cell Biosci.* 2016;6:12. Published 2016 Feb 13. doi:10.1186/s13578-016-0077-7

APA Li, D., Guo, J., Wang, S., Zhu, L., & Shen, Z. (2017). Identification of novel methylated targets in colorectal cancer by microarray analysis and construction of co-expression network. *Oncology Letters*, 14, 2643-2648. doi:10.3892/ol.2017.6506

de Freitas Junior JC, Morgado-Díaz JA. The role of N-glycans in colorectal cancer progression: potential biomarkers and therapeutic applications. *Oncotarget.* 2016;7(15):19395–19413. doi:10.18632/oncotarget.6283

Studentship report - CRISPR-Cas generation of a blood cancer model cell line

Introduction

Acute myeloid leukemia (AML) is a form of malignant cancer characterized by unusual cell division leading to a rise in myeloid-progenitor cell population. AML is presently very challenging to treat, primarily due to a lack in understanding of the pathways that contribute to the disease's development, but also as the condition primarily affects elderly individuals resulting in many traditional treatment methods being unsuitable due to the extensive damage experienced by non-target tissue (Lowenberg *et al*, 1999).

This difficulty in finding suitable treatment methods has led to a key interest in researching the condition and pathways believed to be involved in its development, with research currently being carried out at the University of Worcester, where I was fortunate to experience my summer studentship. Here, the role of the Hedgehog signaling pathway in blood cancers is currently being investigated by Dr Amy Cherry.

Aim

To develop a blood cancer model cell line by the knockout of *Sufu*, the negative regulator of Hedgehog signaling.

Objectives

Culture the K562 blood cell line

Knockout the *Sufu* gene in a blood cell line using CRISPR-Cas technology.

Determine effectiveness of knockout by qPCR to measure *Sufu* expression.

Monitor Hedgehog pathway activity by qPCR to measure GLI-1 expression levels.

Methods

K562 cell culture

K562 cells are grown in a complete RPMI growth media, supplemented with 10% fetal bovine serum, 2 μ M glutathione and 4 μ M penicillin, within a T25 culture flask. Cells are passaged at 4-day increments by diluting 1 ml of previously cultured media and diluting with 4ml of sterile serum (approximately 10⁵ cells in 5ml of media).

Cell health is checked regularly under light microscopy, cell counts, and trypan blue exclusion assays carried out every two days. 200 μ l of growth media is taken from a culture, centrifuged at 300xRPM for 5 minutes, before the supernatant is aspirated and pellet resuspended in 200 μ l 1x PBS (stopping cell division). 20 μ l of this PBS solution is then added to a fresh centrifuge tube and diluted with 20 μ l trypan blue, prior to a 5-minute incubation period, after which 20 μ l may be added to a clean hemocytometer and a cell count for viability performed.

PCR Primer Optimization

Using *in silico* experiments, through the use of freeware packages SerialCloner and PCR Primer BLAST (NCBI, no date), PCR parameters including melting temperatures, product lengths and bind locations were predicted.

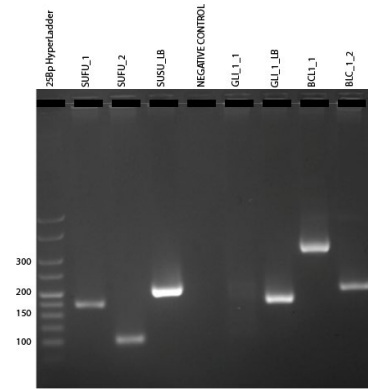
Using these predicted parameters, several touchdown PCRs were conducted with varying touchdown ranges and number of cycles. Ultimately, 10 cycles of PCR touchdown between 60 °C and 50 °C was seen to be most reliable, with standard PCR being conducted for another 25 cycles (95 °C for 45s, 50 °C for 45s, 72 °C for 60s) before a 5 minute extension period at 72 °C for 5 minutes. The products of these PCRs were then run on varying concentrations of agarose gel (1%, 2%, 2.5% and 3%) at differing times until an optimum image was reached, best showing expected banding of the PCR product.

Results

The aim of the project was to develop a blood cell line with the *Sufu* gene knocked out in order to promote Hedgehog signaling which would activate cell growth and proliferation creating a good model for the study of blood cancers. In order to monitor whether the *Sufu* gene had been successfully knocked out and to monitor the level of Hedgehog pathway activity in cells I needed to determine gene expression of *Sufu* itself, and *Gli1* and *Bcl2*, the products of Hedgehog pathway activation. This can be accomplished with qPCR

Optimization of PCR conditions for *Sufu*, *GLI1* and *Bcl2*

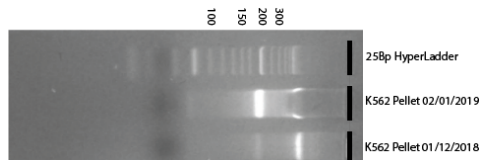
Before attempting qPCR, the effectiveness of primers was tested in a standard PCR reaction, using a plasmid expression vector as a DNA template. *SUFU_1*, *GLI_1_LB*, and *Bcl2* primer pairs were all seen to successfully amplify DNA resulting in clear single bands. Both remaining *Sufu* primers managed to amplify DNA however showed evidence of non-specific binding, demonstrated by a secondary band when imaged. Additionally, *GLI_1_1* failed to amplify DNA.



A touchdown protocol was followed due to the significant difference in melting temperatures predicted between samples through *in silico* testing and is intended to briefly amplify each primer at their optimum temperature so they may be more easily amplified at a lower suboptimal temperature. Whilst non-specific binding was observed in lanes containing *SUFU_2* and *SUFU_LB* with *GLI_1* failing to appear on the gel, clear bands were observed in *SUFU_1*, *GLI_1_LB*, *Bcl2* (lanes 1, 6, 7, 8 respectively). These primer pairs were then recommended for use within the qPCR protocol due to a lack of smearing and high fidelity when run on gels.

qPCR

The primers which were shown to be successful for standard PCR were used for qPCR reactions. K562 cells were cultured and growth and cell death monitored by cell counting with Trypan blue staining. Pellets of 1×10^6 cells were used for RNA extraction following a BioLine RNA Isolation Kit. RNA samples were extracted from two K562 cell pellets and examined on a 1% agarose gel.



Using RNA samples isolated from 01/12/2018 K562 Pellets, all primers were tested once again in a touchdown qPCR experiment. Primer pairs *SUFU_LB*, *GLI_1_LB* and both *Bcl1* primers were seen to amplify RNA resulting in a clear band when visualized on a 2%

agarose gel, and thus used in later qPCR experiments. Banding was also visible in negative controls leading to concerns of contamination. Due to the difficulties in optimizing the qPCR, the CRISPR reaction was not attempted at this time, whilst new reactants are sourced, and primers are designed.

Value of Studentship

During the studentship, I had numerous opportunities not otherwise presented under the course of my standard undergraduate studies. I was invited to attend the post graduate research conference used new procedures and equipment not otherwise available to me such as qPCR using the LightCycler 480-II. I was also trained in other techniques not related to the main project such as gel filtration chromatography using the Äkta pure.

Whilst summer provided a great opportunity to learn new techniques within the laboratory, the opportunity was most valuable in developing my ability to problem solve. This was best demonstrated as gel agarose repeatedly failed to visualize correctly, showing a high degree of smearing and without a ladder. Whilst in a traditional learning environment, this error would likely be overlooked and substituted with model data, being given the opportunity to investigate and resolve the matter through attempting new variations of the gel until the problem could be better understood. This opportunity has confirmed my desire to pursue a research career into the medical field as I believe this path provides a means to continue learning, even after completing higher education.

Deviations from Proposal

Initial plans for this studentship aimed to produce a *Sufu* knockout blood cell line, through CRISPR gene editing and to monitor cell growth and replication in relation to Hedgehog pathway activity. During the project, I cultured the cell line and began the development of the protocols for monitoring gene expression. However, since these were not fully optimized the gene knockout stage was not undertaken. However, whilst working in the research group, I also got experience in auxiliary research, such as purifying previously expressed proteins.

Further Use of Research

Optimized protocols from this studentship will directly aid in the further research expected to be conducted at the University of Worcester to aid in confirming CRISPR indel mutations when investigating the role of the Hedgehog pathway in blood cancer.

References

Aberger, F. et al. (2017) 'Acute myeloid leukemia – strategies and challenges for targeting oncogenic Hedgehog/GLI signaling', *Cell Communication and Signaling*, 15(1), p. 8. doi: 10.1186/s12964-017-0163-4.

Lowenberg, B., Downing, J. R. and Burnett, A. (1999) 'Acute Myeloid Leukemia', *New England Journal of Medicine*. Massachusetts Medical Society, 341(14), pp. 1051–1062. doi: 10.1056/NEJM199909303411407.

NCBI (no date) Basic Local Alignment Search Tool, U.S. National Library of Medicine. Available at: <https://blast.ncbi.nlm.nih.gov/Blast.cgi> (Accessed: 5 March 2018).

INVESTIGATION INTO THE POSSIBILITY OF A GLUCOSE-DEPENDENT SWITCH CONTROLLING UTERINE RECEPTIVITY THROUGH ALTERED PHOSPHORYLATION OF MYPT1

INTRODUCTION AND AIMS

The processes that occur during the receptive phase of the menstrual cycle to make the uterine epithelium receptive to embryo implantation are poorly defined. Current research suggests that loss of epithelial polarity in the uterine epithelium may be a necessary step for facilitating embryo implantation (Whitby et al., 2017). Indeed, in mice that maintain uterine epithelial polarity, the embryo fails to implant (Aplin and Ruane, 2017).

One possible mechanism by which uterine epithelial cells lose polarity is through dephosphorylation of contractile myosin light chain (pMLC) associated with zona-occludin 1 (ZO-1) at tight junctions. This results in a decrease in the effectiveness of the tight junctional barrier leading to decreased epithelial polarity. Myosin light chain phosphatase (MLCP) is responsible for dephosphorylating pMLC and includes the myosin-targeting subunit MYPT1 (Grassie et al., 2011). MYPT1 is subject to differential phosphorylation. When MYPT1 is phosphorylated at residues Thr-696 or Thr-853 by RhoA-associated kinase (ROCK), the activity of MLCP is inhibited and MLC remains phosphorylated (Qiao et al., 2014).

However, the mechanism through which MYPT1 is activated in uterine epithelial cells is unknown. It is known to be subject to O-linked GlcNAcylation carried out by the enzyme O-GlcNAc transferase (OGT). Recent research has shown that MYPT1 is more heavily GlcNAcylated in high glucose concentrations (unpublished). As a result, it has been suggested that both glucose level and GlcNAcylation state alter the phosphorylation of MYPT1 and thus its activity.

The notion of a glucose-dependent switch controlling uterine receptivity is particularly interesting when considering the application to assisted reproductive technology (ART). ART often fails when the embryo fails to implant in the uterus. By understanding the mechanisms underlying uterine receptivity, new techniques may be developed which improve the outcomes of ART.

This project aimed to determine whether the phosphorylation state of MYPT1 is under the control of a glucose-dependent switch.

MATERIALS AND METHODS

Cell Culture. Ishikawa cells were cultured in flasks in 5mM glucose Dulbecco's modified Eagle's medium (DMEM) supplemented with fetal bovine serum (FBS) and antibiotics. Cells were maintained at 37°C in an environment containing 5% CO₂.

The cells were then grown in one of four conditions: 5mM glucose, 5mM glucose with 0.1% v/v concentration of ROCK inhibitor Y27632, 17mM glucose with 0.1% v/v concentration of OGT inhibitor OSMI. The cells were incubated for 3 days at 37°C in an environment containing 5% CO₂.

Pull Down. Using beads coated in wheat-germ agglutinin, a pull-down was performed to enrich for GlcNAcylated proteins.

Western Blotting. Protein lysates were obtained from the cultured Ishikawa cells. Protein concentration was assayed and solutions were made up containing 50µg of protein. Lysates and pull-down samples were loaded into a 7% acrylamide SDS-PAGE gel alongside a pre-stained protein ladder (Cell Signalling Technology) and run in a 1X Tris-glycine electrophoresis buffer at 200V for 60 – 90 minutes. Proteins were then transferred to a nitrocellulose membrane for 2 hours at 200V. Membranes were blocked in PBS containing 4% w/v bovine serum albumin (BSA) at room temperature for one hour, then incubated with primary antibody for two hours. The membranes were then washed with PBS and incubated with secondary antibodies for one hour, washed and read using a Licor Scanner.

RESULTS

In the Ishikawa cell lysates, there was no significant difference ($P > 0.05$) between the amount of MYPT1 found in lysates from different environments. The amount of pMYPT (T853) in each sample was also found not to change between the samples (Fig. 1). There was no significant difference between any of the samples ($P > 0.05$).

Following the pull-down, the amount of GlcNAcylated MYPT1 that was phosphorylated at T853 was not found to significantly change between the different conditions ($P > 0.05$) (Fig.2).

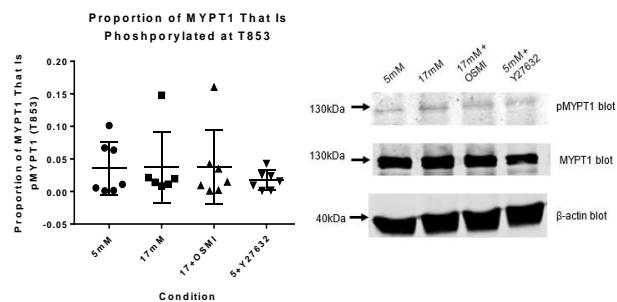


Figure 1: Results of Western blots showing the proportion of total MYPT1 that is phosphorylated at T853.

The proportion of MYPT1 that was phosphorylated was not significantly different between the different conditions ($P > 0.05$).

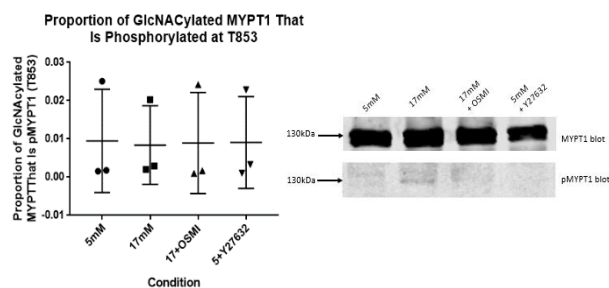


Figure 2: Results of Western blots showing the proportion of GlcNAcylated MYPT1 that is phosphorylated at T853.

The proportion of GlcNAcylated MYPT1 that was phosphorylated was not significantly different between the different conditions ($P > 0.05$).

DISCUSSION

In neither the Ishikawa cell lysates nor the lysates subjected to a GlcNAcylation pull-down, the level of MYPT1 phosphorylation at the residue T853 did not significantly change between the different glucose conditions. This suggests there is not a glucose-dependent switch that alters the phosphorylation state of MYPT1 in endometrial cell lines.

Alternatively, MYPT1 could be phosphorylated at another site that was not detected using the antibody I used. The state of this phosphorylation site may be altered in the different conditions.

FUTURE RESEARCH

Future research into determining whether there is a glucose-dependent switch that alters MYPT1 phosphorylation in endometrial cells would involve use of other antibodies to examine other potential phosphorylation sites in MYPT1. The antibodies I used were specific to the phosphorylation site at residue T853 and did not produce a particularly strong band when examined using the Licor scanner. As a result, the phosphorylation site at T853 may need to be further examined using another

antibody specific to T853-phosphorylated MYPT1 that produces a stronger band when used for Western blotting.

OUTCOME OF THE STUDENTSHIP

This studentship has proven to be invaluable to me as a student. It has given me the opportunity to develop my skills and confidence in the lab (something I am certain will be useful in my future studies and career) and also given me a chance to learn what life as an academic researcher is truly like. This experience will certainly help inform the decisions I must make regarding my next steps following the completion of my degree. I would like to thank the Biochemical Society for providing the funding that has allowed me to pursue this opportunity and the Maternal and Fetal Health Research Centre for giving me this opportunity.

SUPERVISOR'S COMMENTS

Eva worked hard, produced some good data and will present a poster at the Fertility 2020 meeting. Support appreciated. [John Aplin].

REFERENCES

- Aplin, J. D. & Ruane, P. T. (2017). 'Embryo-epithelium interactions during implantation at a glance', *Journal of Cell Science*, 130(1), p. 15.
- Grassie, M. E., Moffat, L. D., Walsh, M. P. & MacDonald, J. A. (2011). 'The myosin phosphatase targeting protein (MYPT) family: A regulated mechanism for achieving substrate specificity of the catalytic subunit of protein phosphatase type 1 δ ', *Archives of Biochemistry and Biophysics*, 510(2), pp. 147-159.
- Qiao, Y.-N., He, W.-Q., Chen, C.-P., Zhang, C.-H., Zhao, W., Wang, P., Zhang, L., Wu, Y.-Z., Yang, X., Peng, Y.-J., Gao, J.-M., Kamm, K. E., Stull, J. T. & Zhu, M.-S. (2014). 'Myosin phosphatase target subunit 1 (MYPT1) regulates the contraction and relaxation of vascular smooth muscle and maintains blood pressure', *The Journal of biological chemistry*, 289(32), pp. 22512-22523.
- Whitby, S., Salamonsen, L. A. & Evans, J. (2017). 'The Endometrial Polarity Paradox: Differential Regulation of Polarity Within Secretory-Phase Human Endometrium', *Endocrinology*, 159(1), pp. 506-518.

Introduction

House mice (*Mus musculus domesticus*) have an obligate proteinuria and excrete Major Urinary proteins (MUPs) in their urine. These protein pheromones elicit fascinating chemical signatures that have multiple roles in communication and recognition. The 'individual signatures' of these proteins in scent marks are significant for many behaviours of animals like the house mice such as mate discrimination, marking territory and much more. The specific area of research I have followed will help gain new understanding of major urinary proteins (MUPs) and their multiple roles including delayed release of pheromones, individuality identification and recognition. If better understood, it is possible that these proteins could suggest new control methods to reduce the negative impacts of rodent pests.

Aims of the project:

One of the challenges of using modern 'bottom up' proteomic approaches rely on digestion of the protein into peptides leading to disconnection of peptide fragments that could potentially carry unique post-translational modifications. The aim of the 8-week project was to develop a 'top down' approach to help the scientific community with the problem of analysing the natural complexity of MUPs obtained from house mice. The strong similarities between their amino acid sequences and the high level of polymorphism of MUPs impose a challenge in identifying and profiling these important proteins. By exploring ways in which the electrophoretic separation of MUPs using SDS-PAGE and Native-PAGE gels can be optimised, a method for recovering enough protein using 'top down' approaches can be formulated for profiling by mass spectrometry. This would allow the development of new approaches to identifying and characterising MUPs.

Description of the work carried out:

SDS-PAGE and Native-PAGE gels:

The first couple of weeks was an introduction to analysis of MUPs by Native and SDS-PAGE gels. This involved learning how to cast and run samples of MUPs from C56BL/6J mice with different methods of staining them for easier visualisation. Different concentrations of buffer and gradient gels were tested to explore how these proteins behave and to find optimal conditions for separation.

Protein extraction method:

A top down approach to protein extraction (communicated by Dr Takemori, Ehime University) featured rapid extraction in the absence of reducing agent, preserving structure of proteins in the gel. Time was spent on further optimisation to maximise the recovered volume of protein which was then re-analysed on Native and SDS-PAGE gels. In the final weeks a tryptic digest was performed on

a C57BL6/J MUP recovered from an SDS gel. The recovered peptides were profiled on the mass spectrometer, delivering information on the identity of MUPs in the sample.

Results and outcomes:

The protein extraction method revealed that it is possible to re-run recovered protein from a Native gel onto a repeat Native and SDS gels and produce bands. A surprising find was that single bands, when cut from a Native gel resulted in multiple bands on an SDS gel repeat (Figure 1). This is an indication that the separate bands seen were in fact a mixture of proteins. After failing to separate individual proteins contained in a single band it is clear that the separation of MUPs based on their Isoelectric point or their molecular weight alone will be challenging.

Original 15% Native

Repeat SDS

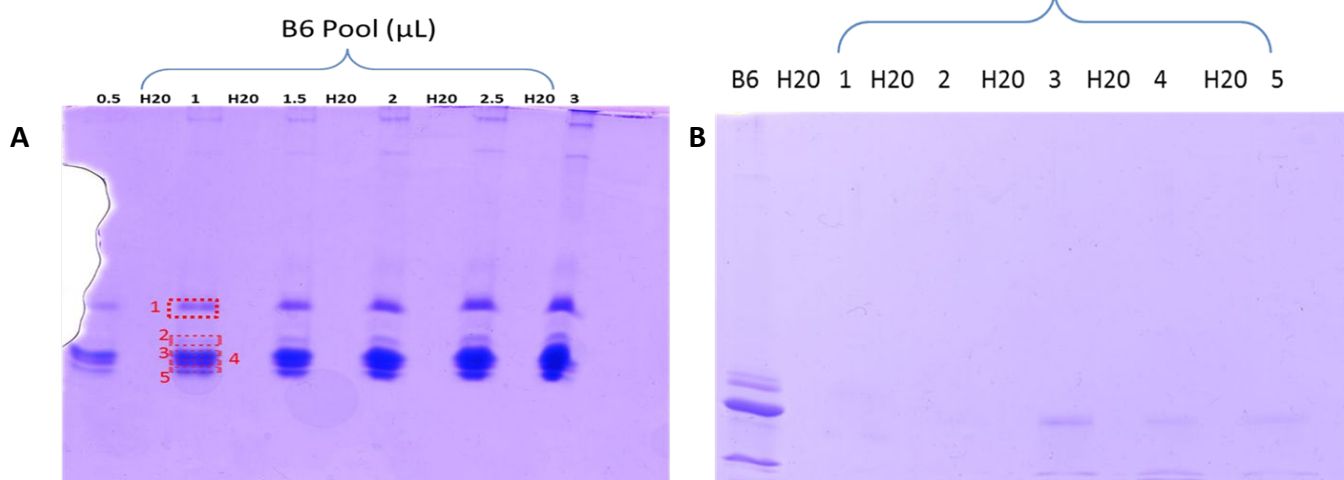


Fig 1: A. An image of B6 Pool ran on a 15% Native gel. The 5 Red boxes indicate the protein bands that were cut out. B. Using the optimised extraction method, these bands were re-run on a repeat SDS gel producing multiple bands.

Future directions in which the project can be taken:

The complexity of MUPs in the urine is challenging. The goal, of recovery of individual MUPs from urine, could be taken further by developing and improving the protein extraction protocol to increase volume of recovered protein. This may include improving technique used to concentrate the protein or the extraction solution used. This would result in a clearer visual of the bands on the repeat gels.

The molecular basis of hexokinase phosphorylation substrate specificity

Student: Joanne Mattocks; Supervisor: Dr Shamus Burns

Introduction

Hexokinases play a key role in carbohydrate metabolism, initiating the first step in glycolysis, by phosphorylating glucose to glucose 6-phosphate (G6P). Hexokinases may use either ATP, polyphosphate (PPi) or a combination of the two as substrates, but the choice of substrate is highly specific to the enzyme. Phosphorylation by ALL1371, a polyphosphate-dependent hexokinase discovered in *Anabaena*, is strictly dependent on the presence of magnesium, suggesting this plays a key role in the catalytic mechanism of the enzyme.

Aims

The aim of the project was to identify how polyphosphate binds to the ALL1371 enzyme as a substrate and how it is then metabolised to G6P, using ^{31}P NMR. This was to develop an understanding of how the active site of hexokinases are organised to obtain discrete specificity for ATP or PPi. The effects of varying concentrations of magnesium (Mg^{2+}) in the reaction was also investigated using both ^{31}P NMR and UV-Vis spectrophotometry.

Methods

Protein Expression and Purification: *E. coli* cells, containing ALL1371 or human HK4 plasmids, were selected for via antibiotic resistance screening. Expression and isolation of the enzymes was conducted using established methods.

NMR Assay: 0.7 ml samples containing 5 mM methylene diphosphonate (MDP) (as an internal reference), 50 mM glucose, 7.5 mM MgCl_2 , 1 mM NAD^+ , assay buffer (Davidson and Arion, 1987), 5 mM hexametaphosphate (HMP) (for ALL1371) or ATP (for human HK4) and 30 μl of the appropriate enzyme supernatant, were prepared. These were run at 301K in a Bruker 600MHz NMR. ^1H , ^{13}C and ^{31}P spectra were obtained in an interleaved fashion every 10 minutes for 360 minutes. Final spectra were obtained at 20 hours. A 0mM MgCl_2 sample was also run under the same conditions.

Magnesium dependency assay: A 96-well plate was prepared with each well containing 150 μl solution of 100mM glucose, 0, 1, 2, 4, 7.5, 15 or 30 mM MgCl_2 , assay buffer (see

above) and either 5 mM HMP (ALL1371) or 5 mM ATP (human HK4) and 5 μl enzyme (ALL1371 or human HK4). Controls included 0 mM glucose plus high and low concentrations of yeast HK with ATP assay buffer and 7.5mM MgCl_2 . The assay was run on a Spectrostar Nano UV-Vis spectrophotometer.

Results and Discussion

ALL1371 cleaves terminal phosphates until only triphosphate remains.

The NMR spectra show the metabolism of the polyphosphate chains and the subsequent formation of G6P.

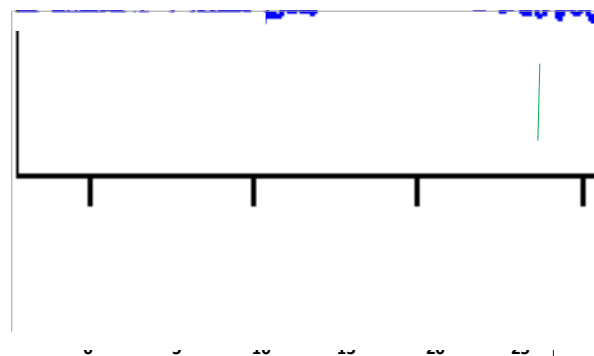


Fig 1: Stacked ^{31}P NMR spectra taken at the start, mid-point and end of the reaction. Initially, four β peaks are visible (-18 to -24 ppm) as well as the γ peak (-6 ppm). As the reaction progresses, G6P appears (~-2 ppm). At the end of the reaction a single β peak (-18 ppm) and γ peak (at a 1:2 ratio) are visible (-6 ppm). (Spectra at 180 and 0 min are shifted by -1 and -2 ppm respectively for clarity).

As the doublet at ~2 ppm appears, indicating the formation of G6P, the peaks visible in the ~-21 to -24 ppm region disappear, showing the metabolism of the polyphosphate chains (Fig. 1). These peaks represent the β regions of the polyphosphate chains; we hypothesise that different chain lengths appear at discrete shifts as shown (see Fig 1 - β_1 , 2, 3 and 4). This hypothesis now needs to be tested (see 'Future Work').

Furthermore, the peak at -6-7 ppm, which represents the terminal γ phosphates in all polyphosphate chains, decreases as a second discrete γ peak in the same region appears. We propose that this indicates phosphate is first cleaved from the ends of the chains, as the total

area of these peaks remains unchanged. Metabolism from the centre of the chain would cause a doubling of the $\gamma:\beta$ ratio, which is not observed.

We also propose that the peak at -18.5 ppm, which has a 1:2 ratio with the final γ peak is triphosphate. This represents another original finding – P₃i cannot be metabolised beyond triphosphate, possibly explaining why this enzyme cannot utilize ATP. Whether the triphosphate has an inhibitory effect on the enzyme is yet to be determined (see 'Future Work').

Continual replacement of shorter chain lengths accounts for metabolic 'lag'.

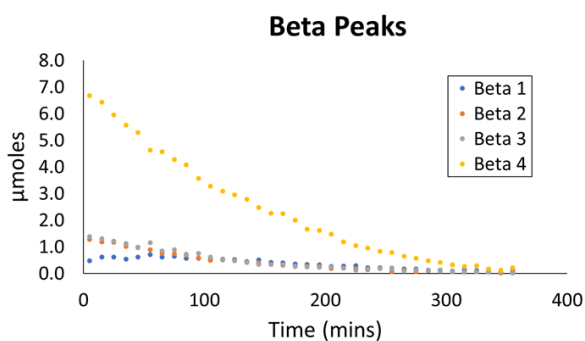


Fig. 2: Metabolism of each β peak throughout the experiment; a lag time of around 60 mins is observed in β peak 1.

Analysis of the individual β peaks (Fig. 2) suggests preferential utilization of longer chain lengths. However, the apparent pause in metabolism of the shorter chains might arise from the longer chains being shortened one phosphate at a time, increasing the abundance of shorter chains in the sample. Therefore, it may simply be the effect of replacement which gives the appearance of slower metabolism of the shorter chains – further kinetic analysis will help to determine the origin of this apparent lag.

Magnesium concentration has an impact on the activity of ALL1371.

The NMR assay spectra clearly show discrete P₃i peaks (see Fig. 1). However, at 0 mM MgCl₂, these individual peaks are no longer visible, instead merging and overlapping into one region (see Fig 3). When 7.5 mM magnesium was added to this sample, the peaks could be seen to separate, indicating changes in the surrounding environment of the phosphates, suggesting the complexing of the magnesium with the phosphate, resulting in structural changes.

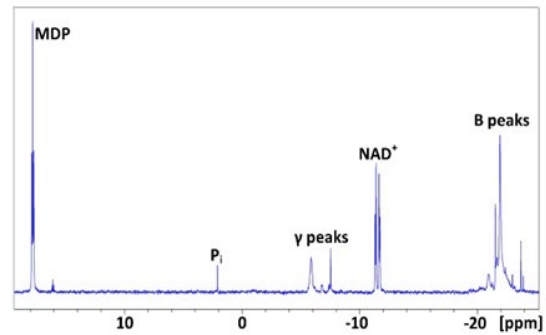


Fig 3: At 0mM Mg²⁺ the discrete peaks visible in the initial NMR spectra (see Fig. 1) are seen to merge together, indicating a change to the environment when magnesium cations are absent.

In addition, the UV-Vis assay indicates an optimal concentration of 7.5 mM Mg²⁺ in ALL1371, concordant with the discontinuous glucokinase assay method (Davidson & Arion, 1987), although concentrations as low as 2 mM do still facilitate some low-level enzymatic activity. At the upper end of the scale, 30 mM Mg²⁺ caused a decrease in activity but not cessation.

Future Work

Further work during my placement year will build on these findings, including: investigating the polyphosphate chain length hypothesis by running the ALL1371 NMR assay with known chain lengths; completing mathematical and kinetic analysis to determine the origin of the β peak 'lag' and identifying the unknown peak at around -21.5 ppm, which could be a useful internal reference.

These experiments will be repeated with the strictly polyphosphate-dependent mammalian glucokinase (PPGKm) (Ali, Wathes, Swali, Burns, & Burns, 2017) to establish whether the mammalian enzyme operates with a similar enzymatic mechanism.

Finally, further investigation into the effects of varying magnesium concentrations and the role of magnesium and other divalent cations in the catalytic mechanism will also be conducted.

Departures from Original Proposal

Due to time constraints, one aim of the original proposal which was not covered was the inhibition of ALL1371 by triphosphate and NTPs. This objective is to be covered during my research placement year and forms a further aim for future work.

Value of Studentship

Student:

Participating in the studentship has given me invaluable research experience, allowing me the opportunity to apply the techniques and knowledge obtained throughout my first two years of undergraduate study. I have also gained experience in new techniques, such as NMR, and developed skills in problem solving, experimental design and data analysis. The project has given me the confidence to develop my own hypotheses and has allowed me to experience first hand the thrill of discovering something completely new! This has confirmed my aspirations to pursue a PhD and a career in active research.

Supervisor:

The project was very successful and will lead to publication of the results in a peer-reviewed journal in 2020, once the kinetic work is complete, and taking the work to a biochemical society meeting. Several original, unexpected and exciting findings have been made that challenge the existing view of how the active site of hexokinases work. The project has allowed Jo the opportunity to work in a research lab, conduct a project and explain new findings. I believe it has convinced her to undertake a career in biochemical research and she is already thinking about PhDs.

Acknowledgements

Many thanks to Dr Shamus Burns for supporting my application and supervising the project, to Shaun Daly for sharing his expertise and day-to-day support in the lab, to Neil McLay for his NMR expertise and to the team of lab technicians for my lab induction and equipment training.

References

- Ali A. *et al* (2017). *Biochemistry and Biophysics Reports*, 12, 151–157.
- Davidson A. L. & Arion W. J. (1987). *Archives of Biochemistry and Biophysics*, 253 (1), 156–167.
- Klemke F. *et al* (2014). *Microbiology*, 160 (Pt 12), 2807–2819.
- Tanaka S. *et al* (2003). *Journal of Bacteriology*, 185 (18), 5654–5656.



Dissecting molecular mechanisms of astrocytic atrophy in Alzheimer's disease

Student: Jamie Austin
Supervisor: Dr Vicky Jones

Introduction

Astrocytes are one of the most abundant cells of the central nervous system and regulate the transmission of electrical impulses within the brain and play an essential role in maintaining brain homeostasis. They are essential for synaptic support and are therefore fundamental in memory formation and cognition. These roles are congruent upon the astrocytes achieving proper physical contact and connection with neurones and other astrocytes. The finding of abnormal astrocyte morphology in the earliest stages of Alzheimer's disease (AD; Figure 1) therefore presents an interesting new insight into how these cells might contribute to the disease process (Olabarria *et al.*, 2010, Jones *et al.*, 2017). Unfortunately, the cellular mechanisms that underly these findings remain poorly studied.

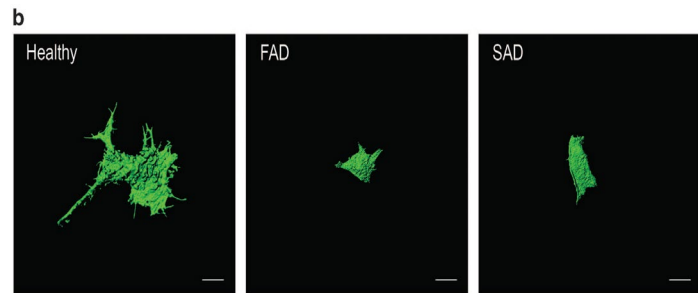


Figure 1. Exemplar 3D IsoSurface renders of astrocytes constructed from serial confocal z-stacks display clear differences in cell size and overall Morphology (Jones *et al.*, 2017)

The homologous Cas-protein family genes *CASS4* and *NEDD9* have previously been identified in genome-wide association studies (GWAS) as risk factors in the development of late-onset AD (Lambert *et al.*, 2013; Li *et al.*, 2007). It is predicted that the SNPs identified for each of these genes alter their protein expression levels and thus contribute to their pathological function²². Both *CASS4* and *NEDD9* are known to be involved in cytoskeletal rearrangements and stabilisation and extracellular matrix attachment, thus it is likely that they influence cellular morphology. To date, however, there are no studies investigating the mechanisms by which *CASS4* and *NEDD9* contribute to AD.

Emerging work by Ulzheimer *et al.* (2019) has demonstrated that RNAi-mediated knockdown of either *CASS4* or *NEDD9* induces astrocytic atrophy mimicking that reported in AD models. To exclude the possibility that these findings might represent off-target effects, rescue studies (where normal levels of each of the protein are restored, post-knockdown) are essential.

Aims

The aim of this internship project was to create RNAi-resistant expression vectors for *CASS4* and *NEDD9* using site-directed mutagenesis, which could be used for rescue experiments.

Method

Stbl3 *E. coli* Transformations:

In order to amplify the CASS4 and NEDD9 expression vectors, they were transformed into *Escherichia coli* (*E. coli*) which were grown prior to plasmid extraction. Briefly, 1 μ l of existing plasmid prep was added to 50 μ l of competent *E. coli* (ThermoFisher, Altricham, UK) and incubated on ice for 30 minutes. The *E. coli* cells were heat shocked at 42 °C for one minute and returned to ice for two minutes prior to the addition of 500 μ l SOC medium and incubation at 37°C for 1 hour in a shaking incubator. The recovered cells were plated to LB agar plates containing 50 μ g/ml kanamycin to permit selection of transformed bacterial cells. Colonies were picked to 10 ml LB broth containing 50 μ g/ml kanamycin and grown overnight prior to plasmid extraction using the Monarch plasmid miniprep kit (New England Biolabs) according to manufacturer's specifications.

Designing site-directed mutagenesis PCR primers:

RNAi-mediated knockdown of gene expression is mediated by the binding of a carefully-designed siRNA to a complementary region of the gene-of-interest's mRNA transcript. This leads to degradation of the transcript prior to translation. For rescue experiments, expression vectors must be created which are not susceptible to this degradation. This is achieved by altering the nucleotide sequence of the gene so that the siRNA no longer binds to it. Hence, mutagenic primers were designed to induce multiple silent mutations in the regions of the expression vectors for NEDD9 and CASS4 to which the siRNA binds. Primers were designed by eye and checked using the OligoEvaluator™ online calculator (Sigma-Aldrich, Gillingham, UK).

Site-directed mutagenesis

Site-directed mutagenesis was performed using the Phusion Site-Directed Mutagenesis kit (New England Biolabs, Hitchin, UK) according to manufacturer's protocol (a variation of PCR). Initial test reactions were performed using only the positive control and a negative (no polymerase) control to establish a working method. Later, experimental reactions were performed on 50 μ l reaction mixes containing; 50-150 ng DNA template (either CASS4 or NEDD9 expression vector), 1X HF buffer, 0.5 μ M forward and reverse primers, 200 μ M dNTPs, 0-5% DMSO and 1U Phusion polymerase. Cycling conditions were; initial denaturation of 30 s at 98 °C; 18 cycles of denaturation (10 s, 98 °C), annealing (15 s, temperatures as specified) and extension (5 mins, 72 °C); and a final extension of 72 °C for 10 minutes. Reactions were carried out in a Techne 3Prime thermocycler (Cole-Parmer, Stone, UK). Positive (kit-supplied) and negative (polymerase-free) control reactions were carried out simultaneously. Agarose gel electrophoresis (1% w/v) was then performed alongside a full-scale DNA ladder for comparison and the resulting gel imaged to determine the effectiveness of the mutagenesis reaction.

Results and Discussion

Amplification of NEDD9 and CASS4 expression vectors by transformation to *E. coli* were successful, yielding 275.6 ng/μl and 292.0 ng/μl of plasmid DNA, respectively, which could be used as templates for the subsequent mutagenesis reactions.

In the first stage of the internship it was necessary to develop a reliable and reproducible mutagenesis technique. A number of attempts to generate a positive PCR product however no bands were seen in the positive control lane (date not shown). A fresh batch of the mutagenesis kit was procured. Using this new kit, a clear band at the expected size of 10 kb was evident in the positive control lane (Figure 2, lane 3) indicating that the issue had been down to a defective kit component, most likely the polymerase. The negative control (lane 2) revealed no bands, suggesting that there was no contamination of the reaction components.

The mutagenesis reactions proper were initially attempted using 150ng of each of the DNA templates however this resulted in the template appearing too strongly in the gel electrophoresis image, potentially obscuring visualisation of the intended PCR product (data not shown). Subsequent mutageneses were therefore performed using 50 ng of the template DNA. Reactions performed with annealing temperatures between 45 °C and 55 °C at 2-degree intervals were undertaken for both CASS4 and NEDD9. In all cases, the positive control reaction was successful, and the negative control lane showed no contamination, although the template DNA was still faintly visible (Figure 3, lanes 3 and 4, respectively). Unfortunately, in all cases, the test reaction lane was indistinguishable from that of the negative control (for example, Figure 3, lane 2). Despite several attempts to alter the reaction conditions, including the addition of DMSO (to relax any primer secondary structure) and lengthening of the extension time, the mutagenesis reactions for both NEDD9 and CASS4 remained unsuccessful.

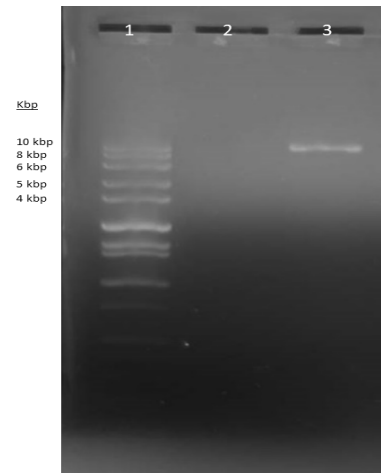


Figure 2. UV image of a positive control for the PCR method at 10kbp

- 1 – Full Scale DNA Ladder
- 2 – Negative Control
- 3 – Positive Control

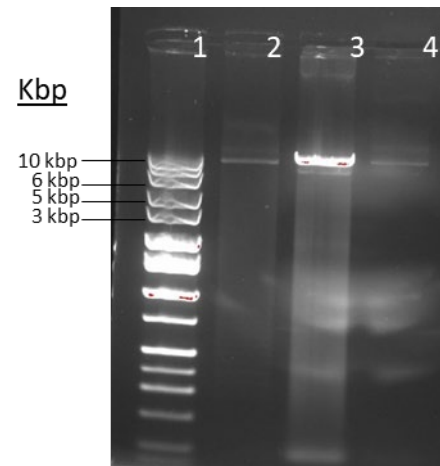


Figure 3. UV image of CASS4 PCR with 50ng of template, with a 6-minute extension time at 45°C

- 1 – Full Scale DNA Ladder
- 2 – Cass4 PCR
- 3 – Positive Control
- 4 – Negative Control

Future directions

Although the expression vectors were not produced during the period of this internship, the materials and procedures used will be recorded and can be used as a starting point allowing someone to take over the project. Specifically, the next logical step would be to redesign the primers to try again. Outside of this, a different polymerase enzyme could be trialed or, since the backbone vectors which CASS4 and NEDD9 were cloned into were quite large, the gene-of-interest could be sub-cloned into a smaller vector which might be more accessible for the mutagenesis reactions.

Value of studentship to me

The studentship has reinforced my passion and drive for a career in research. Whilst the experimental procedures did not always go to plan, I enjoyed the problem-solving and trouble-shooting that was required to overcome these problems and found the progress I made highly rewarding. After these 8 weeks the idea of a postgraduate position in a molecular biology-based lab seems highly attractive and I have gained a greater insight into the work carried out in professional research labs. I would like to thank the Biochemistry Society and my supervisor, Dr. Vicky Jones, and her lab for this opportunity that has been enjoyable, educational and invaluable.

Value of studentship to lab

Not every experiment works out how we plan. Yet every failed experiment tells us something new about what we are trying to achieve. Jamie's dedicated and methodical approach has given us valuable information on how to create these vectors going forward. We are in the process of designing a new mutagenesis approach which we hope will be successful and permit us to undertake essential rescue experiments.

References

Jones, V., Atkinson-Dell, R., Verkhatsky, A. and Mohamet, L. (2017). Aberrant iPSC-derived human astrocytes in Alzheimer's disease. *Cell Death & Disease*, 8(3).

Lambert, J., Ibrahim-Verbaas, C., Harold, D., Naj, A., Sims, R., Bellenguez, C., Jun, G., DeStefano, A., Bis, J., Beecham, G., Grenier-Boley, B., Russo, G., Thornton-Wells, T., Jones, N., Smith, A., Chouraki, V., et al. (2013). Meta-analysis of 74,046 individuals identifies 11 new susceptibility loci for Alzheimer's disease. *Nature Genetics*, 45(12), pp.1452-1458.

Li, Y., Grupe, A., Rowland, C., Holmans, P., Segurado, R., Abraham, R., Jones, L., Catanese, J., Ross, D., Mayo, K., Martinez, M., Hollingworth, P., Goate, A., Cairns, N., Racette, B., Perlmutter, J., O'Donovan, M., Morris, J., Brayne, C., Rubinsztein, D., Lovestone, S., Thal, L., Owen, M. and Williams, J. (2007). Evidence that common variation in NEDD9 is associated with susceptibility to late-onset Alzheimer's and Parkinson's disease. *Human Molecular Genetics*, 17(5), pp.759-767.

Olabarria, M., Noristani, H., Verkhatsky, A. and Rodríguez, J. (2010). Concomitant astroglial atrophy and astrogliosis in a triple transgenic animal model of Alzheimer's disease. *Glia*.

Introduction

The Smaug protein was initially studied in the fruit fly *Drosophila melanogaster*, where it has a well characterised function of suppressing the maternal *nanos* mRNA during the maternal to zygotic transition. SMAUG1 is the human homolog of the Smaug gene and is the focus of this project. SMAUG1 has been implicated in a number of diseases, and SMAUG1 mRNA is highly expressed in Alzheimer's disease brain samples¹. Overexpression gives a protective effect in a fly model of myotonic dystrophy type 1 and cultured human myoblasts². SMAUG1 is involved in the deadenylation of mitochondrial mRNAs during oculopharyngeal muscular dystrophy³. SMAUG1 is also an interesting target for study because of its association with mRNA silencing foci^{4,5}. Vts1 (the Smaug homolog in yeast) forms prion like condensates and downregulates genes involved in carbohydrate metabolism⁶. It is not known what set of mRNAs SMAUG1 binds to in humans, and this is a clear goal for future research. The most efficient method to do this would be by using a technique called UV-crosslinking and analysis of cDNAs (CRAC). As a control for this technique, a RNA binding deficient mutant is needed. Therefore, the focus of this project was to generate an RNA-binding deficient mutant of SMAUG1 using a targeted site-directed mutagenesis approach. The sites and amino acid changes used are shown in Figure 1. Two sites within the RNA binding domain containing highly conserved electropositive amino acids were chosen. These electropositive residues were then mutated to alanine. In a previous study a substitutions of serine at the corresponding position impaired RNA binding in the fly homolog of SMAUG1⁷. Three different mutants were made, a site 1 mutant, a site 2 mutant, and a double mutant. RNA binding was assessed using a luciferase assay using a reporter containing three Smaug recognition elements in tandem. In the initial planning of this project, electromobility shift assays (EMSA) were proposed as a secondary test of RNA binding. This was not carried out due to time limitations and initial results from the luciferase assay.

Materials and methods:

Site directed mutagenesis

SMAUG1 mutants were generated using the New England Biolabs Q5 Site Directed Mutagenesis kit. To create the double mutant the plasmid pCMVHisTev2xFLAG-SMAUG1RBDsite2 was mutated using the site1 mutagenic primers. For the PCR step of this procedure 1ng of plasmid template was used. The PCR conditions were as the manufacturer recommended with an annealing temperature of 70C for 15s and an extension time of 2 min 30s. Colonies produced by this procedure were screened and verified by sequencing.

Calcium phosphate transfection of HEK 293 cells

A six well dish was seeded with 500,000 cells per well and incubated overnight at 37C with 5% CO₂. 2µg of plasmid DNA was transfected into each well using a standard calcium chloride transfection. Cells were incubated with this solution at 37C with 5% CO₂ for 6 hours. Following this the media and transfection solution was removed and replaced with fresh media. Cells were grown for 48 hours before harvesting.

SDS-PAGE and Western blotting

Cells were lysed with 50µl of ice cold lysis buffer containing 150mM NaCl, 50mM Tris pH8, and 1% NP-40. A 10% Acrylamide gel was run at 100v for two hours with 20µl of sample per well. The PVDF membrane was probed with anti-FLAG antibody overnight. The membrane then underwent 3x5min washes with TBST. Following this the membrane was incubated for 1 hour with an anti-mouse antibody conjugated with a green fluorophore. The blot was then imaged using an Odyssey imager from LI-COR biosciences.

Dual firefly renilla luciferase assay

Luciferase assays were performed by Dr Gary Loughran, UCC. The reporter plasmid used for this assay is pmirGLO Dual-Luciferase miRNA Target Expression Vector from Promega Corporation. This plasmid has three *nanos* Smaug recognition elements in tandem⁸ cloned into the 3'UTR of the firefly luciferase gene. A 96 well dish was seeded with 30,000 cells per well and transfected with 10ng of the reporter plasmid and 90ng of the respective SMAUG1 plasmid. The control was H₂O instead of a SMAUG1 plasmid. This assay was performed in triplicate. The result of this assay in relative luminescence units was calculated by dividing the firefly fluorescence signal by the renilla fluorescence signal.

Cloning SMAUG1 mutants into the pET24d vector

Each SMAUG1 mutant was cloned into the pET24d vector for protein expression and purification. To prepare cut vector for cloning pET24d-SMAUG1WT was cut with Nco1 and Xho1 and gel. PCR was performed using Thermo Scientific Phusion High-Fidelity DNA Polymerase. The PCR reactions were performed using the GC buffer with the following cycling conditions: initial denaturation 98C 30s, 25 cycles (denaturation 98C 10s, annealing 69.2C 30s, extension 72C 2min), final extension 72C 10min. Ligation was performed overnight at 12C with a vector to insert ratio of 3:1. Colonies were screened by miniprep and restriction digestion with Nco1 and Xho1. Recombinant DNAs will be fully verified by sequencing.

Protein purification

Each pET24d – SMAUG1 mutant was transformed into *E. coli* BL-21 (DE3) cells. These cells were grown in 100ml LB media with kanamycin at 37C until an OD₆₀₀ of 0.6 was reached. Cultures were induced with 1mM IPTG and 3% ethanol. Cultures were then incubated at 25C for 24

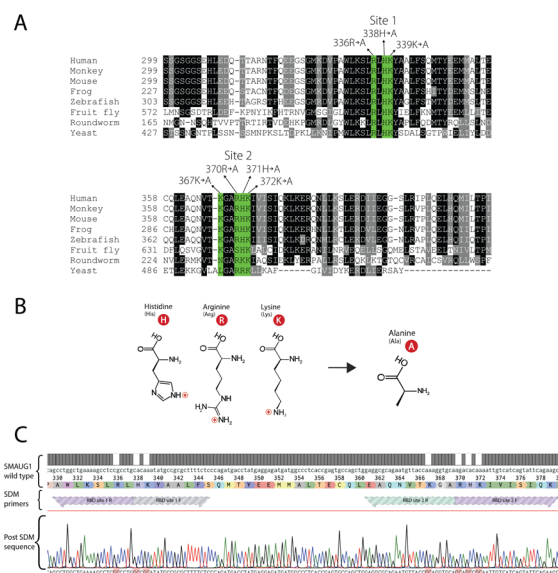


Figure 1. A Multiple sequence alignment showing part of the RNA binding domain. Conserved amino acids are shown in grey and black. Amino acids changed during this project are shown in green. **B** Structures of the mutated amino acids. **C** Sequencing alignment from Benchling showing successful construction of a double mutant.

Generation and Testing of an RNA Binding Deficient SMAUG1 Mutant

hours. Cells were harvested and cleared lysates were produced using standard procedures (Qiagen) with lysis buffer contain 0.3% Sarkosyl. Batch purification was carried out using HisPur Ni-NTA Resin from Thermo Fisher scientific. Samples were then run on a 10% acrylamide gel and stained with Coomassie blue stain.

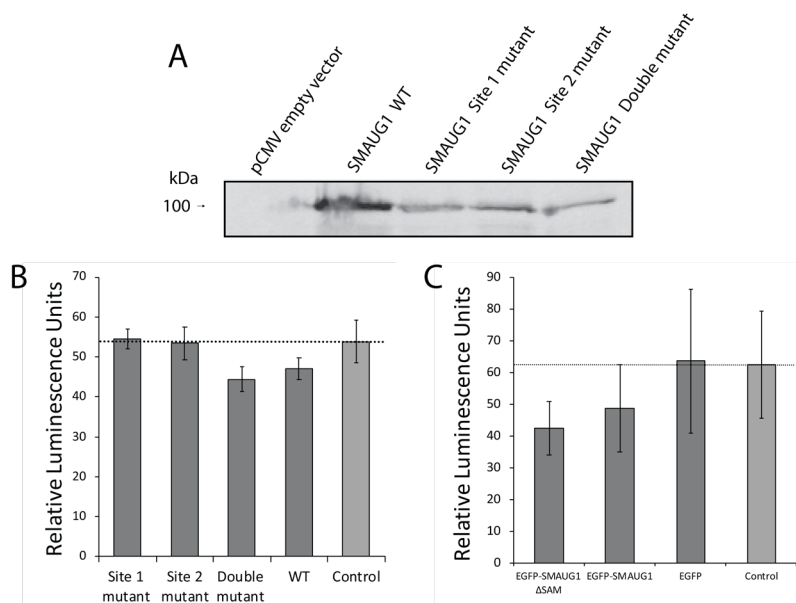


Figure 2. **A** Western blot showing successful expression of each SMAUG1 mutant in HEK293 cells. **B** Luciferase assay for testing the site 1, site 2, and double mutant. The wild type SMAUG1 protein shows repression of the reporter relative to the control. The site 1 and site 2 mutant show derepression of the reporter, producing results similar to the control. The double mutant does not behave as expected and instead shows more repression of the reporter than the wild type. **C** Luciferase assay for testing the SMAUG1-ΔSAM mutant. The wild type SMAUG1 protein shows repression of the reporter relative to the control. The SMAUG1-ΔSAM mutant does not behave as expected and instead shows more repression of the reporter than the wild type.

the wild type SMAUG1. This may suggest that other amino acids besides the ones mutated in this project are important for RNA binding. The mutations introduced by the double mutant may then change the confirmation of the protein in a way that maximises the interaction between these amino acids and the RNA. Following this unexpected result, a second luciferase assay was done using a mutant version of the SMAUG1 protein lacking the SAM domain that is required for RNA binding (Figure 2C). The results of this experiment were again unexpected as the SMAUG1-ΔSAM mutant repressed the reporter more than the wildtype protein. This may have been due to the SMAUG1-ΔSAM mutant being unstable when it is expressed in *E. coli* (Dean lab, unpublished). It's not known how the SMAUG1-ΔSAM mutant was able to bind to RNA better than the wild type protein. In conclusion the site 1 and site 2 mutant derepress the reporter and produce a result similar to the control. Originally the double mutant was expected to have the lowest interaction with the RNA and thus be the best to use as a control for further experiments. However the results here do not support this. Another mutant that may have been suitable for use as a control is the SMAUG1-ΔSAM construct, but this was not also supported by the results. Another concern is that the reporter used in this project only showed a small repression by the wildtype SMAUG1 protein. For future experiments a new reporter could be created that shows a more pronounced effect. Perhaps using the entire section of the *nanos* mRNA containing the SRE elements in the reporter not just the 3xSRE elements in tandem. The RNA binding ability of the site 1 and site 2 mutant could be checked using this reporter and then verified by EMSA. If these mutants still show a low affinity for RNA with the new reporter they could be used as controls, alternatively site directed mutagenesis could be carried out again to create a double mutant by mutating different amino acids. Protein purification carried out during this experiment indicate that additional steps are needed to ensure successful purification.

Value of the studentship to the student

I found my time in the lab this summer incredibly beneficial and enjoyable. I learned a lot of different techniques that will prove very useful to me in the future. I also gained an insight in to academic life and the different routes of postgraduate study like MSc and PhD programs. The entire experience boosted my confidence in myself and in my ambition to do postgraduate study. After this summer I am very excited to start my final year project at university and start applying for postgraduate courses.

to the supervisor

Having supervised many students for summer projects, I can honestly say that John's work made a substantial contribution to our ongoing research on SMAUG1. Based on his findings, we are now re-designing a luciferase reporter and being more conservative with our mutagenesis strategy for SMAUG1. This directly led to two, current final year projects, and his work points to the need for additional steps in SMAUG1 purification. John truly became a full member of the lab and had the opportunity to integrate with other research groups and present his work orally. The Biochemical Society support of undergraduate students is so important to me as a supervisor and provides a real, life-changing research experience to students, like John, at the beginning of their scientific careers.

References

1. Tan, M. G. et al. Genome wide profiling of altered gene expression in the neocortex of Alzheimer's disease. *J. Neurosci. Res.* **88**, 1157–1169 (2010).
2. de Haro, M. et al. Smaug/SAMD4A Restores Translational Activity of CUGBP1 and Suppresses CUG-Induced Myopathy. *PLoS Genet.* **9**, (2013).
3. Chartier, A. et al. Mitochondrial Dysfunction Reveals the Role of mRNA Poly(A) Tail Regulation in Oculopharyngeal Muscular Dystrophy Pathogenesis. *PLoS Genet.* **11**, (2015).
4. Baez, M. V. & Boccardo, G. L. Mammalian smaug is a translational repressor that forms cytoplasmic foci similar to stress granules. *J. Biol. Chem.* **280**, 43131–43140 (2005).
5. Baez, M. V. et al. Smaug1 mRNA-silencing foci respond to NMDA and modulate synapse formation. *J. Cell Biol.* **195**, 1141–1157 (2011).
6. Chakravarty, A. K., Smejkal, T., Itakura, A., Garcia, D. M. & Jarosz, D. F. A Non-Amyloid Prion Particle that Activates a Heritable Gene Expression Program. *SSRN Electron. J.* (2019, pre-print).
7. Green, J. B., Gardner, C. D., Wharton, R. P. & Aggarwal, A. K. RNA Recognition via the SAM Domain of Smaug. *Mol. Cell* **11**, 1537–1548 (2003).
8. Smbirt, C. A., Wilson, J. E., Kerr, K. & Macdonald, P. M. smaug protein represses translation of unlocalized nanos mRNA in the Drosophila embryo. *Genes Dev.* **10**, 2600–2609 (1996).

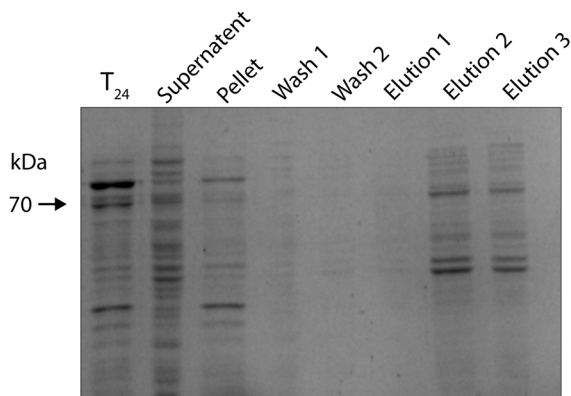


Figure 3. Coomassie gel showing a purification attempt of the SMAUG1 site 1 mutant. Purification of wild type SMAUG1 and other SMAUG1 mutants yielded similar results. This gel shows induction in the lane with the 24 hour post induction sample (T₂₄). The elution samples contained proteins other than SMAUG1, indicating the need for additional purification steps.

Results and conclusion

As can be seen in Figure 1 the double mutant was successfully constructed and verified by sequencing. Prior to the luciferase assay, expression of each SMAUG1 mutant in HEK293 cells was verified by transfection and Western blot (Figure 2A). The results of the first luciferase assay (Figure 2B) showed that the wild type SMAUG1 represses the reporter relative to the control. The site 1 mutant and the site 2 mutant successfully derepress the reporter and produce a similar result to the control. However the double mutant, which was expected to not to bind to the reporter, repressed the reporter more than

Leonard Lee

Supervised by: Dr. Alexander Zhyvoloup,
Jovana Baković and Prof. Ivan Gout

Studying the Effect of Human Islet Amyloid Polypeptide (hIAPP) on Cellular Reactive Oxygen Species (ROS) Production, Oxidative Stress and Protein CoAlation

Introduction

IAPP is a 37-residue peptide hormone co-secreted with insulin by pancreatic β -cells. It acts on the CNS, helping prevent post-prandial spikes in blood glucose concentration by slowing gastric emptying and promoting satiety [1]. IAPP has a high structural homology with amyloid beta, the main component of amyloid plaques found in Alzheimer's patients. Similar to amyloid beta, IAPP has a high propensity of form cytotoxic aggregates. These IAPP amyloid aggregates are often found in pancreatic islet β -cells of patients with Type II Diabetes Mellitus (T2DM), where the formation of amyloid fibrils is believed to contribute to its pathology by inducing cell membrane permeabilisation, endoplasmic reticulum stress, mitochondrial damage and cell death [2]. Studies with INS-1 β cells show that IAPP is internalised and accumulates in the mitochondria, perhaps causing mitochondrial damage and triggering oxidative stress [1]. Immunohistochemistry studies have also identified IAPP deposits in the brain tissue of Alzheimer's Disease (AD) patients, both with and without clinically apparent T2DM [3]. This may provide a partial explanation for the established epidemiological link between T2DM and AD [4], as IAPP deposits may have a similar cytotoxic effect in the brain as it does in the pancreatic islets.

Protein CoAlation is a recently discovered, novel post-translational modification, where the nucleophilic thiol of Coenzyme A forms mixed disulphides with sulfhydryl groups of cysteine residues [5]. In mammalian cells, CoAlation has been shown to be induced in response to metabolic and oxidative stress. Potential functions of protein CoAlation include the prevention of irreversible oxidation of sulfhydryl groups to sulfonic acid states and, thus, act as a protective mechanism against oxidative stress, or in redox signalling, fulfilling similar roles to S- glutathionylation [5].

Project Aims

The aim of this project was to investigate the cytotoxicity, oxidative stress and protein CoAlation induction in INS-1 β (insulinoma), SH-SY5Y (neuroblastoma), HEK293 and HEK293/Pank1 β (pantothenate kinase 1 β) cell lines by IAPP to further our understanding of the role of IAPP amyloidosis in the pathologies of T2DM and AD. The project also aims to assess the antioxidative potential of Coenzyme A and CoAlation in preventing IAPP induced cytotoxicity and oxidative stress, with the hope that this may eventually lead to clinically relevant breakthroughs in the understanding of these pathologies.

Methods

Cell Culture: INS-1 β cells were cultured in RPMI 1640 (+10% FBS, 1% Pen/Strep and β -mercaptoethanol). SH-SY5Y cells

were cultured in DMEM/Ham's F12 (+10% FBS and 1% P/S). HEK293 and HEK 293/Pank1 β cells were cultured in DMEM (+10% FBS and 1% P/S).

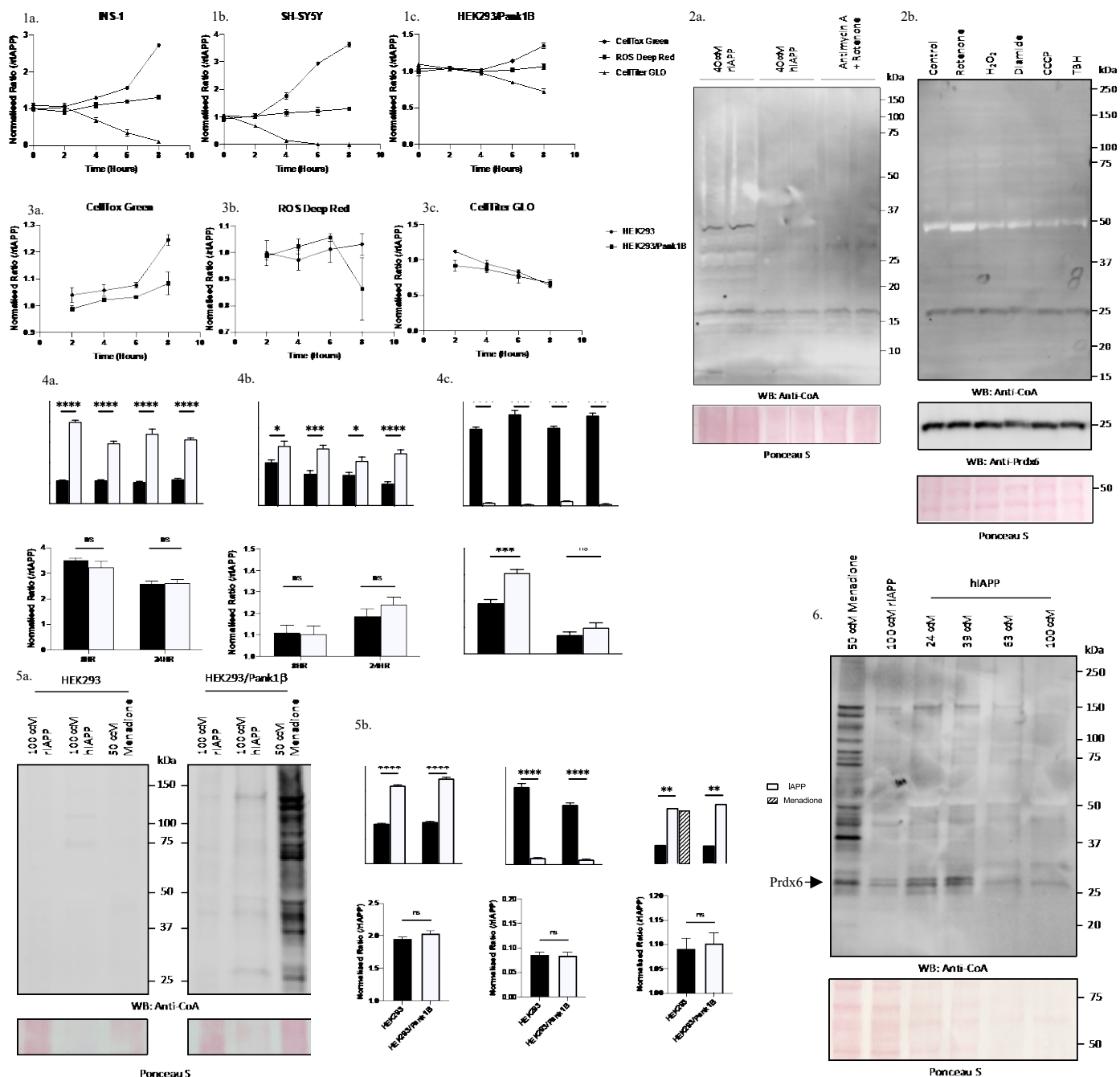
Cytotoxicity, ROS and Viability Assays: Cells were seeded onto half area 96-well plates at a density of 5,000-10,000 cells per well, 24-48 hours prior to treatment. Cells were treated by aspirating media and replacing media with fresh media dissolved with reagent (e.g. rIAPP, hIAPP, Menadione) + 0.1% CellTox™ Green Dye (Promega). Rat IAPP (rIAPP) is a non-amyloidogenic, non-cytotoxic variant of IAPP which was used as a negative control in all experiments throughout this project. Menadione was used as a positive ROS control. An equal volume of PBS + 0.1% ROS Deep Red Dye (Abcam) was added to each well 45 minutes prior to the end of the incubation period. At the end of the incubation period, fluorescence was measured at Ex/Em=650/675nm (ROS Deep Red) and Ex/Em=490/525nm (CellTox Green). After fluorescence measurements, an equal volume of CellTiter-GLO™ (Promega) was added to each well. A double orbital shaker induced cell lysis and luminescence was measured. Fluorescence and luminescence data is presented in the figures as raw values (RFU or RLU) or as normalised ratios against rIAPP control (hIAPP/rIAPP).

Treatment of SH-SY5Y Cells: Cells were seeded on 60 mm culture dishes at a density of 1 million cells per plate, 48 hours prior to treatment. Cells were treated with oxidising agents for 3 hours; rotenone (100nM), CCCP (10 μ M), TBH (200 μ M); or 30 min: H₂O₂ (500 μ M), Diamide (500 μ M). After treatment, the cells were collected by pressure washing and centrifugation (200 g for 5 min). The media was aspirated and cells were lysed in ice cold lysis buffer (homogenisation buffer including 1% Triton X-100, 100mM NEM and protease inhibitor cocktail (PIC)). Lysates were then centrifuged at 21000 g for 10 min at 4°C and the supernatant was analysed by Western Blot.

Treatment of INS-1 β Cells: Cells were seeded on 12 well plates at a density of ~400,000 cells per well, 24 hours prior to treatment. Cells were treated by aspirating media and replacing media with fresh media containing 40 μ M rIAPP, 40 μ M hIAPP or 1 μ M Antimycin A + Rotenone, incubating for 16 hours. After treatment, the cells were collected and lysed as described above.

Treatment of HEK293 and HEK293/Pank1 β : Cells were seeded on 12 well plates at a density of ~200,000 cells per well, 24 hours prior to treatment. Cells were treated by aspirating media and replacing media with fresh media containing 100 μ M rIAPP (non-cytotoxic negative control) or 24-100 μ M hIAPP and incubating for 24 hours or 50 μ M Menadione (30 mins). After treatment, the cells were collected and lysed as described above.

Western Blotting: Protein concentration of cell lysates were determined by BCA assay and samples containing ~10-20 μ g of protein were heated in non-reducing SDS loading buffer for 5 min at 99°C. Proteins were separated by SDS-PAGE on 4-20% gradient gels and transferred to Low Fluorescence PVDF membranes. Membranes were blocked by Odyssey blocking buffer and analysed using anti-CoA and/or anti-Prdx6 western blots. The bands were visualised by infra-red dye-conjugated secondary antibodies and an infra-red imaging system.



(1a) Cytotoxicity, Viability and ROS assays for INS-1 β treated with 40 μ M hIAPP for 0-8 hours ($N=1$); CellTox Green is a membrane impermeant dye which fluoresces green when bound to the DNA of cells with compromised membrane integrity, ROS Deep Red is a membrane permeant dye which fluoresces deep red when bound to ROS, such as superoxide; CellTiter-GLO is a luciferase-based luminescence assay which measures ATP content. (1b) Assays for SH-SY5Y treated with 40 μ M hIAPP for 0-8 hours ($N=1$) (1c) Assays for HEK293/Pank1 β Assays treated with 40 μ M hIAPP for 0-8 hours ($N=1$) (2a) Anti-CoA Western Blot of INS-1 β total cell lysates (TCLs) after treatment with 40 μ M rIAPP, 40 μ M hIAPP and 1 μ M Antimycin A + Rotenone for 16 hours ($N=1$) (2b) Anti-CoA and Anti-Prdx6 Western Blots of SH-SY5Y TCLs after treatment with a panel of agents to induce oxidative stress. ($N=3$) (3a-c) Cytotoxicity, Viability and ROS assays of HEK293 and HEK293/Pank1 β after 2-8 hours of 40 μ M hIAPP treatment ($N=2$) (4a-c) Cytotoxicity, Viability and ROS assays of HEK293 and HEK293/Pank1 β after 8-24 hours of 100 μ M hIAPP treatment ($N=2$) (5a) Anti-CoA Western Blot of HEK293 and HEK293/Pank1 β TCLs after treatment with 100 μ M rIAPP/hIAPP for 24 hours and 50 μ M Menadione for 45 min. ($N=2$) (5b) Parallel measurement of Cytotoxicity, Viability and ROS production in cells under the same conditions as in 5a. (6) Anti-CoA Western Blot of HEK293/Pank1 β TCLs after dose-course treatment of 24-100 μ M hIAPP ($N=1$)

Results and Discussion

INS-1 β is an insulinoma cell line derived from rat pancreatic β -cells commonly used in endocrinology studies because of their glucose concentration-dependent secretion of insulin. The assays for INS-1 β (Fig. 1a) show an acute toxicity to 40 μ M hIAPP and a significant production of ROS. Interestingly, SH-SY5Y cells are similarly sensitive to hIAPP at this concentration and significant ROS production is also detected (Fig. 1b). However, these two cells lines do not appear to show any protein CoAlation when treated with oxidising agents (Fig. 2a, 2b).

Only one CoAlated protein was detected in SH-SY5Y; Peroxiredoxin 6 (Prdx6) and this appeared to be constitutively CoAlated, even in the untreated control. As these are cancer cell lines, they are likely subject to the Warburg effect and are probably more dependent on aerobic glycolysis for ATP production than oxidative phosphorylation. As such, the TCA cycle is likely much less active and, therefore, these cells will have decreased concentrations of Coenzyme A, the essential substrate for protein CoAlation. This decreased concentration of CoA has previously been observed in other established and immortalised cell lines such as HEPG2, MEF and HEK293 [5].

HEK293/Pank1 β is a HEK293 derived cell line generated by the Gout lab which carries a stable transfection of the pantothenate kinase 1 β gene, the enzyme which catalyses the rate determining step of CoA biosynthesis. HEK293/Pank1 β cells show 6-8 fold increased concentration compared to HEK293, a concentration comparable to primary cells obtained from animal tissue [5] and are a better model for protein CoAlation studies. HEK293/Pank1 β cells showed a high resistance to hIAPP and comparatively little increase in cytotoxicity and drop in cell viability after 8 hours of 40 μ M treatment (Fig. 1c) and no significant increase in ROS production. Since HEK293/Pank1 β cells were known to undergo extensive protein CoAlation and exhibit elevated concentrations of CoA [5], it was speculated that CoA and CoAlation were having an antioxidant effect and conferring these cells with resistance against hIAPP induced cytotoxicity.

Experiments comparing the cytotoxicity and ROS production in HEK293 parental cell line (Fig. 3a, b, c) against the HEK293/Pank1 β cell line showed that the hypothesis described above can be rejected as no statistically significant differences between the two cell lines could be observed in any of the assays at any time points at 40 μ M hIAPP treatment. HEK293 appear as robust against hIAPP toxicity at 40 μ M as the HEK293/Pank1 β cell line. Significant cytotoxicity, reduced viability and ROS production were eventually induced in HEK293 and HEK293/Pank1 β cells at 100 μ M hIAPP after 8 and 24 hour treatment (Fig. 4a, b, c), although still no statistically significant difference could be detected between the two cell lines. The results of these experiments suggest that HEK293 cells have a high innate resistance to hIAPP cytotoxicity than INS-1 β or SH-SY5Y cells, but CoA overexpression appears to have no effect on these cells' susceptibility to hIAPP cytotoxicity and hIAPP induced oxidative stress.

Protein CoAlation does appear to be induced in HEK293/Pank1 β cells after 24 hour treatment of 100 μ M hIAPP (Fig. 5a). Although the band intensity of the 100 μ M hIAPP lane is not much greater than the rIAPP control, the protein content is much lower than in the rIAPP control, shown by the Ponceau stain. This was due to the increased membrane permeance induced by hIAPP toxicity and consequent leakage of proteins for analysis. Nevertheless, CoAlation can be detected even at these lower protein concentrations, showing CoAlation is induced in HEK293/Pank1 β cells by 100 μ M hIAPP. It's more difficult to compare the extent of protein CoAlation in the hIAPP treated cells compared to the 50 μ M menadione positive control due to the disparate protein loading. The combined data from Fig. 5a and 5b does suggest that protein CoAlation is mediated by the induction of oxidative stress. HEK293 shows no CoAlation due to the low levels of CoA (Fig. 5a), despite undergoing similar levels of oxidative stress (Fig. 5b).

A dose course experiment (Fig. 6) revealed that protein CoAlation appears to be induced in HEK293/Pank1 β cells by hIAPP concentrations as low as 24 μ M after 24 hours. This is somewhat surprising as significant cytotoxicity and ROS production were not measured at 40 μ M hIAPP (Fig. 1c, 3a-c), although these treatment periods only went up to 8 hours. The strongest CoAlation appears to be a protein with MW~25kDa, most likely Prdx6. CoAlation diminishes at higher hIAPP concentrations but this is most likely due to lower protein loading, evident by the reduced Ponceau staining. For some unknown reason, the BCA assay appears to give incorrectly high

protein concentration measurements of TCLs of cells treated with high concentrations of hIAPP, thwarting efforts to normalise protein loading for SDS-PAGE and resulting in protein underloading. I suspect soluble hIAPP oligomers are contributing to a large absorbance for these samples in the BCA.

Future Directions

It'd be interesting to further explore hIAPP cytotoxicity and hIAPP induced ROS production in INS-1 β and SH-SY5Y cells and its effect on protein CoAlation, as data from these cell lines would have more physiological relevance and clinical significance than studies in HEK293 cells. A transfection of pantotheonate kinase 1 β into these cell lines could increase CoA levels to physiological concentrations and we may detect protein CoAlation when stimulated by metabolic or oxidative stress. Studies could also be extended to primary neurones and pancreatic β cells. Primary cells, containing high concentrations of CoA, have previously been proven to be better models for protein CoAlation [5].

Deparatures from Original Proposal

The original proposal was '*Studying protein CoAlation and the antioxidant effect of coenzyme A in neuronal cells under oxidative and metabolic stress*'. The project deviated quite far from this original proposal as prior to the start of the studentship, Prof. Gout realised the opportunity for collaboration between the Gout lab and Prof. Dan Raleigh's lab which studies pancreatic islet amyloidosis. As such, the project was changed to study the effect of IAPP on oxidative stress and its link to protein CoAlation. Studies on metabolic stress was dropped and were focus was placed on oxidative stress. SH-SY5Y cells were still used as a model for neuronal cells, as outlined in the original proposal, but studies were extended to INS-1 β cells, a model of pancreatic islets, and HEK293/Pank1 β , a model cell line used to study protein CoAlation. Studies proposed on the BV2 (microglial) cell line were omitted.

Value of the Studentship

The studentship has proven to be a valuable experience and has allowed me to gain confidence in the lab to independently design, execute and interpret experiments with a critical scientific method. The studentship has also convinced me to pursue a PhD programme after completion of my Master's. The research that I started over the past months has opened the door to many more avenues of enquiry and started a collaborative effort between these two labs. I hope my work can be continued and it's possible that my data and figures will contribute to one of the lab's future publications.

References

- [1] Kiriya, Y., & Nochi, H. (2018). Role and Cytotoxicity of Amylin and Protection of Pancreatic Islet β -Cells from Amylin Cytotoxicity. *Cells*, 7(8), 95. doi:10.3390/cells7080095
- [2] Raleigh, D., Zhang, X., Hastoy, B., & Clark, A. (2017). The β -cell assassin: IAPP cytotoxicity. *Journal of Molecular Endocrinology*, 59(3), R121-R140. doi:10.1530/JME-17-0105
- [3] Jackson, K., Barisone, G. A., Diaz, E., Jin, L. -, DeCarli, C., & Despa, F. (2013). Amylin deposition in the brain: A second amyloid in alzheimer disease? *Annals of Neurology*, 74(4), 517-526. doi:10.1002/ana.23956
- [4] Janson, J., Laedtke, T., Parisi, J. E., O'Brien, P., Petersen, R. C., & Butler, P. C. (2004). Increased risk of type 2 diabetes in alzheimer disease. *Diabetes*, 53(2), 474-481. doi:10.2337/diabetes.53.2.474
- [5] Tsuchiya, Y., Peak-Chew, S. Y., Newell, C., Miller-Aidoo, S., Mangal, S., Zhyvoloup, A., . . . Gout, I. (2017). Protein CoAlation: A redox-regulated protein modification by coenzyme A in mammalian cells. *Biochemical Journal*, 474(14), 2489-2508. doi:10.1042/BCJ20170129

Imperial College London

The transition from White Light to Far-Red Light Photosynthesis in *C. thermalis*: Back into the Light

Supervisors: Prof Bill Rutherford and Dr. Stefania Viola

Introduction and Aims

Chroococcidiopsis thermalis PCC 7203 is a cyanobacterium capable of growth in either white or far-red light using chlorophyll f [1]. Far-red light growth involves production of special photosystems, where chlorophyll f is involved in primary photochemistry [2].

Understanding the processes occurring when transitioning between far-red light (FRL) and white light (WL) growth are of fundamental interest to the agriculture and biotechnological industries, as it may be possible to engineer crop plants and microalgae to be able to use more of the solar spectrum [3]. The transition involves the changeover of far-red light reaction centres and antennae to their chlorophyll a-containing variants. Preliminary experiments in the host lab indicate that this takes around a week to fully complete, however little else is known.

The aim of this project was to begin characterization of the transition process to obtain biochemical and physiological insights. The activities of photosystems I and II (PSI and PSII) were measured in either red light (RL) or far-red light over the course of the transition period to monitor their levels. Far-red PSII gives high thermoluminescence, 20 times more than WL-PSII [2], and this was monitored during the far-red to visible light transition. PSI does not give rise to thermoluminescence and thus must be monitored separately.

Materials and Methods

Growth and Culture Conditions: *C. thermalis* cultures were grown in BG11 medium in bubbling flasks, under 745nm far-red (near infra-red) light [2]. For transition experiments, cultures were moved to the visible light growth room at the start of the week. Every day 100ml of cells were taken from the culture and whole-cell spectra taken for chlorophyll measurements.

PSI and PSII Activity Measurements: Measurements were made on a Clark-type electrode with either red (665nm) or far-red (745nm) LEDs. Samples were equilibrated in the dark for 60 seconds before light was switched on. PSII measurements were made in the presence of the exogenous electron acceptor system, 2mM potassium ferricyanide and 1mM DCBQ (di-chlorobenzoquinone) to allow measurement of oxygen evolution. PSI activity was measured in the presence of 20 μ M DCMU (to inhibit PSII), the electron donor system, 5mM sodium ascorbate and 50 μ M DCPIP, and the electron acceptor 100 μ M methyl viologen to rapidly relay electrons to O₂. Thus PSI activity was measured as oxygen consumption. Cells were at 10 μ g/ml chlorophyll concentration for all measurements.

Thermoluminescence Experiments: Measurements were made on a thermoluminescence instrument built in-house by Sven de Causmaecker. Samples were at a concentration of 10 μ g/ml chlorophyll. A 532 nm flash was given at 253 K to dark-adapted samples, and then after a 30 second delay, the sample was heated from 253 to 353 K at a heating rate of 1 K/s, and light emission measured.

Results

Thermoluminescence signal decreased to a stable low level in \sim 3 days (figure 1a). This would suggest that almost all FRL PSII has been lost after this point. Figure 1b shows that the PSII activity measurements correlated well with the thermoluminescence experiments, showing almost total loss of activity by day 4.



Figure 1 - Transitioning *C. thermalis* cultures

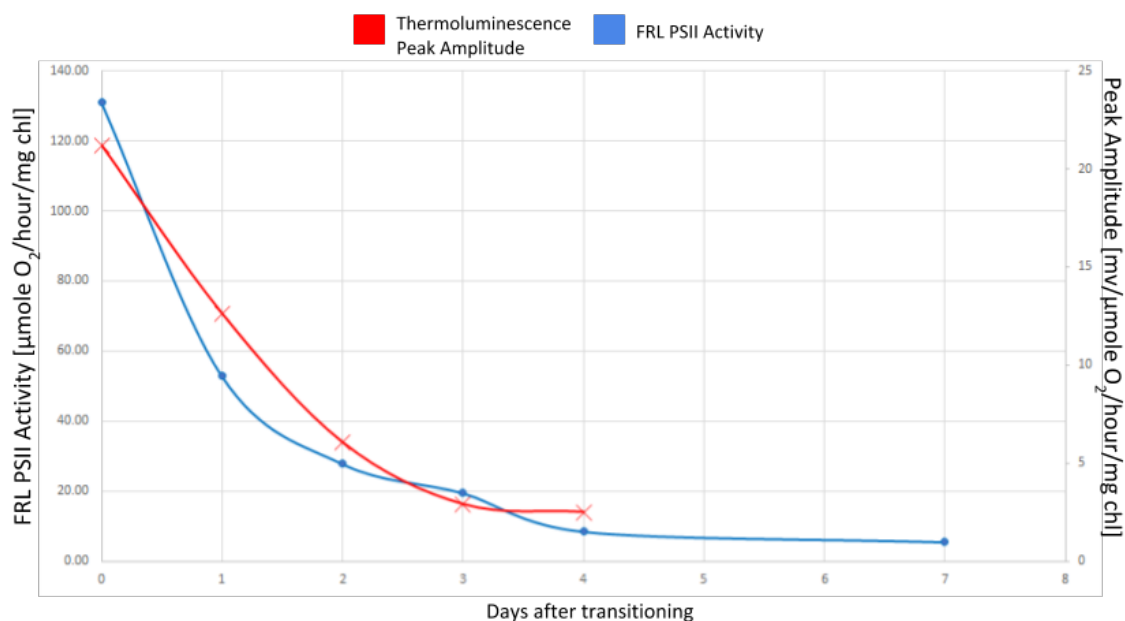


Figure 2 - FRL PSII Activity and Thermoluminescence Peak Amplitude over the transition period

a) FRL PSII Activity. After 4 days almost all FRL PSII activity had been lost. **b) Thermoluminescence Peak Amplitude** - normalized on FRL PSII activity measured at each time point. Both data sets shown are for single measurements, as there were not enough cells for replicates.

PSI activity proved much more difficult to follow over the transition, with no clear trend visible in the FRL or WL data. This suggests that PSI measurements in whole cells do not give reliable data. On two occasions it was noted that the culture bleached completely, and eventually cells died. This indicates that an abrupt transition can be cytotoxic, likely in the form of photochemical oxidative stress.

Future Outlook

The present study showed interesting insights into the transition process. The two ways of monitoring FRL-PSII activity both worked well and showed good correlation, with FRL activity lost in 3 to 4 days. It needs to be demonstrated that RL activity returned. For this we should repeat PSII oxygen evolution measurements, in RL, using isolated oxygen evolving thylakoid membranes.

PSI activity measurements proved difficult in whole cells - this may be due to redox mediators becoming unavailable to reaction centres, instead interacting with cellular compounds. To resolve this, it would be possible to isolate PSI in isolated thylakoid membranes, using cells frozen each day. Thylakoids should be free of reagents that might interfere with activity measurements. Activity could also be assayed in RL or FRL over the transition, using fluorescence measurements at 77 K. For that the lab would need to acquire or build an appropriate instrument.

The transition sometimes resulting in bleaching and cell death is interesting. It may be possible to make the transition less severe by using a lower level of visible light immediately after transition, increasing to normal levels after the process is well under way.

Value of the Studentship

The studentship was immensely valuable to me. I gained experience in biochemical, biophysical, and microbiological techniques. I also learned about day to day life in a lab, experimental design, and data analysis. I am grateful for the opportunity to work in a world-class research environment and interact with experts in the field.

Note from the supervisor: The work moved forward our knowledge of this new subject and sets the scene for future work in the group. The Biochemical Society summer studentships are excellent for getting new studies going and invaluable for providing experience for students. Biochemical Society support is gratefully acknowledged.

References

- Chen, M., Schliep, M., Willows, R., Cai, Z., Neilan, B. and Scheer, H. (2010). *A Red-Shifted Chlorophyll*. *Science*, 329(5997), pp.1318-1319.
- Nürnberg, D., Morton, J., Santabarbara, S., Telfer, A., Joliot, P., Antonaru, L., Ruban, A., Cardona, T., Krausz, E., Boussac, A., Fantuzzi, A. and Rutherford, A. W. (2018). *Photochemistry beyond the red limit in chlorophyll f-containing photosystems*. *Science*, 360(6394), pp.1210-1213.
- Chen, M. and Blankenship, R. E. (2011). *Expanding the solar spectrum used by photosynthesis*. *Trends in Plant Science*, 16(8), pp.427-431.



Using *in vivo* single molecule tracking to study LexA diffusion for different SOS promoters

Student:- Aditya Jalin

Supervisor:- Stephan Uphoff



Introduction:-

The SOS response is a highly conserved response to DNA damage in Bacteria. Cell replication is inhibited and DNA mutagenesis is induced. LexA is an important regulator in the activation of the SOS response. In undamaged cells, LexA exists as a homo-dimer which binds to SOS promoter sites. When the SOS response is initiated, the homo-dimer is cleaved which exposes protease sites in the monomer leading to complete degradation. Hence at any given time there are different species of LexA molecules in the cell. During my internship I used Single-Molecule tracking to calculate diffusion coefficients of individual LexA molecules *in vivo* and study their populations in the cell for different SOS promoters. Strains with a Lex-A halo tag had been previously made in the lab.

Aims & Objectives:-

The aim of the project was to analyse LexA binding/diffusion for different SOS promoters using single molecule tracking in E.Coli AB1157 by: **1)** Comparing the binding affinity of LexA to different SOS promoter sites by increasing the number of SOS promoter sites by transforming cells with a modified pUC19 plasmid containing a promoter site. Since pUC19 is a high copy number plasmid we would be providing several more binding sites for LexA. and increasing the number SOS induced cells by deletion of Δ dam. The dam gene encodes for a DNA methylase. The absence of which causes cells to spontaneously induce the SOS response **2)** Characterisation of SOS gene expression vs LexA degradation in cells with GFP labelled SOS promoters.

Materials and Methods:-

1) P1 transduction:- Δ flhD:mKate2 and LexA3::TC were moved to strains containing PsulA-GFP :: Kan & PdinB-GFP :: Kan using P1 transduction. Δ flhD makes the cell non motile which is useful for imaging using a microfluidics device. Cells with LexA3 express a mutated version of LexA that cannot be cleaved / The cells were then plated on sodium citrate+Kan plates.

Δ flhD:mKate2 was further moved into the constructed strains containing the LexA3 mutant.

2) UV sensitivity test:- LexA3 mutants were selected by plating them on plain LB plates along with a confirmed LexA3 mutant and wildtype strain. The plate was then exposed to a pulse of 50J/m² under a UV lamp. The successfully transduced strains showed a similar phenotype (low survival characterised by fewer and smaller colonies) to the confirmed strain after UV exposure.

3) Plasmid Construction:- pSulA and pDinB promoter sites were inserted into pUC19 plasmid using restriction digestion. EcoRI and XmaI were used to cut the MCS sites. A Blue-White colony test was done for selection

4)Blue-White Colony test:-The pUC19 plasmid contains the Lac promoter and LacZ gene. The restriction digestion disrupts the LacZ gene. Hence the transformed culture was plated on X-Gal+IPTG Plates and the white colonies were selected

5)Microscopy:-A Total Internal Reflection Microscope was used to take the images. Cell cultures expressing LexA-Halo and pSulA/pDinB GFP were prepared and labelled. The Halo-tag were then labelled using JF549 dye..A movie of length 20,000 frames was recorded using a 567nm laser at 50% of the maximum intensity and framerate 7ms. For the GFP a single image was taken at the same location with a 488nm laser at 10% of the maximum intensity.The mean square path of each molecule was measured. The diffusion coefficients were calculated and plotted using MATLAB.

Results:-

Increasing the number of SOS promoters:-

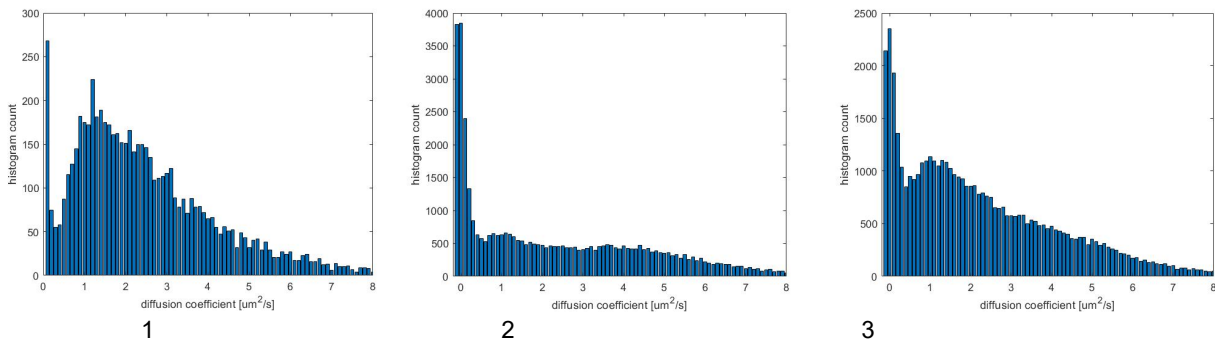


Figure 1: Histogram Count vs Diffusion Coefficient graphs for LexA-Halo molecules in E. coli strains: 1) Wildtype 2)WT with overexpressed pSulA 3)WT with overexpressed pDinBx

By overexpressing the promoter sites we allow more of the free LexA molecules to be bound in the absence of DNA damage. It is observed thaton increasing the number SOS promoters causes the LexA population to shift towards the lower mobility. This is expected as increasing the binding sites for LexA would cause more molecules to exist as a homodimer, bound to the promoter sites.

Characterisation of SOS gene expression vs LexA degradation:-

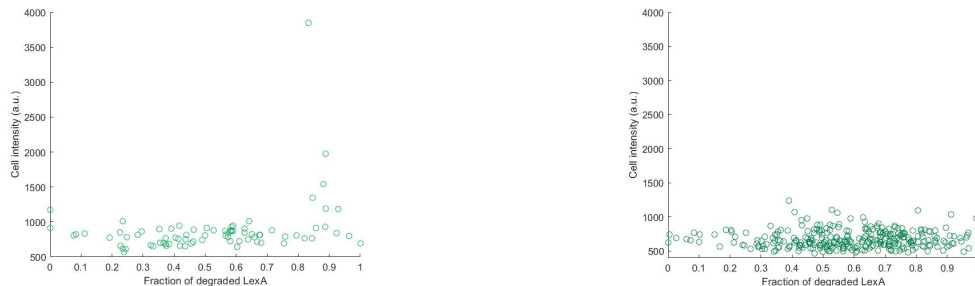


Figure 2: GFP Intensity vs Fraction of degraded LexA for individual cells: 1) WT LexA-Halo PdinB-GFP 2) Δ dam LexA-Halo PdinB-GFP

The goal was to understand how LexA degradation affects gene expression. The dam gene encodes for a DNA methylase which plays an important role in DNA mis-match repair. If a mismatch occurs in non methylated DNA, the mismatch-repair proteins cleave both the strands, causing a double stranded break. This spontaneously induces the SOS response.

It was observed that WT and Δ dam show similar correlation between SOS gene expression vs LexA diffusion.

Future Directions

In my project I used 2 SOS promoters, pSulA and pDinB to study the diffusion of LexA(**Fig1**). This experiment can be taken further by testing the LexA diffusion characteristics for more SOS promoters. Also the control used was WT E.Coli. A more accurate result can be obtained by using a strain with a PUC19 plasmid

For the characterization of SOS gene expression vs LexA degradation(**Fig2**) it would be interesting to study the temporal dynamics using a microfluidics device

Value of the Studentship

This experience has been an amazing opportunity that has helped improve both my theoretical and practical skills. Getting to use the TIRF microscope to do single molecule tracking was incredible and exciting. Apart from the lab skills, I have also learnt important lessons in time management and planning. I sincerely thank the Biochemical Society for providing me with the grant to carry out this internship. I am immensely grateful to my supervisor Stephan Uphoff and Valentine Lagage for helping make the best of this opportunity.

Role and Effect of Serine 222 Phosphorylation of NF- κ B2 in CRISPR/Cas9 Genome Engineered U2OS Osteosarcoma Cells



Sukhmani Kaur

Supervisors – Prof. Neil Perkins, Dr I. Ivanova, Dr J. Hunter

Background

NF- κ B is a fundamental regulator of many cellular processes, and activation results in the production of chemokines and cytokines, when induced by proinflammatory cytokines during inflammation⁽¹⁾. Moreover, it is a key factor involved in the initiation and progression of cancer^(3,4). Mammalian cells possess five NF- κ B subunits, RelA (p65), c-Rel, RelB, NF- κ B1 (p105/p50) and NF- κ B2 (p100/p52), which form homodimeric and heterodimeric transcription factor complexes⁽²⁾. In resting cells, NF- κ B in the cytoplasm is inactivated by members of the inhibitory I κ B family, such as I κ B α . Upon DNA damage and stress, I κ B α is phosphorylated by the IKK complex (including IKK α and IKK β) which signals an E3 ligase complex to degrade I κ B α using the proteasome^(2,3). In the non-canonical (or alternative) pathway, IKK α and NF- κ B inducing kinase (NIK) mediates the induce proteolytic processing of the NF- κ B2 subunit p100 to p52, leading to the induction of p52/RelB containing complexes. The loss of inhibition of NF- κ B allows it to translocate to the nucleus and modulate gene transcription of cell cycle regulating targets such as PLK4, Cyclin B1 and Cyclin D1⁽³⁾. Figure 1 shows the canonical and non-canonical pathways of NF- κ B, including the genes that are targeted by both complexes.

Post-translational modifications, in particular phosphorylation, can be used by the cell to modify NF- κ B and its activity,. This allows for crosstalk with other signalling pathways⁽³⁾. Site-specific phosphorylation of NF- κ B has been widely studied in the canonical pathway, as it can upregulate or downregulate the transcription of target genes. For example, in the non-canonical pathway, IKK α is recruited by NIK to phosphorylate p100 at Serine sites S99, S108, S115, S123 and S872, leading to p100 processing to p52⁽³⁾. This project further investigates the phosphorylation sites in p100/p52 in the non-canonical pathway, which has been less studied.

Aims and Objectives

This project focuses on the role and effect of phosphorylation of Serine 222 (S222) in p100/p52. This site is close to residues involved in p52 DNA binding, and mutation of this residue to aspartic acid to mimic phosphorylation inhibited this essential function. Using three U2-OS osteosarcoma cancer cell lines, generated by the Perkins lab using CRISPR/Cas9 genome engineering, where this site has been mutated to alanine to prevent phosphorylation and one control wild type U2-OS cell line.

- 1. Validate the genotype and p100/p52 expression in the cell lines.** The cell lines generated by genome engineering will be sequenced to confirm the introduced S222A mutation and mRNA levels of p100/p52 validated by qPCR.
- 2. Investigate whether S222 phosphorylation contributes to the regulation of other NF- κ B subunits or p52 specific target genes.** Cytoplasmic protein extracts will be prepared from the U2OS WT and S222 mutant cell lines, to analyse effects on proteins expressed from p52 target genes and processing of p100 to p52.
- 3. Examine the role of S222 in cell survival using a Clonogenic Assay.** To investigate the possible effects of S222 with regards to cell survival, which may allow the cell to proliferate more or less.

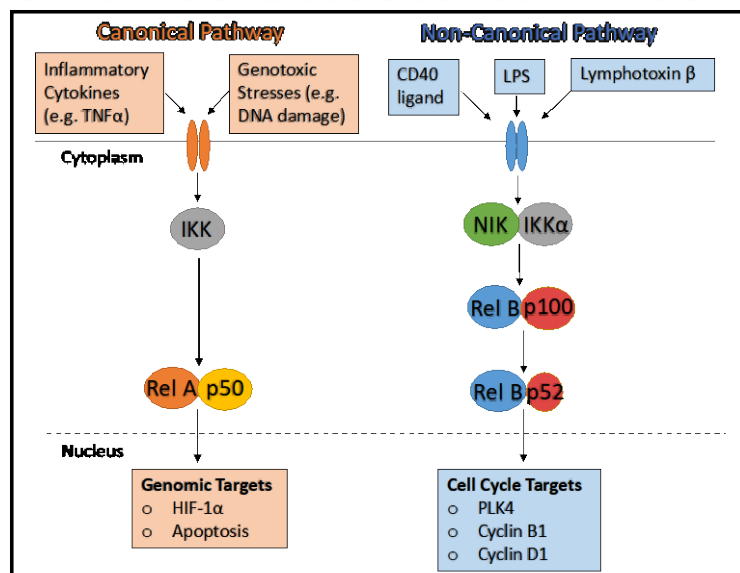


Figure 1. Canonical and Non-canonical NF- κ B pathways. Stimuli that activate both the canonical and non-canonical pathway lead to the activation of IKK complex, which phosphorylates inhibitory molecules leading to their degradation. The non-canonical pathway includes processing of p100 to p52, regulated by NF- κ B inducing kinase (NIK). Active components of NF- κ B associate with their relevant protein to form complexes that translocate to the nucleus to regulate target genes.

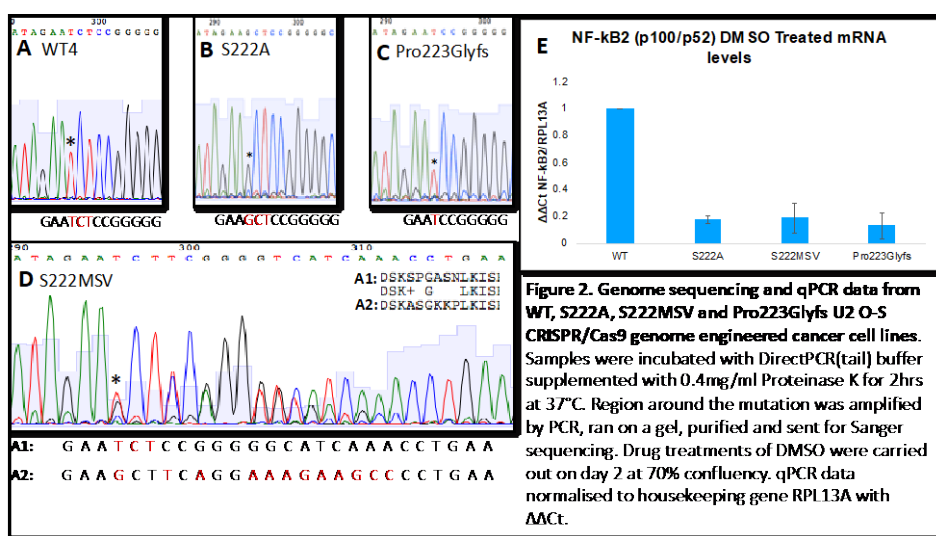
Methods

Protein extraction and Western Blotting – Protein concentration was quantified using a microplate Pierce™ BCA Protein Assay (ThermoFisher Scientific; ref: 23225). Cells were collected by scraping plates, and centrifuged at 300g for 5 minutes in order to aspirate the supernatant. Samples were resuspended in PBS, centrifuged at 300g for 5 minutes and aspirated. TNE buffer (100nM Tris, pH 7.6, 150mM NaCl, 0.5mM EDTA, 1% Triton, 1% NP-40, Phostop Phosphatase, Proteinase inhibitor cocktail tablets from Roche) was added to the samples to resuspend pellets and produce supernatant protein samples. Supernatant protein samples loaded

Sanger Sequencing – Genomic DNA was extracted with the DirectPCR (Tail) buffer supplemented with 0.4mg/ml Proteinase K, incubated for 2 hours at 37°C, followed by 85°C for 10 min. The region around the site of mutation was amplified by PCR, ran on a 1% agarose gel and cut out under UV light. The PCR bands were then gel purified with the Monarch DNA Gel Extraction Kit according to manufacturer's protocol and send to GATC Eurofins Genomics for sequencing.

RNA extraction and Quantitative PCR/Real-time PCR – Total RNA was extracted with the peqGold total RNA extraction kit (VWR) and quantified using a NanoDrop spectrophotometer according to the manufacturer's protocol. RNA samples were reverse transcribed with Quantitect Reverse Transcription Kit, and the cDNA stock was diluted 1:10. Data was generated on a Rotor-Gene Q using the following settings: hold, 95°C for 5 min; cycling, (95°C for 20 s; 58°C for 20 s; 72°C for 30 s) x 40; melting curve, 50-95°C

Results and Discussion

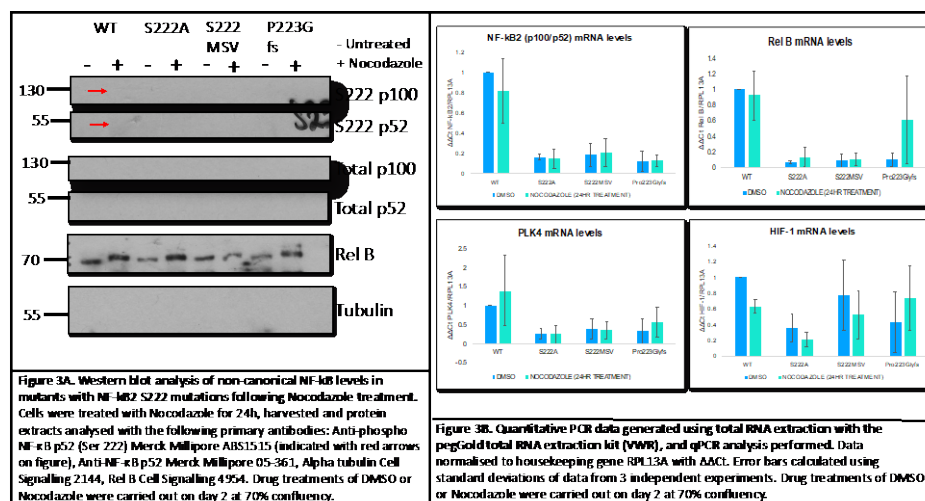


Genetic and mRNA Characterisation of NF-κB2 S222 genome edited U2 O-S cells.

U2 O-S cells generated by the Perkins lab are the main investigative cell used in this project to determine the effects of post-translational modifications on NF-κB2. In order to define the four different cell lines (one wild type, two potential NF-κB2 S222A mutants and one potential NF-κB2 frame shift mutant), genome sequencing was performed by GATC Sanger Sequencing Services (Eurofins Genomics) from extracted genomic DNA to be able to state what mutations the cells have obtained.

Figure 2A shows that the WT cell line contains the sequence encoding a serine residue at site 222, which can be phosphorylated as expected. Figure 2B shows a S222 mutant (S222A) containing the successful mutation at S222 to alanine, which cannot be phosphorylated. Figure 2C shows a S222 mutant (Pro223Glyfs) containing a 2 base pair deletion at S222, resulting in a frameshift of the sequence from a proline at residue 223 to glycine. This could result in a truncated protein or a complete knockout. Figure 2D clearly shows that the second potential NF-κB2 S222A mutant contains a mixture of alleles with varied mutations. One of the alleles contains the WT sequence with no mutations, and the other contains the correct S222A mutation but with added in frame mutations later in the sequence. When protein translations of both alleles are compared, the allele that exhibits the S222A mutation is in fact a missense mutant due to the additional mutations. This cell line will be referred to as the S222MSV (missense variant) further in the text.

To investigate if the mutations we identified influence the mRNA levels of p100, mRNA was extracted from the four cell lines and analysed by qPCR. Figure 2E shows the basal levels of NF-κB2 in the cell lines, and illustrates a clear drop in levels between WT and the three mutants. This suggests that the mutations present in the mutants lead to a decrease in mRNA levels of p100/p52. This could be due to either effects of the mutations on the expression of the gene or by affecting mRNA splicing, due to the close proximity of S222 to an exon/intron boundary.



The effect of S222 phosphorylation effects on the expression of p52 specific target genes.

To investigate the effect of the mutations on protein level of p100/p52 itself and other NF-κB subunits, western blotting was performed following treatment with Nocodazole (tubulin-binding agent that disrupts microtubule assembly and arrests cells within the mitotic cell cycle). Furthermore, quantitative PCR was used to confirm whether the results gathered from the Western Blot data correlated with mRNA levels, or if they resulted from a post-transcriptional process. Following 24 hour Nocodazole treatment, mRNA samples from each cell line were analysed together with RPL13A as a housekeeping gene. Figure 3A

phosphorylated in WT cells following Nocodazole treatment, but not in all other mutants which was expected as the mutation removes the phosphorylation site. Total p100 and p52 levels decrease in S222A and S222MSV, compared to WT, and is absent in Pro223Glyfs, in both untreated and treated cells. Figure 3B shows that the mRNA levels of NF-κB2 in all S222 mutants, either untreated or treated, is less than mRNA levels in WT. Processing of p100 to p52 is not affected by the mutations present in all S222 mutants. Figure 3A shows that levels of RelB are lower in untreated S222 mutants compared to WT, possibly due to low levels of total p100 and p52 leading to less RelB/p52 complexes. However, RelB is induced in all Nocodazole treated cells. mRNA levels of RelB shows low levels in S222 mutants, which does not correlate with results gathered from Western Blotting. This suggests that RelB undergoes post-transcriptional modifications in order to increase its protein levels, whilst mRNA levels are lower and stable. This could be due to either preventing RelB degradation or increasing the translation rate of RelB.

To understand if S222 phosphorylation affects the transactivation ability of p52, the levels of several target NF- κ B genes were analysed. PLK4 is a direct NF- κ B target gene involved in centrosome duplication⁽⁵⁾, and figure 3B shows mRNA levels are lower in S222 mutants compared to WT in both treated and untreated cells. Other targets of NF- κ B2 were investigated including Cyclin B1 and Cyclin D1, which also showed that mRNA levels were lower in S222 mutants compared to WT (data not shown). On the other hand, HIF-1 α contributes to cellular processes occurring during hypoxia, and is regulated mainly by the canonical NF- κ B pathway⁽⁶⁾. Consistent with this, HIF-1 α mRNA levels showed no change between all cell lines, in both treated and untreated cells. Overall, Western and qPCR analysis confirms that S222 mutants lose the ability to generate full length, functioning p100/p52 but processing is preserved. Due to this effect, the ability of the mutants to regulate target genes, such as PLK4, is compromised.

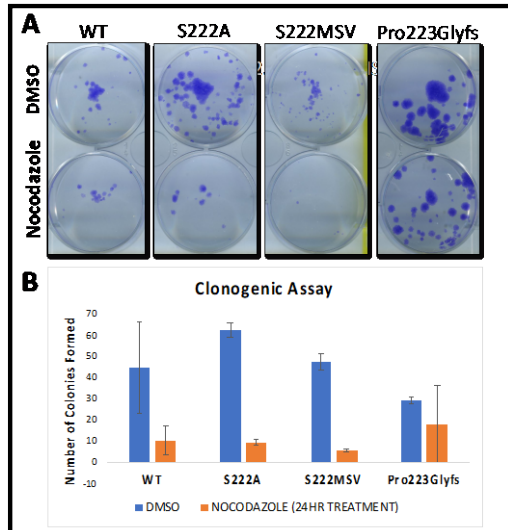


Figure 4. Clonogenic Assay showing the ability of each engineered cell line to generate clones following Nocodazole treatments. A. Photos of cells treated with DMSO and Nocodazole (how much) for 24h, then seeded at 100 cells/well in 6 well plate and cultured until colonies formed in regular DMEM. **B.** Graph depicting the number of colonies counted and plotted with error bars representing the standard deviation from two independent experiments. Drug treatments of DMSO or Nocodazole were carried out on day 2 at 70% confluency.

Role of S222 Mutants on Cell Survival using Clonogenic Assay

To investigate the ability of each cell line to form clones, 100 cells were seeded into each well for each cell line in a 6 well plate to perform a Clonogenic assay. Figure 4 shows S222MSV formed smaller colonies in untreated conditions, compared to WT. In addition to this, treatment with Nocodazole appears to have a larger effect on this cell line as there were fewer colonies compared to WT and S222A. The Pro223Glyfs mutant cell line formed larger colonies but at a smaller frequency in untreated conditions, and when treated with Nocodazole produced larger colonies at a similar frequency. When investigating the growth rate of U2-OS cells, RealTime Glo assay showed that the growth rate of WT, S222A, S222MSV and Pro223Glyfs was not statistically different (data not shown). This suggests that the mutations do not affect the growth rate of S222 mutant cell lines, however may have an effect on the ability to form clones. The data gathered from the clonogenic assay shows that WT, S222A and S222MSV form similar number of colonies, and the addition of Nocodazole inhibits the colony formation potential of these cells. The Pro223Glyfs cell line may also have a similar colony forming potential after Nocodazole, therefore these cells may be more resistant to spindle formation defects.

Overall, these findings illustrate the vital role of post-translational modifications in terms of Serine 222 phosphorylation within the NF- κ B2 non-canonical pathway. mRNA levels of p100/p52 are depleted following phosphorylation, and this has a negative effect on p52 regulated specific target genes such as RelB and PLK4. Genes which are independent from the non-canonical pathway remain at a stable level (e.g. HIF-1 α). This phosphorylation does not affect the growth rate of cells, but

may have an effect in terms of clone formation particularly in Pro223Glyfs cells which have similar colony formation before and after treatment. Previous experiments have showed that depletion of p100/p52 by siRNA led to an increase of cells in G₂/M phase⁽⁵⁾. Since S222 mutations also reduced the levels of p100/p52 it would be interesting to investigate what stage of the cell cycle the WT and S222 mutants are in by FACS profiling.

This project has determined the importance of post-translational NF- κ B2 modifications within the non-canonical pathway, and will lead to further investigation into this widely unknown area.

Departures from Proposal and Future Work

Due to time constraints, the PC3 prostate cancer cell line was not investigated and the U2OS osteosarcoma cells were mainly used.

In this project, cells were treated with Nocodazole for 24 hours but studies have shown different effects with longer treatment times. Furthermore, in order to distinguish what stage of the cell cycle the cells are in when untreated and treated, FACS profiling would be beneficial.

Value of Studentship

This studentship has been an invaluable experience that has allowed me to improve my skills and gain confidence in performing practical techniques. I have developed a range of practical skills during the 8 weeks, enabling me to work independently in a lab environment. I was able to apply the theories I have learnt during my degree to a practical setting, and have expanded my knowledge about scientific procedures. The placement has enabled me to see what a career in research entails, and has inspired me to carry on in further study after my undergraduate degree to pursue a PhD. I was lucky enough to work in a lab that was encouraging and supporting, and for that I am very grateful.

References

- Perkins ND. Integrating Cell-signalling pathways with NF- κ B and IKK function. *Nature Reviews Molecular Cell Biology*, 2007;8: 49-62
- Perkins ND. The diverse and complex roles of NF- κ B subunits in cancer. *Nat Rev Cancer* 12, 121-132.
- Christian F, Smith EL, Carmody RJ. The Regulation of NF- κ B Subunits by Phosphorylation. *Cells*. 2016;5(1).
- Webster GA, Perkins ND. Translational Cross Talk between NF- κ B and p53. *Molecular and Cellular Biology*, 1999;19(5): 3485-3495.
- Ledoux AC, Sellier H, Gillies K, Iannetti A, James J, Perkins ND. NF- κ B regulates expression of Polo-like kinase 4. *Cell Cycle*, 2013;12(18): 3052-3062.
- Ivanova IG, Park CV, Yemm AI, Kenneth NS. PERK/eIF2 α signalling inhibits HIF-induced gene expression during the unfolded protein response via YB1-dependent regulation of HIF1 α translation. *Nucleic Acids Research*, 2018;46(8): 3878-3890.

The aims of the project

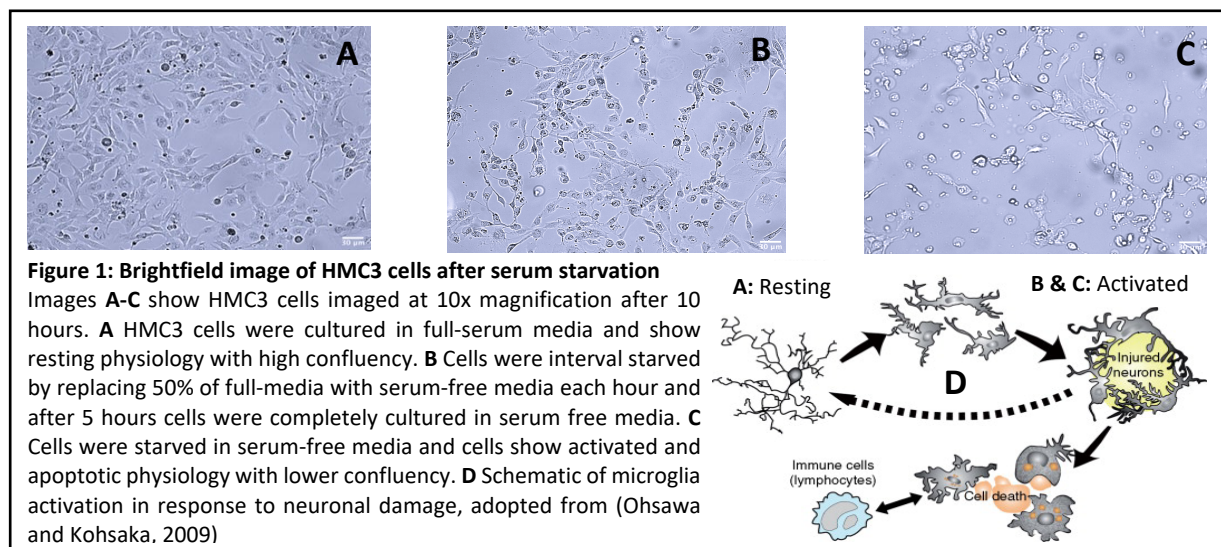
- Understand the importance of changing physiology in microglia
- Measure endogenous G protein-coupled receptor (GPCR) presence with PCR in HMC3 cells
- Investigate GPCR dimerisation using recombinantly overexpressed tSA201 cell models

A description of the work carried out

Microglia contribute significantly to the homeostasis of the brain by continuously monitoring the cerebral environment (Simon, Obst and Gomez-Nicola, 2019). The fluent pro- and anti-inflammatory immune response makes microglia particularly important to understand the progression of neurodegeneration (Sarlus and Heneka, 2017). My work was specifically targeted at studying purinergic receptors P2Y₁ & P2Y₁₂, which are involved in mediating inflammatory signals between microglia and neurons (Figure 1 **D**) (Hidetoshi, Makoto and Inoue, 2012). By studying dimerisation between P2Y₁ and P2Y₁₂ I learned fundamental skills in cell culture, Quantitative Real-Time PCR (RT-PCR), Co-immunoprecipitation, Glutathione S-transferase (GST) pull down, Western blotting and experienced the use of confocal microscopy.

HMC3 cells (ATCC_CRL3304) were used in this study. These cells are immortalized by incorporating a dominant oncoprotein gene, which allow them to replicate endless and prove to be a viable alternative to limited available primary culture microglia from rodents (Dello Russo et al., 2018). A stable culture environment (37°C, pH 7.2) is crucial for optimal growth. The cells were cultured in media enriched with essential amino acids, sugars and minerals (full-serum) as well as antibiotics. Once cells were confluent (density of cells in flask 80%, reference Figure 1 **A**), which was determined visually using a brightfield microscope, the cells were passaged for experimentation.

Throughout the project I experienced that the cell division rate decreased and more cells underwent apoptosis towards the 35th passage. Recent research reported that the physiology, relating to antigen expression, phagocytic activity and apoptosis rate of HMC3 is considered stable up until the 35th passage (Dello Russo et al., 2018). To understand better the importance of a stable culture environment I carried out cell-starvation experiments (Figure 1).



RT-PCR was carried out in HMC3 cells to confirm purinergic P2Y₁ and P2Y₁₂ GPCR expression. Extracted mRNA was quantified and tested for purity using the thermofisher Nanodrop. With the use of Reverse-Transcriptase the mRNA was reverse transcribed into complementary DNA (cDNA). I incorporated a DNase purification step to increase the purity of the mRNA prior to reverse transcription. RT-PCR involved working in absolute clean environment, as well as troubleshooting and understanding the importance of positive control and negative control and normalization of extracted mRNA.

Next, transfections were carried out in HMC3 and tSA201 cells with plasmids containing either the P2Y₁ or P2Y₁₂ gene, linked with a HA-tag gene and a fluorescence protein gene (eg. Green Fluorescence Protein, GFP). The HA-tag and GFP allowed for analysis of potential co-interactions between P2Y₁ or P2Y₁₂ in Western Blot (Figure 3) and fluorescence microscopy.

Assessment of results and outcomes

First HMC3 cells were tested for the P2Y₁ & P2Y₁₂ gene presence. Figure 2 shows PCR cycle threshold results for P2Y₁. P2Y₁₂ was not detected, however previous research confirmed the gene is present in HMC3 (Dello Russo et al., 2018). Closer analysis of the primer nucleotide sequence lead to the evaluation of testing a custom designed primer.

	Un-transfected		Transfected	
	HMC3 (A)	HMC3 (B)	HMC3 P2Y ₁	HMC3 P2Y ₁₂
mRNA conc. (ng/μl)	779.2	839.8	179.3	233.4
A260/A280	2.07	2.06	2.08	2.04

Table 1: Amount of mRNA in elute-solution (ng/μl) extracted, tested in Nanodrop. A260/A280 provides a precise estimate of protein contamination. Proteins primarily absorb 280 nm UV-wavelength due to amino acid side chains with aromatic ring structures. Pure RNA has an absorption ratio of 2.

Table 1 shows that extracted mRNA in elute-solution has a high degree of purity, which is important to avoid interference of protein contaminants in the reverse transcription reaction and the PCR itself. From the transfected HMC3 (Table 1) a much lower amount of mRNA (ng/μl) was extracted. The magnet transfection method used, is reported to have the highest transfection efficiency out of 4 commonly used transfection methods, but can stress the cells and induce lower overall transcription (Smolders et al., 2018). The extracted mRNA results allowed me to learn more about the optimization of the transfection method.

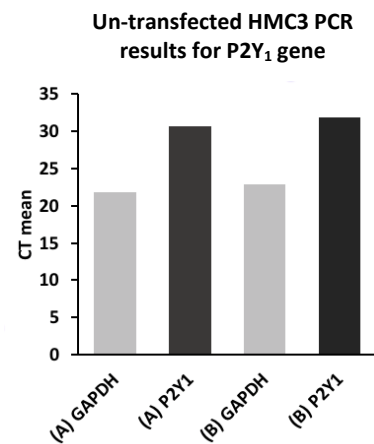
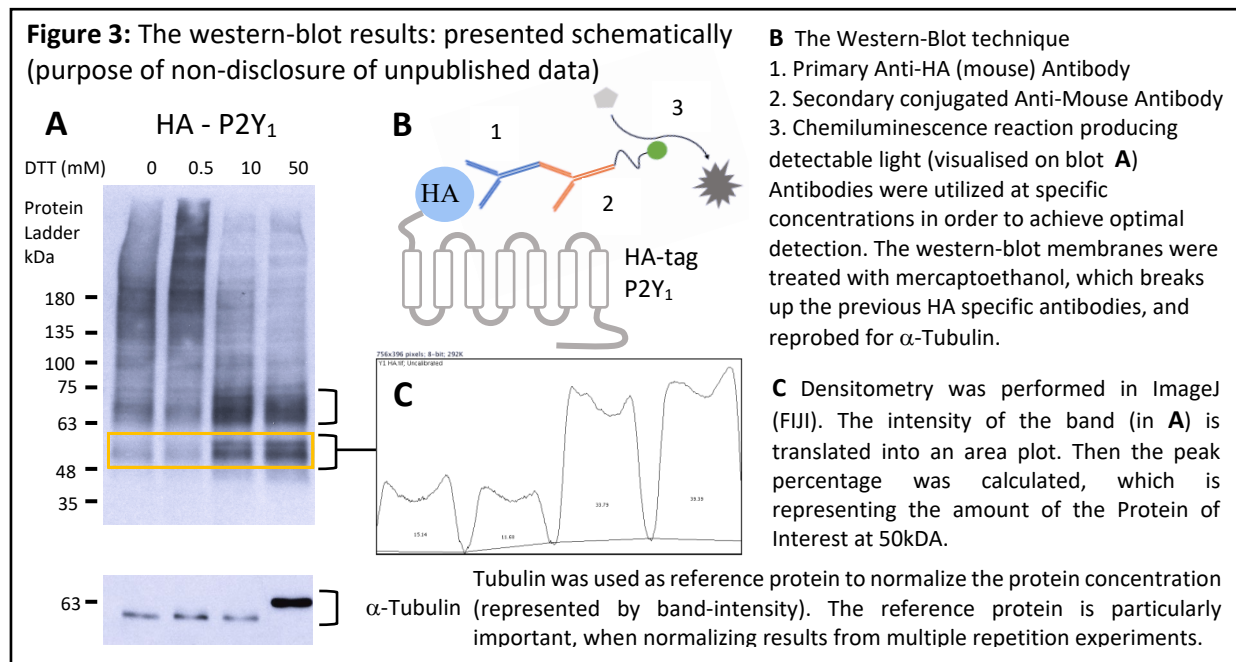


Figure 2: Showing PCR cycle number when fluorescent threshold is reached for amplified Gene; either GAPDH (reference gene) or P2Y₁ in HMC3 sample A or B



Future directions in which the project can be taken

The direction of the project is moving towards understanding the role of P2Y₁ and P2Y₁₂ dimerisation in microglial function. Studies will be conducted using activity assays to measure the various signaling pathways downstream to these receptors.

Departures from the original proposal and value of studentship

The focus was shifted from PAR-1 signaling to purinergic GPCR in microglia. This change allowed me to experience a wide range of techniques, which are currently employed for the ongoing research and I was able to contribute meaningful data for publication. I believe, through completing my internship funded by The Biochemical Society, I have acquired the knowledge and skills that can help me follow my aspiration of researching microglial inflammatory signaling in neurodegeneration in the future.

Biochemical Society Summer Studentship 2019

University of Bradford

Supervisor: Dr Ritchie Williamson

Student: Zulaikha K Yasir



Introduction

Alzheimer's disease is a progressive neurodegenerative disorder with currently no known cure or disease modifying treatment. There are 850,000 people living with Dementia here in the UK and AD accounts for up to 50-75% of all Dementia cases. There are 4 current drugs that offer symptomatic relief, that too for a limited time. A number of pathologies such as cardiovascular disease, diabetes and neurodegeneration have been identified by their altered O-GlcNAcylation. In order to fully understand the molecular changes that lead to Alzheimer's, it is important to identify which proteins alter and at which stage.^{1,2}

O-GlcNAc is an O-linked β -N-acetyl glucosamine, important in disease-related signalling and enzyme regulation. O-GlcNAcylation is regulated by two enzymes, O-GlcNAc transferase (OGT) and O-GlcNAc Hydrolase (OGA).^{3,4} Post translational modifications (PTM) such as phosphorylation, acetylation and ubiquitination have confirmed O-GlcNAc is responsible for cellular response in stressful conditions. However, there is not enough evidence yet to confirm glucose deprivation can result in increased O-GlcNAc levels, when associated with OGA.^{4,5} The purpose of this research was to identify the proteins bearing the O-GlcNAc modification. In order to identify protein bearing the O-GlcNAc moiety, an OGA-trap methodology has been developed. Here, a bacterial orthologue of OGA with a single amino acid substitution (D298A) in the active site was generated. The substituted amino acid is proton donor for hydrolysis of the O-GlcNAc.⁷ As such, the generated orthologue could bind to O-GlcNAcylated proteins but not hydrolyse the O-GlcNAc. Attaching a Halo protein to the OGA allowed for subsequent purification of O-GlcNAcylated proteins through affinity resin. The project aimed to develop a similar system using human and mouse OGA.

Project Aims

1. Expression and purification of mouse OGA and human OGA.
2. Characterisation of expressed proteins by western blotting and activity assays.
3. Application of expressed proteins to mouse brain homogenates to enrich for O-GlcNAcylated proteins.
4. Western blotting of enriched proteins using a panel of commercial antibodies against known O-GlcNAcylated proteins.

Methods

Generation of bacterial orthologues of OGA. Glycerol stocks of plasmids containing N-terminally Halo-tagged C-terminally hexa-His-tagged *CpOGA* were streaked on agar plates and incubated overnight at 37 °C. The next day a single colony was selected and cells grown overnight at

37 °C in Luria-Bertani medium containing 50 μ g/ml kanamycin (LB-Kan) and used to inoculate fresh LB-Kan. Cells were grown to OD 600, readings were taken after a few hours using a spectrophotometer. Once cells reached an OD600 of 0.6-0.8, cultures were transferred to 18 °C and incubated with 250 μ M IPTG and harvested after 16 H by centrifugation at 3,500 r.p.m (4 °C).

Cell pellets were then resuspended in 20 ml of lysis buffer containing 50 mM Tris, 250 mM NaCl at pH 7.5 (lysis buffer was supplemented with protease inhibitors, DNase and lysozyme. Cells were lysed using a sonicator and the lysate cleared by centrifugation at 15,000 r.p.m for 30 min at 4 °C. Cleared lysate was passed through a syringe filter and loaded onto a HisTrap column. The column was then washed with 10 volumes of lysis buffer. Flow through was measured for protein content and washes continued until the flow though did not contain any protein. His-tagged protein was then eluted with imidazole (250 mM) by incubation and mixing for 2 h at room temperature. Eluted protein was then concentrated using viva spin concentrators and buffer exchanged into tris buffered saline. Concentrated protein was stored as a 20% v/v of glycerol at -80 °C.

Generation of human OGA

To generate human OGA, two plasmids were obtained. The first plasmid contained sequence for the first half of the protein and the second plasmid contained sequence for the second half of the protein. Both plasmids were transformed into Dh5alpha cells and a mini prep of each was performed to generate DNA. The two plasmids work together in order to express human OGA. Once the DNA was prepared this was transformed into BL21 cells. Protein expression and purification was performed as described above.

Polycrylamide gel electrophoresis (PAGE)

Protein purification was determined by PAGE. 10% acrylamide gels were prepared and approximately 10 μ g of protein (in 4x Laemmli buffer) was loaded onto the gel. Gels were run at 180 V for 1 h. The gel was removed and stained with Coomassie Blue R gel stain (10% v/v glacial acetic acid, 45% v/v methanol, 0.05% w/v Coomassie Brilliant Blue R) for 1 h at room temperature. The gel was then de-stained with multiple washes of destain (5% v/v glacial acetic acid, 40% v/v methanol). Stained gels were then scanned using the Bio-Rad imaging system.

Results

Purified CpOGA protein was successfully expressed and purified. Both wild type and mutant CpOGA was generated and confirmed by PAGE.

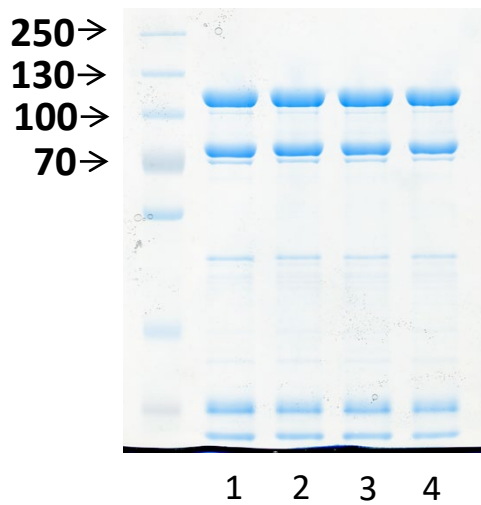


Fig 1. Purification of CpOGA. Wild type (lanes 1 and 2) and mutant D298A CpOGA (lanes 3 and 4). Purified proteins were separated on 10% acrylamide gels and proteins identified by Coomassie stain.

The protein species at approximately 130 kDa represent the full length CpOGA with the Halo link protein. The protein species at approximately 70 kDa represent the CpOGA alone without the Halo sequence. This suggests cleavage of the protein at some point during the purification. The purified protein was then tested to see if it could capture O-GlcNAcylated proteins. From Fig 2 below we can see that the D298N CpOGA was able to trap the O-GlcNAcylated proteins (lane 2) and that the wild type CpOGA did not trap any O-GlcNAcylated proteins (lane 1).

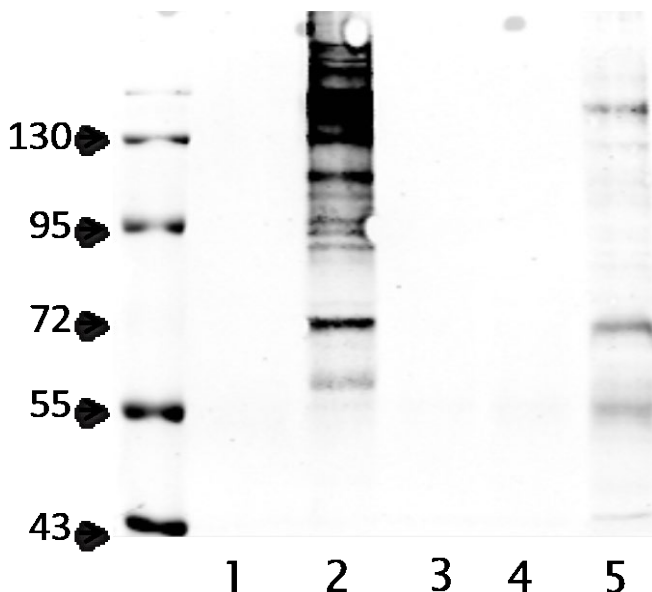


Fig 2. Western blotting of brain lysates incubated with different CpOGA protein preparations. Brain homogenate was incubated with purified CpOGA protein and western blotted for O-GlcNAcylated proteins.

Future Directions

Now that we have purified the human OGA the next step will be to link to a halo protein. Once the halo-linked protein has been made. Point mutation scan then be generated to make the human equivalent of the CpOGA D298A protein. From this we will be able to generate a mouse specific version of these proteins, again by mutagenesis. The human and mouse proteins share 97.8% sequence similarity.

Value of Studentship

I have thoroughly enjoyed my time in the lab and it was hugely beneficial for me to conduct western blots and gel electrophoresis, as it ties in nicely with the theory I have studied in my degree. This invaluable experience has taught me the importance of research and has allowed me to develop and hone a large skill set including: teamwork, time management and the ability to take down notes quickly and efficiently. As a Clinical Sciences' student, we are not given much time in the labs to experience basic lab skills such as pipetting. However, this project has allowed me to even grow bacterial cultures and purify proteins. I was even lucky enough to observe Dr Ritchie remove some mice brain! I am extremely fortunate to have had the opportunity to conduct a 2 month research project alongside reputable researchers. This project will help me with my final year Neuroscience module and has supported my decision to apply for a Master's degree in Neuroscience.

Value to lab

Zulaikha's work has taken the lab forward in generating species specific OGA trapping methodologies. This will increase the toolkit available for researcher exploring protein O-GlcNAcylation in health and disease. Zulaikha's dedication and commitment to the project was obvious from the start and her work has established the base from which we can now develop these methodologies. This has accelerated our work to develop these tools and we would welcome Zulaikha back if the opportunity arose.

References

1. Bond, M., & Hanover, J. (2015). A little sugar goes a long way: The cell biology of O-GlcNAc. *The Journal Of Cell Biology*, 208(7), 869-880. doi: 10.1083/jcb.201501101
2. Selvan, N., et al. (2017). A mutant O-GlcNAcase enriches Drosophila developmental regulators. *Nat Chem Biol*, 13(8): 882-887
3. Nie, H., & Yi, W. (2019). O-GlcNAcylation, a sweet link to the pathology of diseases. *Journal Of Zhejiang University-SCIENCE B*, 20(5), 437-448. doi: 10.1631/jzus.b1900150
4. Gong, C., Liu, F., Grundke-Iqbal, I. and Iqbal, K. (2006). Impaired brain glucose metabolism leads to Alzheimer neurofibrillary degeneration through a decrease in tau O-GlcNAcylation. *Journal of Alzheimer's Disease*, 9(1), pp.1-12.
5. Dias, W., & Hart, G. (2007). O-GlcNAc modification in diabetes and Alzheimer's disease. *Molecular Biosystems*, 3(11), 766. doi: 10.1039/b704905f
6. Maher, P. and Schubert, D. (2009). Metabolic links between diabetes and Alzheimer's disease. *Expert Review of Neurotherapeutics*, 9(5), pp.617-630.
7. Gong, C., Liu, F., Grundke-Iqbal, I. and Iqbal, K. (2006). Impaired brain glucose metabolism leads to Alzheimer neurofibrillary degeneration through a decrease in tau O-GlcNAcylation. *Journal of Alzheimer's Disease*, 9(1), pp.1-12.

Summer Internship Report from Kavi Shah

Redesign of the chloroplast genome towards a synthetic organelle

Overall aims of research

Chloroplasts of algae are naturally evolved for **efficient light absorption, and carbon fixation** which can be used to provide energy and building blocks for synthesis of novel products. It is possible to achieve a high level of expression of foreign genes due to multiple copies of the plastome. Therefore, the manipulation of **phototrophic organisms** is important in driving **sustainable production** of a wide range of products from biofuels to phytochemicals. The group of Alison Smith is working to generate a minimal chloroplast genome as genes have an energy cost and can interfere with the desired pathway when producing high value compounds. It will also group pathways and complexes together to enable easy future engineering of the plastome. *Chlamydomonas reinhardtii* is a mixotrophic organism with a single chloroplast, meaning many photosynthetic genes are dispensable under heterotrophic growth conditions. This makes it an ideal organism for the engineering of a minimal chloroplast.

The minimal plastome project will also provide insights into the components necessary and sufficient in constituting a genome as well as improve our understanding of the structure of the chloroplast genome. It will also present the way large scale changes in the chloroplast genome affect the chloroplast and whole organism. Sequential deletion can provide an insight into the evolution of plastid genomes over time as well as the miniaturisation of genomes. Chloroplast engineering also improves our understanding of the use of less well characterised phototrophic organisms like algae in future synthetic biology. This allows synthetic biology to progress beyond the model systems of *E. coli* and yeast.

Aims of Summer Internship:

In this summer internship I worked towards refactoring the genes for the cytochrome b6f complex by deleting the *pet* genes. The cytochrome b6f complex contains multiple genes both in chloroplast and nucleus and has not been refactored before, although individual genes have been knocked out. After sequentially deleting all the genes, the eventual aim will be to put them in a single locus in the chloroplast genome. The second aim was to optimise the selection process when deleting genes from the chloroplast to minimise false positive background colonies and speed up selection process to achieve homoplasmy.

Work carried out

I designed and constructed using Start-Stop Assembly, a deletion plasmid to delete the *petA* and *petD* genes from the chloroplast genome which are together at a single locus. This plasmid contained a left homology arm and right homology arm and a positive selective marker to replace native region with the deletion cassette through homologous recombination. The positive selection marker *aadA*, confers resistance to streptomycin and spectinomycin and is used to select to homoplasmy, where all the multiple copies of the chloroplast genome contain the deletion. The plasmid also contained a direct repeat identical to the left homology arm and negative selection marker *codA* conferring sensitivity to 5-fluorocytosine for the removal of the selection cassette. I transformed this deletion plasmid into the chloroplast using biolistic transformation and plated in top agar with spectinomycin for the first round of selection.

I helped transformed *Chlamydomonas* with deletion plasmids for *petG*, *petL* and *petB*, and carried out four rounds of positive selection to select towards homoplasmy through picking and streaking colonies (every 8-12 days) in increasing antibiotic concentrations. I then genotyped the strains using the PHIRE kit for DNA extraction and PCR, and continued with another round of selection as homoplasmy had not been reached.

I performed multiple experiments to try and characterise the strains being used and optimise the antibiotic concentrations in the selection process. e.g. spectinomycin 200 µg/ml for the first round of selection.

Results and Outcomes

The genotyping of *petB* and *petL* deletions showed successful transformation and deletion although not yet homoplasmic. This is important as it validates the method of designing the construct, transformation and selection as well as genotyping. I transformed the *petAD* deletion plasmid into *Chlamydomonas* and will see if

it was successful after selection and genotyping. After all the different *pet* genes have been deleted, including the ones in the nucleus individually, they can then be sequentially deleted in the same cell line. Optimisation of antibiotic concentrations used in selection process of the CC-1690 strain will increase the yield of true deletion colonies and increase the speed of selection to homoplasmy.

Skills gained

I have gained a lot of experience and skills in experimental techniques. I have gained a lot of experience in cultivating and working with *Chlamydomonas*. I have also gained experience in all the processes that are involved in designing and assembling a plasmid in *E. coli*. This includes designing the construct in SnapGene software, utilising the Start-Stop Assembly method with type II restriction enzymes to create scar-less constructs, PCR, running gels, gel extraction of DNA, restriction digests, bacterial transformation, minipreps and midipreps, and interpreting DNA sequencing results. I have also gained experience in transformation of algae using biolistics and electroporation and selection processes through different plating methods including starch plating and plating in top agar, and streaking and picking of colonies. Another important experimental skill I have gained is in independently planning, carrying out and evaluating experiments.

I have also gained a lot of other skills that are important including presenting and communication skills from the final presentation given at the end of the internship as well as a poster seminar as well as regular meetings with my supervisors, journal club sessions and brainstorming and troubleshooting sessions with the lab as a whole.

Departures from the proposal

Construction of *petAD* deletion construct took longer than expected due to issues in amplifying multiple short repeats through PCR and mutation of a transposable element native to the chloroplast genome in *E. coli*. This resulted in redesign of the deletion construct and meant I only did first round of selection after transformation. As mentioned in the proposal as an alternative if creation of a construct was taking too long, I also helped transform and select three different gene knockouts as mentioned above.

Future directions

There are multiple exciting future directions that this project can be taken in. This includes investigating methods to temporarily reduce copy number by different growth conditions. e.g. in the dark or different media conditions and inhibitors that could potentially be added. This would reduce selection time to homoplasmy which is currently one of the bottlenecks of transforming the chloroplast. After successfully transformed, the copy number could be increased again to provide the benefits of high expression of transgenes. Another possible topic that is being investigated further down the line in this project is the way codons can be optimised for the chloroplast. This will be important when refactoring complexes adding genes from the nucleus or distantly related organisms. The long-term project of working towards a synthetic chloroplast genome is still in its early stages and the minimisation and rearrangement of the genome will provide unique insights for the use of synthetic biology in algae and the chloroplast.

Conclusion

This summer internship has been an exciting, memorable, and rewarding experience that has helped me make the decision to pursue a career path in research. I would like to thank everyone in the lab, and Pawel Mordaka and Alison Smith, as well as the Biochemical Society who helped make this internship possible.

Comments from the lab

Kavi was the ideal summer student – enthusiastic, hard-working and a team player, in particular he was always happy to rack tips! He learnt the skills necessary to carry out chloroplast synthetic biology quickly and was able to generate several constructs which we will use as part of the minimal plastome project. He also helped with preliminary experiments to test a method to transform *Chlamydomonas* using bacterial conjugation and episomes, during which time he learnt which controls need to be considered to establish a new method. He presented his work at a poster session and to one of our lab meetings. We hope that Kavi can use his lab experience to complete his final year successfully, and are very pleased that he is considering a career in research as a result of his time in the lab.



Are Translated lncRNAs Preferentially Localised to the Cytoplasm?

Biochemical Society Summer Vacation Studentship 2019

Student: Sulaiman Sulaiman

Supervisor: Dr Julie Aspden

School of Molecular and Cellular Biology
University of Leeds
UK



UNIVERSITY OF LEEDS

Introduction

The RNA family of biomolecules comes in many flavours, which can be grouped into two main categories, based on whether the RNA molecule encodes a peptide sequence. Of these two categories, non-coding (ncRNA) do not encode peptides and of this is a subset known as long non-coding RNA (lncRNA), which are defined as being >200nt in length. These lncRNAs have no large (>300nt) open reading frames (ORFs) thus not thought to be translated into proteins.

lncRNAs provide a wide range of functionality to a cell which are necessary for the proper survival and functioning, ranging from regulation of gene expression (e.g. RNA splicing) and scaffolding for proteins [1]. However, some lncRNAs contain small open reading frames (smORFs), meaning they can associate with ribosomes and may be translated to produce small peptides. In fact, translation of lncRNAs has been recently seen in a number of organisms [2].

Aims/Questions

1. Are translated lncRNAs transcripts being preferentially localised to the cytoplasm of the cell? And if so, is this localisation property shared across all transcripts of the gene or just to specific subset of transcripts
2. Are translated lncRNAs transcripts more conserved than non-translated lncRNAs? This would indicate to some evolutionary pressure to keep them.

Methodology

Preliminary work in the group had identified a number of lncRNAs expressed in a human neuroblastoma cell line (SH5Y5Y) and the subset of these which are translated had been determined.

Using the IDs for these lncRNAs which had been identified, the subcellular localisation expression levels were retrieved from previously published datasets in a number of different cell types (lncAtlas [3] and GENCODE v7 [4] were used). The data for each set was marked as to whether the lncRNA transcript/gene was identified as being translated or not. As a control for the localisation of translated RNAs, randomly selected protein-coding RNAs were used (from GENCODE v24 GTF genome annotation) and were passed through the same databases to retrieve the relevant localisation data, Figure 1.

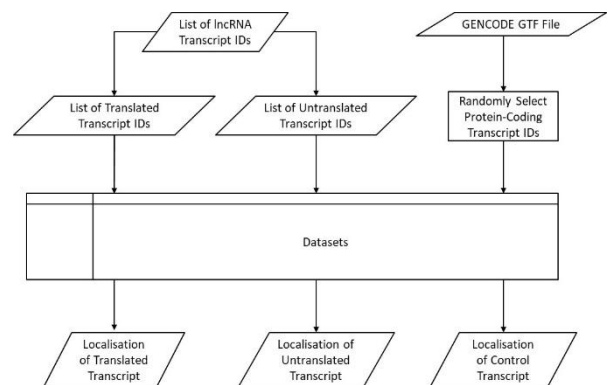


Figure 1 Flowchart for the generation of localisation data for the various sets of data: translated/untranslated lncRNA and random mRNA

The data was then normalised (equation 1), by taking the ratio of cytoplasmic level relative nuclear level, which provides a dimensionless quantity, the log (base 2) of this value was then taken to better identify preferentially cytoplasmic or nuclear transcripts/genes.

$$R_{CN} = \lg \left(\frac{[\text{Cytoplasm}]}{[\text{Nucleus}]} \right) \quad (1)$$

Results & Discussion

Data for only 37.8% of the translated lncRNA transcripts and 13.8% of untranslated lncRNA transcripts could be retrieved from GENCODE. Even then, there were indications that translated lncRNA transcripts were localised to the cytoplasm. Using the lncATLAS data was more fruitful, being able to recover 96.8% of translated lncRNAs and 97.6% of untranslated lncRNAs. However, this data is at gene level and not transcript specific, but it provided data for related cell-lines, most of the subsequent analysis was performed using lncATLAS dataset.

To determine if there are features of translated lncRNAs that are different from untranslated lncRNAs I assessed the number of cell-lines each lncRNA was expressed in (Figure 2). Untranslated lncRNAs generally have a more restricted

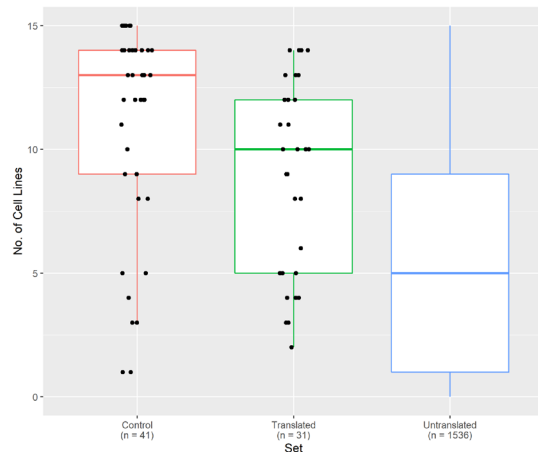


Figure 2 Number of cell-lines in which various untranslated lncRNA, translated lncRNA and mRNA genes were expressed in

there was no conservation with humans across any of the species, with 6 exceptions where it would indicate conservation between humans and fruit flies. Rather interestingly some of the species more closely related to humans did not show conservation in these otherwise conserved transcripts, indicating that there is a lack of data for these transcripts which may otherwise be conserved, showing that there may be a lack of conservation data for these lncRNAs.

What is quite clear is that translated lncRNA is preferentially exported out into the nucleus, compared to its untranslated counterpart, indicating that may be inferring some functional advantage. The preliminary data for conservation indicates that their may be some conservation of some translated lncRNA, but this would need to be compared with untranslated lncRNA to see if its significant.

Future Directions

Beyond this project it would be beneficial to further develop the data relating to the transcript level subcellular expression. This would require curating a dataset manually from published data, by merging other datasets, and/or experimentally determining the subcellular. It would then be possible to place more confidence in the conclusions being made about the relationship between localisation and lncRNA translation. It would also be interesting to compare localisation of the overall gene and that of individual lncRNA transcripts. It might be then possible to identify any exons (or even motifs) which are key for exporting translated lncRNAs.

Furthermore, finding out how much sequence level conservation between the translated lncRNA (in particular within the translated regions), but what may be a necessary first step is to verify no transcripts were given as false negative, especially given that LNCipedia only returned conservation between drosophila and humans, but not any much closely related species. With this conservation data answering whether translated lncRNA are more conserved than their untranslated counterparts would be possible and may also provide hints at whether the observation noticed in Figure 2 has some evolutionary pressure.

expressed compared to translated lncRNAs and mRNA controls. The median number of cell lines in which a translated lncRNA gene (10) was expressed was higher than untranslated (5). This may indicate an underlying evolutionary pressure suggesting a broader function for these translated lncRNAs.

I next sought to establish the sub-cellular localisation of these lncRNA sets in different cell-lines. To start with, I focused on SK.N.SH and SK.N.DZ which were most related to the original neuronal cell-line: SH5Y5Y. In both these cell lines we find that translated lncRNAs are preferentially localised to the cytoplasm and the untranslated lncRNA being preferentially localised in the nucleus (Figure 2).

To assess levels of conservation, data was retrieved from LNCipedia [5], as simple Boolean values for various species. Preliminary results from the translated set of lncRNA, indicated that in most cases it

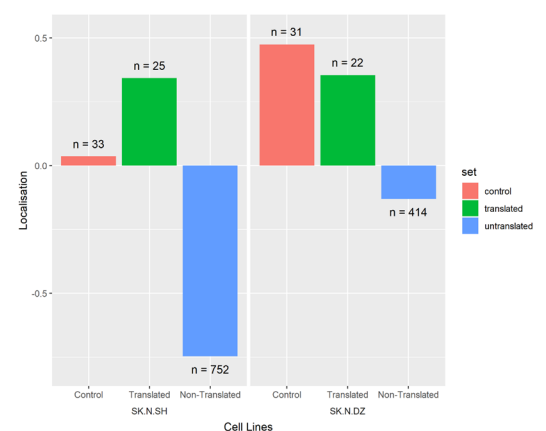


Figure 2 Median localisation of all genes (retrieved from lncATLAS) for the SK.N.SH and SK.N.DZ cell lines

References

- [1] L. Ma, V. B. Bajic, and Z. Zhang, "On the classification of long non-coding RNAs," *RNA Biol.*, vol. 10, no. 6, pp. 924–933, 2013.
- [2] Z. Ji, R. Song, A. Regev, and K. Struhl, "Many lncRNAs, 5'UTRs, and pseudogenes are translated and some are likely to express functional proteins," *Elife*, 2015.
- [3] D. Mas-Ponte, J. Carlevaro-Fita, E. Palumbo, T. H. Pulido, R. Guigo, and R. Johnson, "LncATLAS database for subcellular localization of long noncoding RNAs," *RNA*, 2017.
- [4] T. Derrien *et al.*, "The GENCODE v7 catalog of human long noncoding RNAs: Analysis of their gene structure, evolution, and expression," *Genome Res.*, 2012.
- [5] P. J. Volders *et al.*, "Lncipedia 5: Towards a reference set of human long non-coding rnas," *Nucleic Acids Res.*, 2019.

Characterisation of the Necrosis and ethylene-inducing peptide 1-like protein (NLP) family from *Leptosphaeria* species.

David James, Dr Georgia Mitrousia, Dr Pryank Patel.

Project aims and background

Brassica napus, more commonly known as Oilseed rape, is a major crop used for the production of Rapeseed (Canola) oil. Worldwide, it is one of the largest sources of vegetable oil and, subsequently, protection from disease is vital for its continuing viability as a commercial crop. Winter crops are at a greater risk of the fungal infection phoma stem canker, (Blackleg disease) than the summer crops grown in other regions, so the development of novel methods of pathogen control is vital for both commercial interests and for consumers. The fungal pathogens *Leptosphaeria maculans*, and *Leptosphaeria biglobosa* are responsible for phoma stem canker and infect plants by first establishing themselves as lesions on leaves. The growth of the pathogen continues down the petiole of the leaf, and eventually the stem becomes infected (West, Kharbanda, Barbetti & Fitt, 2001). Severe infection can lead to devastating crop losses, of up to £100 million per year (Mitrousia, Huang, Siddique & Fitt, 2017). This project explored necrosis and ethylene-inducing peptide 1-like proteins (NLPs), which are a family of proteins that have been associated with cell death, ethylene production and immune responses through infection in host organisms, looking at their role in the context of oilseed rape (Feng, et al., 2014). There is evidence to suggest that NLPs are present in both bacteria and fungi as well as oomycetes (Garcia, et al., 2007). NLPs contain key features which are thought to contribute to their ability to trigger cell death, and considered to be important virulence factors (Feng, 2014). Previous research has identified a highly conserved heptapeptide motif thought to play a key role in NLP function (Ottmann, et al., 2009; Schouten, Van Baarlen & Van Kan, 2008). This motif, 'GHRHDWE', forms a cation pocket on the outer surface of the protein and may play a role in binding to glycosylinositol phosphoryl ceramides (GIPCs) on the plasma membrane of plant cells (Lenarčič, et al., 2017; Ottmann, et al., 2009), suggesting that these sphingolipids may act as a possible toxin receptor, presenting a possible mechanism of action. Importantly, NLPs only have an effect upon eudicotyledons, such as oilseed rape, and this is likely due to the difference in length between the GIPCs present in eudicots and monocots (Lenarčič, et al., 2017). Further research has also identified that the NLP receptor is unlikely to be a protein, as protease treatment of membrane vesicles prior to application of NLPs did not prevent their function (Lenarčič, et al., 2018).

In this project, based upon previous findings, mutations were targeted towards aspartate and histidine residues located within a proposed cation pocket of the NLP proteins, as these are thought to be responsible for binding Mg^{2+} and Ca^{2+} ions, and may also play a role in interacting with the polar heads of membrane lipids, involved in inducing responses *in vivo* (Ottmann, et al., 2009). Additionally, hexose sugars were found to bind to a pocket in the protein, and bound Mg^{2+} ions appear to be involved in this interaction, with binding to

hexose causing part of the GIPC to be contained within the protein. (Lenarčič, et al., 2017). This previous work was unable to determine whether the *in vivo* response to NLPs was due solely to Mg^{2+} , or Ca^{2+} ions, but found that calcium chelation treatment prevented NLP activity, and as such determined that it may be Ca^{2+} binding which is crucial, especially given that the proteins act in a calcium-rich environment (Ottmann, et al., 2009). Primarily, this project aimed to explore whether there is a difference in the response to NLPs between two cultivars of *B. napus*, here called G1 and G7, as well as to characterise the specific response, using pre-existing methods to build upon knowledge of these members of a wider family of proteins. Additional work included the production of mutants of the NLP proteins of *L. maculans* and *L. biglobosa*, building upon previous work in similar proteins from other organisms, and exploring whether the characteristics of NLPs are shared within what is widely regarded to be a far reaching, yet highly conserved protein family.

Methods

The first part of the project was dedicated to preparation of recombinant NLP proteins, for use in downstream applications. Expression of the NLPs, NLP_LM1 and NLP_LB, was carried using Rosetta-Gami 2 cells in lysogeny broth (LB) growth media induced with 1 mM IPTG. When expressed, the protein has a small ubiquitin-like modifier (SUMO) tag attached, allowing purification via Ni^{2+} -affinity chromatography. Proteins were purified firstly by following a well-established wash and refolding protocol using either 7M Guanidine-HCl, or 8M Urea (Singh, Upadhyay, Upadhyay, Singh & Panda, 2015), followed by an affinity purification using Nickel-bound HisTrap columns (GE Life Sciences). The proteins were subsequently dialysed into buffer, for infiltration of cotyledons, from which the tag was cleaved using SUMO protease produced in-house. The protein was concentrated using MilliPore Amicon Ultra-15 centrifugal filter units, to the desired final volume, giving a concentration of 4.44 μ M. The second purification of NLP_LM1, with a yield of 4.44 μ M, was washed using urea and gave a considerably higher yield than previous expressions attempted. Further to purification of the NLPs, electrolyte leakage assays were carried out, using purified NLP_LM1 and previously purified NLP_LB, following a protocol from Ottmann, 2009. To carry out the assays, 0.5 μ M of NLP, and NLP buffer were infiltrated into previously germinated and sown *Brassica napus* cotyledons of two different cultivars, G1 and G7, the seeds of which were obtained from John Innes Centre (Norwich, UK). The leaf discs cut without infiltration were used as a blank control. A solution of 10 μ L was used for each infiltration. Leaf discs were cut and rinsed for 30 minutes in 1ml deionised water. After rinsing, and addition of fresh deionised water, conductivity measurements (μ S) were taken at 0, 1, 2, 3 and 4 hours using a FiveEasy F30 Benchtop Meter (Mettler Toledo) as demonstrated in Figure 1.

To confirm the results of the electrolyte leakage assay, an infiltration assay, allowing observation of the phenotypic response to NLP infiltration in dicotyledons over a one-week period, was carried out. In this case, concentrations of 0.5 μ M

and 1 μM recombinant NLP_LB were used, and once again, the protocol was identical to that described by Ottmann, 2009, with the exception of the additional 1 μM NLP_LB solution. NLP buffer alone was also infiltrated, as a control, to confirm that this did not influence phenotype.

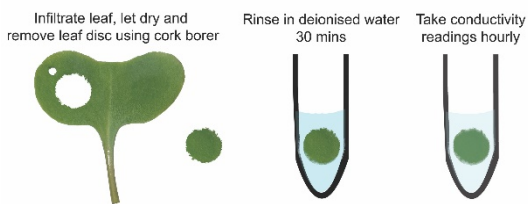


Figure 1: Overview of an electrolyte leakage assay, for the assessment of the cytotoxic effects of NLPs in *Brassica napus*.

Due to the arrangement of cotyledons in *B. napus*, it is possible to infiltrate both concentrations of NLP as well as NLP buffer and also retain a blank portion, on each plant. The arrangement of infiltration is shown in Figure 2, with the punch hole indicating the orientation.

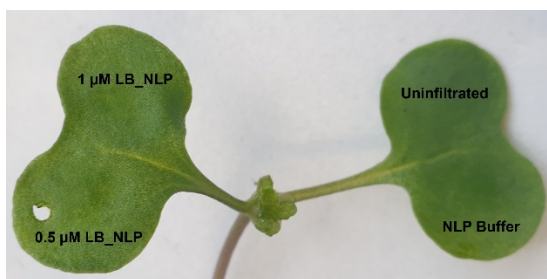


Figure 2: Diagram demonstrating the arrangement of infiltration of NLP and buffer into each cotyledon.

The final part of the project aimed to produce mutant NLP proteins, with mutations targeted to a specific motif in each protein, GHRHDWE, which is thought to play a major role in the function of NLPs *in vivo*. As such, we wished to ascertain whether the same was true of NLPs *in vivo*. To generate mutants, site-directed mutagenesis was

carried out, using a Q5 SDM kit (New England Bioscience). The PCR programme was run as follows:

Initial denaturation- 98°C- 2 minutes
25 Cycles- 98°C- 20 seconds (Denaturation)
 55°C- 30 seconds (Annealing)
 68°C- 7 minutes (Extension)
Final extension- 68°C- 8 minutes

The resulting mutant PCR products were treated with a KLD enzyme mix, which contains the endonuclease *DpnI* and thus cleaves the template DNA, while also phosphorylating and circularising the desired PCR product. Following this, DH5- α derivative competent cells were transformed with the mutant construct, and plated. Colony PCR was used to confirm the identity of colonies, using the designed mutant primers. and plasmid DNA was extracted from these using a GenElute MiniPrep kit (Sigma-Aldrich).

Results

The results for the NLP_LB infiltration assay (Figure 3) demonstrate that there is a phenotypic difference between the cultivars G1 and G7. In G7, NLP_LB at a concentration of 0.5 μM , induced small areas of necrosis and chlorosis, and at a concentration of 1 μM , these regions are particularly pronounced. In G1, this phenotype is not observed at either concentration. Additionally, the controls show that there is no response to infiltration of buffer, or in uninfiltrated leaves. Further studies would be needed to determine the cause of this phenotypic difference, but the difference in the response between cultivars is significant. Results for the electrolyte leakage assays (Figures 4-5) were analysed using a two-way ANOVA, and a Tukey's multiple comparisons test. The results show that there is a significant difference in the conductivity increase between infiltration of NLP and NLP buffer and NLP and uninfiltrated leaf discs, in G7 but not in G1 ($P < 0.01$ for NLP vs. NLP buffer in G7), for NLP_LB. For NLP_LM1, the result is also significant ($P < 0.05$ NLP vs. NLP buffer in G7),

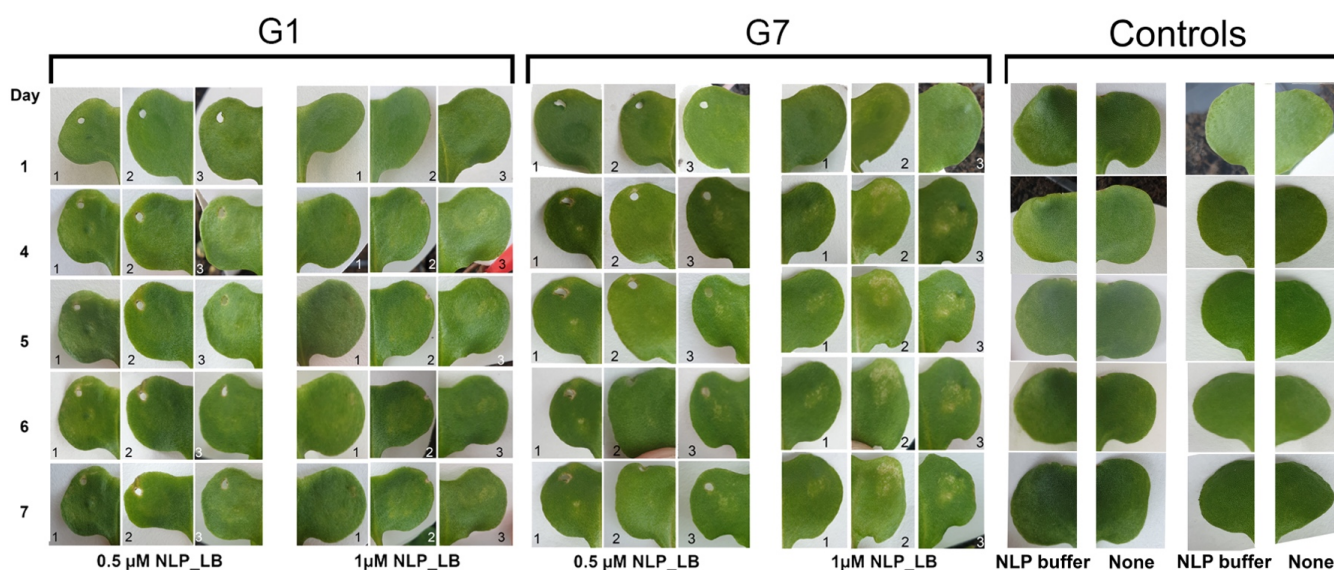


Figure 3: An infiltration assay for infiltration of 0.5 μM and 1 μM NLP_LB in the *Brassica napus* cultivars G1 and G7, demonstrating the necrotic response in each cultivar over a seven-day period. The difference in response between G1 and G7 closely mirrors the trends seen in the electrolyte leakage assay with the same protein, indicating a difference in response between the two cultivars.

from hours 2-4, but not at hour 1. It is of note that the data from the electrolyte leakage assays, and that obtained from the infiltration assays, is concordant. The results highlight a clear phenotypic and quantitative difference in the response to identical NLP infiltration, between cultivars. This presents an interesting proposition that there may be a degree of insensitivity to NLP activity within one of the cultivars, this

Departures from the original proposal

Whilst most of the project aims were met, we were unable to complete a few of them, due to time constraints. In particular, while one NLP mutant, LM1 H126G, was produced, we were unable to carry out expression trials, and as such, unable to use any expressed protein to carry out infiltration or electrolyte leakage assays. Therefore, it is still not yet known whether these mutants act differently *in vivo*. However, the production

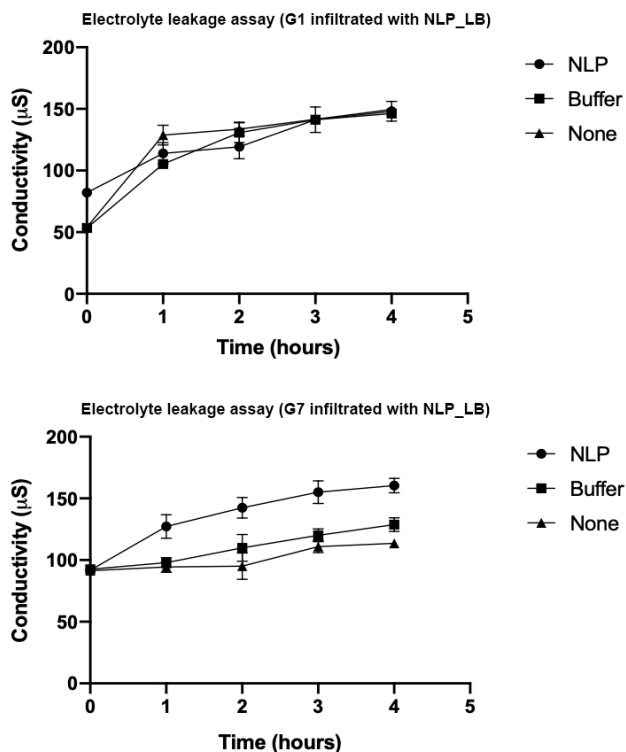


Figure 4: Electrolyte leakage assays for NLP_LB in the cultivars G1 and G7. The graphs demonstrate a significant difference ($P < 0.05$) in conductivity between NLP buffer and NLP_LB as well as between uninfiltrated leaf discs and NLP_LB at all time points in G7 but at no time points in G1, indicating a difference in response to infiltration with NLP_LB between cultivars.

being G1. However, as the studies have not focused upon the differences in gene expression in response to NLP infiltration, we cannot speculate a mechanism by which the response differs. As such, it is wise to include this as a potential avenue for further work.

Regarding SDM work, the resultant amplicons have, as of yet, not been sequenced, and as such no comment can be made regarding the efficacy of mutant production.

Future directions

As previously discussed, it is necessary to further explore the significance of response differences between the *B. napus* cultivars G1 and G7. Additionally, the monitoring of changes in gene expression, specifically genes associated with pathogenic responses, such as *PR1* and *PAD3* should be carried out, in tandem with infiltration assays. Monitoring mRNA changes for these, and potentially other genes, via RT-qPCR will give a greater insight into what is happening at a molecular level.

Further to this, the confirmation of mutants, and expression of these, is vital to verify that the behaviour of these NLPs, *in vivo*, and the significance of the conserved motif, matches that of those previously characterised.

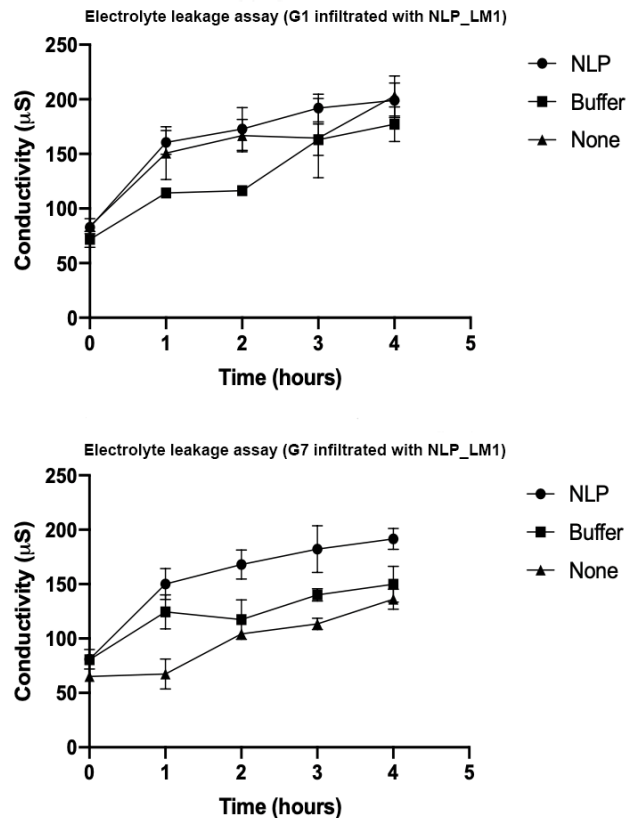


Figure 5: Electrolyte leakage assays for NLP_LM1 in the cultivars G1 and G7. The graphs demonstrate a significant difference ($P < 0.05$) in conductivity between NLP buffer and NLP_LM1 2-4 hours post infiltration in G7, but at no time points in G1, indicating a difference in response to infiltration with NLP_LM1 between cultivars.

of one mutant means that the PCR protocol has been optimised for future use, and that there is potential for these mutant proteins to be further explored in the future.

Value of the studentship to the student and lab

I have learned a great deal from spending time in a research laboratory. In particular, I feel that it has better equipped me with knowledge of how research works, and how to deal with setbacks, and as such feel that it has encouraged me to pursue a career in scientific research. Additionally, it has given me valuable hands-on experience. It has definitely encouraged me to consider further post-graduate study after my undergraduate degree is completed.

References

- Feng, B. Z., et al. (2014). *BMC Plant Biol.*, 14, 126.
- Garcia, O., et al. (2007). *Mycol. Res.*, 111(4), 443-455.
- Lenarčič, T., et al. (2017). *Science*, 358(6369), 1431 LP-1434.
- Mitrousis, G. K., et al. (2018). *Plant Pathol.*, 67(6), 1339-1353.
- Ottmann, C., et al. (2009). *PNAS*, 106(25), 10359 LP-10364.
- Schouten, A., et al. (2008). *New Phytol.*, 177(2), 493-505.
- Singh, A., et al. (2015). *Microb. Cell Fact.*, 14, 41.
- West, J. S., et al. (2001). *Plant Pathol.*, 50(1), 10-27.

Using PCR as a technique for the development of an ultrasensitive assay for the diagnosis of Type 1 Diabetes.

Jack Eames, Dr Michael Christie
School of Life Sciences – University of Lincoln



Abstract

Manipulating the power of qPCR has led to an immunoassay that is up to 10,000 times more sensitive than others - can it now be used to early diagnose Type 1 Diabetes? qPCR was used to amplify DNA fragments between the immunocomplexes to gain data about the amount of antibodies present in the samples. The positive samples gave a mean cycle time of 5.49, whilst the negative samples gave a mean cycle time of 5.61. There was no differentiation between the samples, however diagnostics of the techniques involved will help us locate the faults within the assay.

Introduction

The production of an ultrasensitive assay for the early detection of Type 1 Diabetes is crucial for patients who are at high risk of developing the autoimmune disease; this early detection would consequently mean that treatment could be implemented earlier, such as immune intervention therapy, resulting in the progression of the disease slowing down and preventing secondary complications (Villalta *et al.*, 2005; Naserke *et al.*, 1998). Conventional assays used in clinical settings, such as Luciferase Immunoprecipitation system (LIPS) and Radioimmunoassay (RIA), vary in their sensitivity to detect low levels of antibodies – this was predominantly highlighted by recent international workshops designed to standardise the detection of antibodies associated with Type 1 diabetes. Antibody detection by agglutination PCR (ADAP) is recognised as being up to 10,000 times more analytically sensitive than other clinical enzyme-linked immunoassays, enabling this new assay to become the forefront of autoimmunity diagnosis (Tsai *et al.*, 2018). The ADAP platform works by manipulating the multivalent binding properties of antibodies to power the agglutination of antigen-DNA conjugates; this proximity then enables ligation of DNA fragments to form full-length DNA amplicon, which can then be quantified by the use of qPCR – the quantification can then be used to calculate the levels of antibodies present in the sample (Tsai *et al.*, 2018).

Aims

With international workshops highlighting that there wasn't an assay with a high enough sensitivity to standardise globally, we aimed to create one that would defeat this variation in sensitivity and give forth to a new early detection system for Type 1 Diabetes. We aimed to do this by:

- Coupling DNA tags to target proteins
- Incubating DNA-tagged proteins with serum samples
- Capturing antibody-protein complexes and amplifying the DNA tags

Methods

The methodology was derived from Tsai *et al.* (2016) and Tsai *et al.* (2018):

5µl of each serum sample was added to a v-bottom well plate in duplicates. A mix of 4A and 4B conjugated IA2-GST antigen were diluted by IMP buffer to create a 1:20 dilution - 20µl of the diluted antigen was then added to each well and it was incubated overnight for the immunocomplexes to form. 10µl of 50% suspension Protein A Sepharose was added to each well and shaken for 30 minutes. Contents of each well were then transferred to corresponding 0.5ml Eppendorf tubes; wells were additionally washed twice with 100µl of water, also being transferred to the appropriate tube. The Eppendorf tubes underwent centrifugation at 5000 RCF for 2 minutes, with the supernatant being aspirated with a vacuum pump afterwards – the pellet was washed a further 3 times with 0.5ml IMP Buffer and 2 times with 0.5ml Molecular Water (supernatant aspirated each time). 10µl of Master Mix (340µl Molecular Water, 60µl Ampligase Buffer, 0.6µl Bridge Oligo, 2.4µl Ampligase Enzyme) was added to each tube and then incubated at 37°C for 30 minutes. Contents of each Eppendorf were then transferred to a PCR plate ready for preamplification, with 35µl of Master Mix (910µl Molecular Water, 400µl 5x GoTaq Clear Buffer, 40µl Nucleotide Mix, 20µl Forward Primer, 20µl Reverse Primer, 10µl GoTaq Polymerase) – contents of plate then amplified by PCR (95°C for 10 min, 95°C for 15s, 56°C for 30s, 12 cycles). After amplification, all samples were diluted 1:20 and transferred to 0.2ml qPCR tubes and ran on a real-time qPCR machine (95°C for 10 min, 95°C for 30s, 56°C for 1 min, 40 cycles).

Results

The results came back inconclusive from the immunoassay, with no clear differentiation amongst the volunteer (negative samples) and positive patient samples. The negative samples gave fluorescence readings within close proximity of that of the positive samples (shown in both figure 1 and 2). The positive samples gave a mean cycle time (ct) (taken at the threshold) of 5.49,

whilst the negative samples gave a mean cycle time of 5.61.

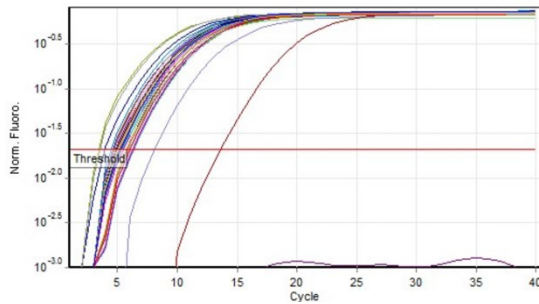


Figure 1: Fluorescence signal emitted at interval cycle times for each sample.

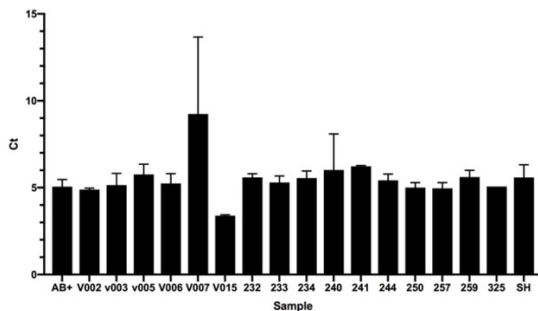


Figure 2: Cycle time for each sample at a fluorescence signal of $10^{-1.7}$.

Discussion

The positive samples would be expected to appear earlier during the fluorescence reading as immunocomplexes would've allowed the ligation of DNA fragments and consequently full-length DNA amplicons to form. Additionally, antigen should've been washed away for the negative samples during the capturing stage as no immunocomplexes should've formed due to the absence of antibodies – this consequently means that no signal should've been obtained from the negative samples during qPCR. We came to theorise three ideas that may have resulted in this lack of differentiation: Firstly, there might be some non-specific binding within our samples that is allowing the antigens, in the absence of antibodies, to proceed to the later stages of the assay and thus produce false positive results. Secondly, we thought that the temperatures suggested in similar papers may not be specific for our antigen and that is allowing any other proteins/DNA to be replicated and emit a signal. And finally, we believe that our capturing system using the Protein A Sepharose might still be allowing foreign material to remain in our samples.

This led us onto running many diagnostic trials to try and discover what was wrong with the assay. We ran gradient preamplification PCRs to try and discover an optimum temperature for the reaction

to occur under, our results actually indicating that an annealing temperature of approximately 68°C produced a better distinction between the results, especially when compared to that of lower temperatures. Tests were performed to see if primer dimers were forming within the samples and if this formation is what emitted false signals across the samples, however an agarose gel showed us that this wasn't occurring, leading us on to further conclude that it maybe be due to non-specific binding.

Studentship

I had a great time working on this summer project with my supervisor Mike; I feel that it's given me a good-grounding for my third year research project and allowed me to reaffirm my love for laboratory research. It's allowed me to see the problem solving and specific techniques involved with conducting research, as well as teaching me that not everything will always work first time around.

Acknowledgements

I would like to give a thank you to Dr Michael Christie for allowing me the opportunity to collaborate on this project, as well as a thank you to Dr Forough Torabi Baghkomeh, Melissa Tombs and Chelsy Cliff for providing me support throughout my studentship.



References

- Naserke, H.E., Ziegler, A.G., Lampasona, V. and Bonifacio, E. (1998) Early development and spreading of autoantibodies to epitopes of IA-2 and their association with progression of Type 1 Diabetes. *Journal of Immunology*, 161(12) 6963-6969.
- Tsai, C.T., Robinson, P.V., Cortez, F.D., Elma, M.L.B., Seftel, D., Pourmandi, N., Pandori, M.W. and Bertozzi, C.R. (2018) Antibody detection by agglutination-PCR (ADAP) enables early diagnosis of HIV infection by oral fluid analysis. *Proceedings of the national academy of sciences of the United States of America*, 115(6) 1250-1255.
- Tsai, C.T., Robinson, P.V., Spencer, C.A. and Bertozzi, C.R. (2016) Ultrasensitive Antibody Detection by Agglutination-PCR (ADAP). *ACS Central Science*, 2(3) 139-147.
- Villalta, D., Renato, T.B., Tonutti, E. and Bizzaro, N. (2005) The laboratory approach to the diagnosis of autoimmune disease: Is it time to change? *Autoimmunity Reviews*, 6(6) 359-365.

The importance of the RNA exosome in childhood-onset neurological diseases and neurodegeneration

Student: Annabel Kunzemann Supervisor: Dr Claudia Schneider
The Institute of Cellular and Molecular Biosciences, Newcastle University



Introduction

A vital participant in ribosome maturation is the RNA exosome: an evolutionarily conserved, ribonuclease complex composed of nine catalytically inert protein subunits and associated enzymes (1). Defects in the ribosome biogenesis pathway provokes stabilisation of the tumour-suppressor p53, resulting in cell cycle arrest and apoptosis. Mutations in genes encoding the exosome subunits EXOSC3, EXOSC8 and EXOSC9 cause childhood-onset neurodegenerative diseases ('exosomopathies') such as spinal muscular atrophy and cerebellar hypoplasia (2). Yet, the impact of such mutations on human ribosome production and associated p53-dependent signalling pathways, which may lead to apoptosis, is unclear.

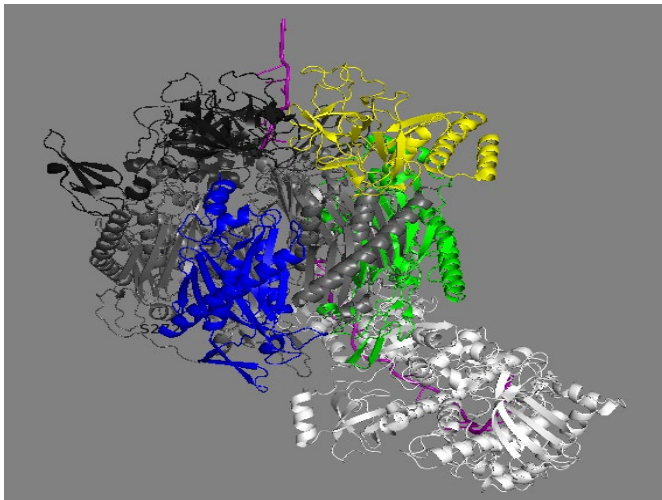


Figure 1 Structure of the Human Nuclear Exosome. EXOSC3 in yellow, EXOSC8 in blue, EXOSC9 in green and RNA in pink. Modified from (3).

Under normal cellular conditions, the ubiquitin-protein ligase MDM2 binds p53 leading to its degradation. Defects in the ribosome biogenesis pathway cause MDM2 to take a divergent route and bind the 5S RNP, a critical complex that forms part of the large subunit of the ribosome. This provokes the stabilisation of the tumour-suppressor p53, ultimately leading to programmed cell death (4).

Project Aims

The first aim of my project was to assess how depletion of core exosome subunits such as EXOSC3 and EXOSC8 affects ribosome production and p53 levels in HCT116 cells.

My second aim was to create human expression plasmids through the cloning of the RNAi-resistant wild-type EXOSC3

gene into a pcDNA5 plasmid. This EXOSC3-pcDNA5 plasmid would be modified to produce EXOSC3 mutants such as those present in 'exosomopathies'.

My third aim was to perform a tetracycline induction in HCT116-FlpIn cells containing a wild-type or mutant EXOSC8-pcDNA5 plasmid with a tetracycline promoter already available in the lab. The tetracycline concentration at which the endogenous and exogenous EXOSC8 levels are the same is an accurate depiction of the concentration of tetracycline required to mimic native conditions.

Methods

Depletion of core exosome subunits EXOSC3 and EXOSC8

A siRNA-mediated 3-day knockdown of core exosome components in HCT116 cells (colorectal cancer cell line) was carried out in a 24-well plate with 40,000 cells in each of 3 wells corresponding to GL2 control, EXOSC3 and EXOSC8 knockdowns. Knockdowns were then harvested, a pellet obtained and a Western Blot conducted. In turn, qualitative and quantitative analysis of different protein levels (i.e. p53, EXOSC3, EXOSC8) was carried out.

Creating human expression plasmids encoding wild-type and mutant FLAG-tagged versions of EXOSC3

Through blunt end cloning, a wild-type EXOSC3 gene was inserted into a 'shuttle' PJET vector. This plasmid was later inserted into *E. coli* cells via an *E. coli* transformation. Cell cultures were set up to amplify these *E. coli* cells followed by a plasmid mini prep to solely extract plasmid DNA. A restriction digest was carried out to cut out EXOSC3 from the 'shuttle' vector. This preliminary step was performed so that EXOSC3 could then be ligated into a pcDNA5 vector through the same procedure as detailed above. Then, site-directed mutagenesis of the EXOSC3-pcDNA5 plasmids was conducted in a PCR reaction. After producing each plasmid, DNA was sent for sequencing to ensure that the ligation and mutagenesis was successful.

Performing a tetracycline induction in HCT116-FlpIn cells containing wild type and mutant pcDNA5-EXOSC8 plasmids

The induction was carried out in a 24-well plate with 40,000 cells in each well. Wild-type EXOSC8, EXOSC8-A2V (Mutant 1), EXOSC8-S272T (Mutant 2) were used with tetracycline concentrations 0, 1, 100, 10,000 ng/ml. Cells were incubated for 3 days, pellets obtained and a Western blot conducted.

Results and discussion

Western blot of siRNA-mediated knockdowns of EXOSC3 and EXOSC8 in HCT116 cells:

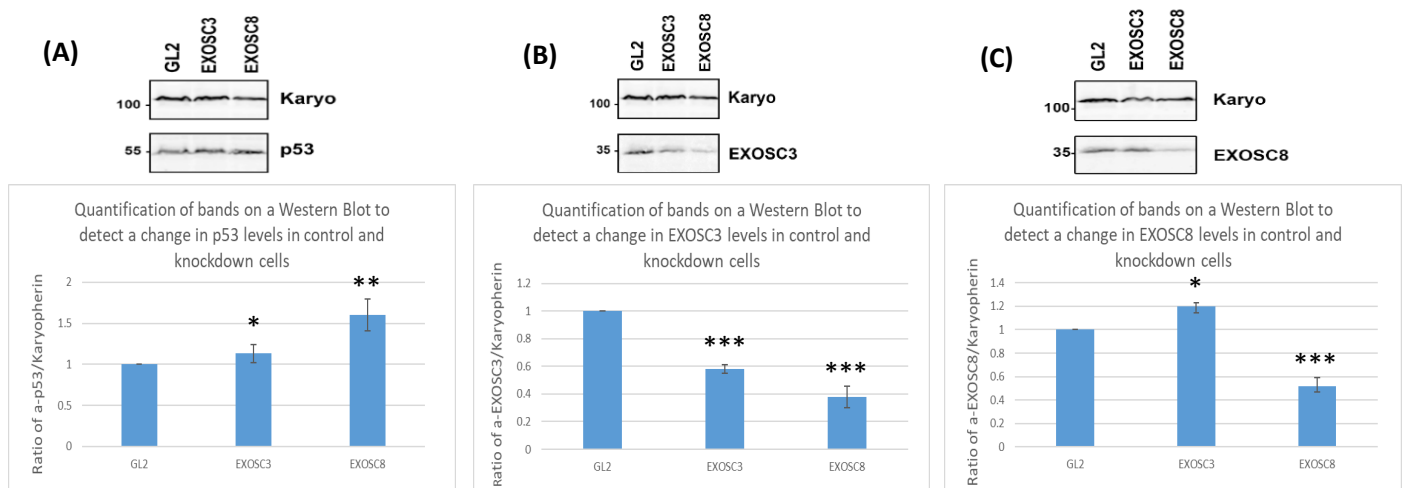


Figure 2 (A) Western Blot of GL2 (control), EXOSC3 and EXOSC8 knockdowns probed with antibodies α -Karyopherin (~100kDa) and α -p53 (55kDa). The graph below shows the change in p53 levels in the knockdowns compared to GL2. (B) Western Blot of GL2, EXOSC3 and EXOSC8 knockdowns probed with antibodies α -Karyopherin (~100kDa) and α -EXOSC3 (~30kDa). The graph below shows the change in EXOSC3 levels in the knockdowns compared to GL2. (C) Western Blot of GL2, EXOSC3 and EXOSC8 knockdowns probed with antibodies α -Karyopherin (~100kDa) and α -EXOSC8 (~30kDa). The graph below shows the change in EXOSC8 levels in the knockdowns compared to GL2. Error bars represent standard error and statistical analysis was performed using an unpaired t-test. *p* values: <0.05 (*), <0.01 (**), <0.001 (***). Results are significant and not due to chance.

In the Western blot, α -Karyopherin was used as a loading control, which allowed for a comparison between the overall protein levels and other specific proteins (i.e. p53). My results showed that p53 levels rose in knockdowns EXOSC3 and EXOSC8 when compared to the control as indicated in the graph in Figure 2(A). As shown in Figure 2(B), a knockdown of EXOSC3 decreases levels of EXOSC3. Interestingly, a knockdown of EXOSC8 also decreases levels of EXOSC3 but to an even larger extent than an EXOSC3 knockdown. This implies that EXOSC3 stability is dependent on the presence of EXOSC8. EXOSC8, being part of the core exosome may act as a structural support for EXOSC3, which assembles as part of a cap on top (see Figure 1).

Western Blot of Tetracycline induction in HCT116-FlpIn cells expressing wild-type and mutant EXOSC8-pcDNA5 plasmids:

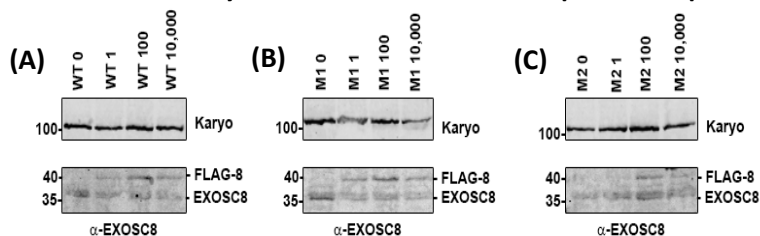


Figure 3 Western blot of cells with (A) wild type EXOSC8 pcDNA5 plasmid (WT), (B) EXOSC8-A2V pcDNA5 plasmid (M1), (C) EXOSC8-S272T pcDNA5 plasmid (M2). Each wild type and mutant cell line was treated with an increasing concentration of tetracycline: 0, 1, 100, 10,000 ng/ml. All samples were probed with α -Karyopherin at ~100kDa and α -EXOSC8 at ~35-40kDa. FLAG-8 at ~40kDa corresponds to EXOSC8 with a FLAG tag expressed from the exogenous plasmid which is heavier than the endogenous EXOSC8 at ~35kDa.

The expression of endogenous EXOSC8 at ~35kDa remained relatively constant across the samples. As shown in Figure 3(A), expression of wild-type FLAG-8 increased with increasing tetracycline concentrations because of the presence of a tetracycline promoter in the pcDNA5 plasmid. Expression of Flag-8-S272T (M2) is lower compared to wild type. Despite mutations EXOSC8-A2V and EXOSC8-S272T, FLAG-EXOSC8 is still expressed in these mutants.

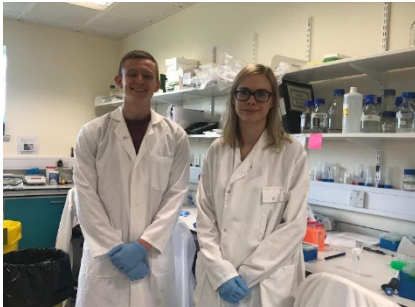
Future directions: The HCT116-FlpIn cells containing pcDNA5-EXOSC8 mutant plasmids were frozen at -80° and will be used in further experiments to assess p53 levels in wild-type compared to mutant cell lines.

Departures from original proposal: Following the creation of human expression plasmids encoding RNAi-resistant mutant versions of EXOSC3, a transient transfection of these mutants into HCT116-FlpIn cells was intended to be carried out to discern if the mutations affect protein stability. However, the cells became infected and due to time constraints, this was not retried.

Value of studentship: This studentship was very enjoyable and of great value to me. It was very inspiring to work around research experts on a project in a subject area that greatly interests me. I learned a range of new scientific techniques and methods such as RNAi-mediated knockdowns of endogenous proteins, site-directed mutagenesis using PCR and analysis of protein levels using western blots. Most importantly, it has provided me with an insight of what a career in research would entail and orientated me in possible career options.

References:

- (1) Schuller J, Falk S, Fromm L, Hurt E, Conti E. Structure of the nuclear exosome captured on a maturing preribosome. *Science*. 2018;360(6385):219-222.
- (2) Müller J, Giunta M, Horvath R. Exosomal Protein Deficiencies: How Abnormal RNA Metabolism Results in Childhood-Onset Neurological Diseases. *Journal of Neuromuscular Diseases*. 2015;2(s2):S31-S37.
- (3) Weick, E.M., Puno, M.R., Januszky, K. *et al.* Helicase-Dependent RNA Decay Illuminated by a Cryo-EM Structure of a Human Nuclear RNA Exosome-MTR4 Complex. *Cell*. 2018;173: 1663.
- (4) Sloan K, Bohnsack M, Watkins N. The 5S RNP Couples p53 Homeostasis to Ribosome Biogenesis and Nucleolar Stress. *Cell Reports*. 2013;5(1):237-247.



Student:
**Matt
Graham**
Supervisor:
**Sophie
Nyberg**

Background

Amyotrophic lateral sclerosis (ALS) is a fast progressing neurodegenerative disease, categorised by the targeted destruction of both upper and lower motor neurones. Prognosis is poor, with the onset of death usually seen within 5 years as a result of neuromuscular respiratory failure. ALS is as complex as it is devastating, with a multitude of mutations contributing to a range of different molecular pathways that lead to motor neurone death: oxidative stress, excitotoxicity, neuro-inflammation and protein aggregation are just a small sample of these [1]. Furthermore, approximately 10% of cases are familial (fALS), whilst 90% are sporadic (sALS); of the former, 70% of the causative genes are known (such as C9orf72 and SOD1) whereas only 15% of these genes are known in the latter. Therein lies the complexity of treating ALS; ambiguous genetic origins eliciting a variety of molecular pathways in patients, that all ultimately conclude in motor neurone death. Animal models of ALS are largely limited to the SOD1^{G93A} mutation. However, the disease can also be modelled in human cells by genetically reprogramming patient fibroblasts into motor neurones and their support cells, such as astrocytes. Such models of ALS have elucidated toxic factors secreted by the astrocyte as causing destruction of motor neurones in ALS [2]–[5].

Less well documented is the role diseased astrocytes may have on the integrity of the Blood Brain Barrier (BBB). The BBB is composed of a tight junction of endothelial cells that lines blood vessels in the brain, selectively allowing the entrance of specific molecules. The BBB poses a challenge in developing novel drugs for ALS as it prevents the entry of >98% of small molecule drugs. There is therefore an impetus to develop a unique *in vitro* human ALS model of the BBB in order to explore new treatments for the disease. Such is the efficacy of the healthy BBB that it has become a major clinical challenge developing drugs that can penetrate it. As such, there is also a requirement to develop a healthy *in vitro* model of the BBB in order to test the penetrative capacity of new drugs.

Project Aims

The primary aim of this project is to develop an ALS disease model of the BBB utilising a novel triple co-culture of motor neurones, astrocytes and BBB cells. We postulate that this model could be used to study the impact diseased astrocytes of different genetic subtypes have on barrier integrity. In

doing so, we hope to provide a model upon which new treatments for ALS can be explored. In conjunction with this, we aim to develop a healthy model of the BBB in order to establish a method of testing the ability of new drugs to penetrate the BBB.

Methods

This project was carried out with several different induced pluripotent stem cell lines (iPSCs): MIFF, GM and CS. All were obtained from healthy control donors.

Differentiating human derived iPSCs: the initial protocol used to differentiate iPSCs into brain endothelia was based on the work carried out by *Lippman et al* [6][7]. Human derived iPSCs were first expanded on a Matrigel coated 6 well plate in a culture of E8 medium. After 3 days, differentiation was initiated by switching to unconditioned media (UM) which was replaced daily for 5-6 days, leaving a mixture of Neuronal Precursor Cells (NPCs) and endothelial cells. The media was then changed to Endothelia Media (EM) in order to drive a more specific line of endothelial differentiation. This media was replaced every 2 days for 10 days, and supplemented with 20 ng/ml basic Fibroblast Growth Factor (bFGF) every 3 days. 10 μ M of Retinoic Acid (RA) was added directly to each well plate daily.

Endothelial Purification: for each cell line, a 6 well plate and a 96 well plate were coated with 20 μ g/ml fibronectin and 0.5 mg/ml type I collagen, and both were incubated for 4 hours. The mixed population of NPCs and endothelia were lifted from the well plates using an Accutase incubation period of 5 minutes at 37°C. These cells were placed in EM and centrifuged at 200g for 4 minutes. The resulting pellet was re-suspended, and the number of cells counted using a haemocytometer. This value dictated the cell density that was seeded on to each of the coated well plates.

Characterising the BBB cells: the early BBB model was interrogated using Western Blots, Immunocytochemistry staining and quantitative PCR (qPCR). We define BBB endothelial cells as those that express endothelial markers such as nestin, in addition to highly upregulated expression of tight junction markers (ZO-1 and occludin) and specific transporter proteins (PGP, Glut-1 and PepT).

Astrocyte, motor neurone and endothelia co-culture: once fully differentiated, endothelial cells were seeded on to a 96 well plate and exposed to a number of triple co-cultures, making up a healthy control and 2 disease models:

- Endothelia + healthy iAstrocytes + motor neurones
- Endothelia + SOD1 iAstrocytes + motor neurones
- Endothelia + C9orf72 iAstrocytes + motor neurones

Each culture condition was imaged after 1 day and after 3 days using an InCell high throughput screening microscope. The number of surviving motor neurones were calculated in each condition using semi-automated software, with the corresponding rate of motor neurone survival calculated.

Results and Discussion

Through a series of Western Blots, qPCRs and extensive imaging techniques, we were able to demonstrate the successful differentiation of endothelial cells specific to the BBB.

Analysis of the BBB proteins: PGP is a drug efflux transporter protein that is highly upregulated within the BBB. Western Blot analysis of our MIFF and GM cell lines demonstrated high levels of PGP upregulation when compared to the standard human umbilical vein endothelial cell line HUVEC. This result was further validated by the immunocytochemistry staining of PGP within these cells (figure 1).

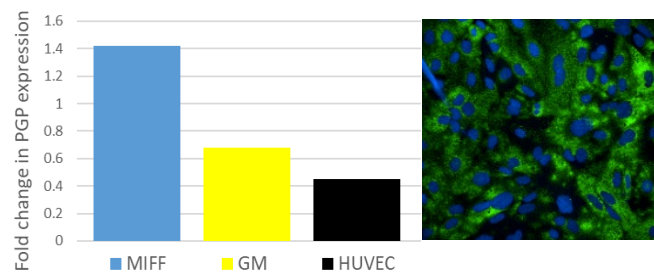


Figure 1: (left) quantitative western results displaying PGP upregulation within the MIFF and GM cell lines; (right) immunocytochemistry staining for PGP (green).

Other transport proteins specific to the BBB were also highly upregulated within the cells. qPCR analysis showed a 13x fold increase in *SLC15A1* expression (a gene coding for the peptide transporter PepT 1 found within the BBB) in the GM cell line when compared to the HUVEC cell line (figure 2). Within this analysis, the tight junction marker occludin was also shown to be upregulated within both the MIFF and GM cell lines; a 5x and 20x fold increase were seen respectively. The same qPCR delivered an interesting result in the upregulation of nestin within the MIFF cell line. Whilst traditionally thought to be an NPC marker, emerging evidence suggests that nestin is expressed within proliferating endothelial progenitor cells, which this result corroborates [8].

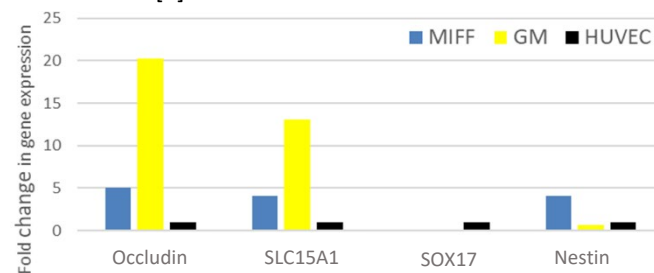


Figure 2: qPCR analysis displaying high upregulation of occludin and *SLC15A1*, and the presence of nestin within the MIFF cell line.

Further immunocytochemistry staining revealed high levels of the tight junction markers Z-O1 and occludin, and the glucose transporter Glut-1 (figure 3). The combination of these proteins is highly characteristic of endothelia found within the BBB. The complete absence of any SOX17 (a BBB marker present within the Wnt/ β -catenin signalling pathway) implies the primer may not have worked.

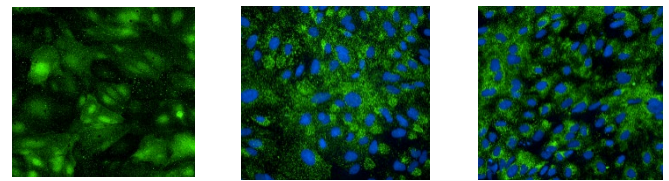


Figure 3: immunocytochemistry staining of: (left) occludin, (middle) Z-O1 and (right) Glut-1. The abundance of all 3 proteins is indicative of BBB endothelia.

Analysis of the ALS disease models: using high throughput microscopy imaging, the 3 different triple co-cultures were imaged after day 1 and day 3 (figure 4).

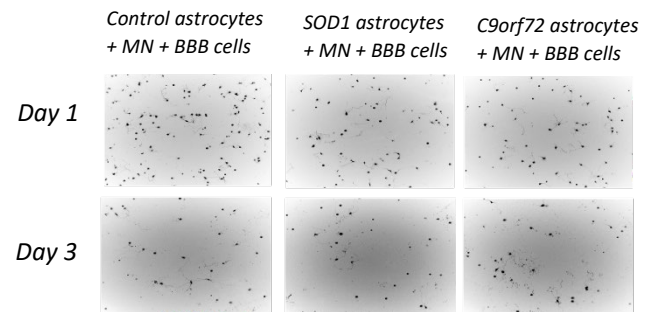


Figure 4: high throughput images displaying motor neurones in each of the triple co-cultures after day 1 and day 3.

In order to assess the viability of this triple co-culture model, the number of surviving motor neurones on day 3 were calculated (figure 5).

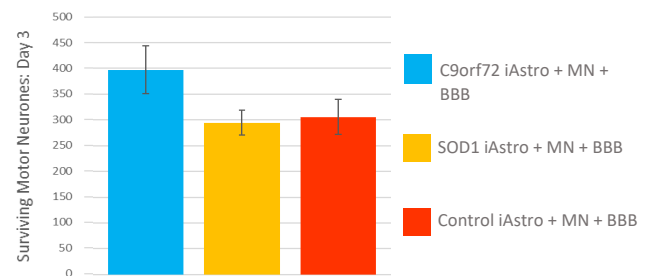


Figure 5: ratio of surviving motor neurones day3:day1.

Figure 5 displays a higher rate of motor neurone survival within the healthy control model when compared to the 2 ALS disease models. This corresponds with the existing literature, where it has been well documented through novel co-cultures that ALS diseased astrocytes are toxic to motor neurones [9]. Figure 6 builds on this result by proving that these diseased astrocytes are also toxic to BBB endothelial cells. This simultaneously increases the validity of the model, whilst also providing evidence for the pertinence of the BBB within ALS.

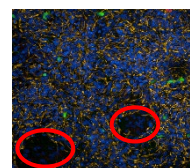


Figure 6: staining showing BBB endothelial cells (CS cell line) growing away from SOD1 astrocytes (circled in red).

Future Work

Further optimisation is required in to form a continuous monolayer of endothelia, which can then be used as a BBB permeability assay e.g. for drug screening. The effect of astrocyte-mediated toxicity to the BBB, and how this may affect motor neurones, also requires further investigation.

Acknowledgements

I would like to thank the Biochemical Society for providing me with the opportunity to undertake this project through their Student Summer Vacation Studentship. The studentship first exposed me to the process of applying for a grant, an experience that will be invaluable as I hope to commence a PhD in regenerative medicine next year. The project also gave me the opportunity to experience the realities of scientific research; both the excitement felt after a successful experiment, and the frustration that comes with disappointing results. In such, the studentship allowed me to develop my resilience and perseverance;

both intrinsic to a career in research. I was also able to develop a variety of technical lab skills – including cell culture, western blotting, immunocytochemical staining and qPCR – which will stand out upon applications to PhD positions.

I would also like to thank Sophie Nyberg, and all the other researchers in Laura Ferraiuolo's lab, for making me feel so welcome throughout the placement and providing me with advice and guidance whenever it was needed. In turn, I was able to help Sophie with day to day experiments, carry out repeat experiments unsupervised and validate her results.

References

- [1] L. Ferraiuolo, J. Kirby, A. J. Grierson, M. Sendtner, and P. J. Shaw, "Molecular pathways of motor neuron injury in amyotrophic lateral sclerosis," *Nat. Rev. Neurol.*, vol. 7, no. 11, pp. 616–630, 2011.
- [2] A. M. Haidet-phillips *et al.*, "Astrocytes from Familial and Sporadic ALS Patients are Toxic to Motor Neurons," vol. 29, no. 9, pp. 824–828, 2012.
- [3] M. et al Nagai, "Astrocytes expressing ALS-linked mutated SOD1 release factors selectively toxic to motor neurons," vol. 10, no. 5, pp. 615–622, 2013.
- [4] K. Meyer, L. Ferraiuolo, C. J. Miranda, S. Likhite, S. Mcelroy, and S. Renusch, "Direct conversion of patient fibroblasts demonstrates non-cell autonomous toxicity of astrocytes to motor neurons in familial and sporadic ALS," vol. 111, no. 2, pp. 829–832, 2014.
- [5] F. Paolo, D. Giorgio, G. L. Boulting, S. Bobrowicz, and K. C. Eggan, "Human Embryonic Stem Cell-Derived Motor Neurons Are Sensitive to the Toxic Effect of Glial Cells Carrying an ALS-Causing Mutation," *Stem Cell*, vol. 3, no. 6, pp. 637–648, 2008.
- [6] E. S. Lippmann *et al.*, "Derivation of blood-brain barrier endothelial cells from human pluripotent stem cells," *Nat. Biotechnol.*, vol. 30, no. 8, pp. 783–791, 2012.
- [7] E. K. Hollmann, A. K. Bailey, A. V Potharazu, M. D. Neely, A. B. Bowman, and E. S. Lippmann, "Accelerated differentiation of human induced pluripotent stem cells to blood – brain barrier endothelial cells," *Fluids Barriers CNS*, pp. 1–13, 2017.
- [8] S. Suzuki, J. Namiki, S. Shibata, Y. Mastuzaki, and H. Okano, "The Neural Stem / Progenitor Cell Marker Nestin Is Expressed in Proliferative Endothelial Cells , but Not in Mature Vasculature The Journal of Histochemistry & Cytochemistry," vol. 58, no. 8, pp. 721–730, 2010.7
- [9] L. Ferraiuolo *et al.*, "Dysregulation of astrocyte–motoneuron cross-talk in mutant superoxide dismutase 1-related amyotrophic lateral sclerosis," 2011.

The role of the Rpd3-complex in recycling cell surface proteins

Student: Josephine Ayre

Supervisor: Dr Chris MacDonald

Background

Cell surface membrane proteins (e.g. receptors, transporters, channels), which are critical for myriad cellular functions, continually internalise to endosomes, where they can either be sent for degradation or recycled back to the plasma membrane^{1,2}. Although it has been appreciated for decades in mammalian cells that a direct endosome to surface recycling pathway is critical for many cellular processes, much of the required machinery has not been discovered, let alone understood at a mechanistic level. The MacDonald lab recently discovered that yeast have a direct recycling pathway from endosomes to the plasma membrane. Subsequently, using an engineered synthetic reporter that follows this recycling pathway exclusively, a comprehensive genetic screen of all ~5200 non-essential yeast mutants identified many highly conserved factors that regulates this physiologically important recycling pathway³.

The screen identified 89 mutants with defective localisation of the reporter. **Intriguingly, this blind screen identified all 10 sub-units of the Rpd3-complex components as required for recycling.** These proteins physically interact and comprise a histone deacetylase (HDAC) complex known to regulate gene expression in the nucleus⁴. Although this complex can deacetylate histones, we saw no reason why it could not also act on any protein substrates, including recycling factors. So, we set out to test the hypothesis that the Rpd3-complex has a life outside of the nucleus regulating the cell surface recycling pathway directly.

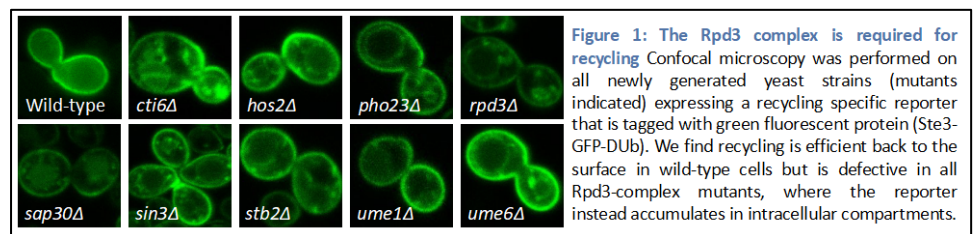
Aims

1. To stably integrate the recycling reporter into yeast null mutants lacking Rpd3 complex members.
2. To create fluorescently tagged versions of Rpd3 to confirm they are functional.
3. To perform localisation of Rpd3 to assess test if it has a role outside of the nucleus.

Results

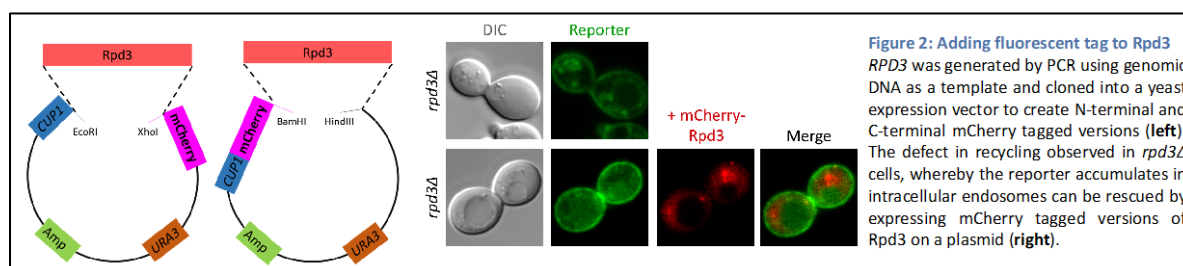
Rpd3 complex is required for recycling

The recycling specific reporter was generated by PCR and stably integrated at the *HIS3* locus (which allows selection on media lacking histidine), via homologous recombination, into *Saccharomyces cerevisiae* null mutant strain lacking components of the Rpd3 complex. We confirmed that recycling was efficient in wild-type cells but was defective in all the null mutants I created (Figure 1). We also revealed there are differential defects amongst the mutants, implying some components of the Rpd3 complex are more important for recycling than others.



Fluorescently tagged Rpd3 is functional

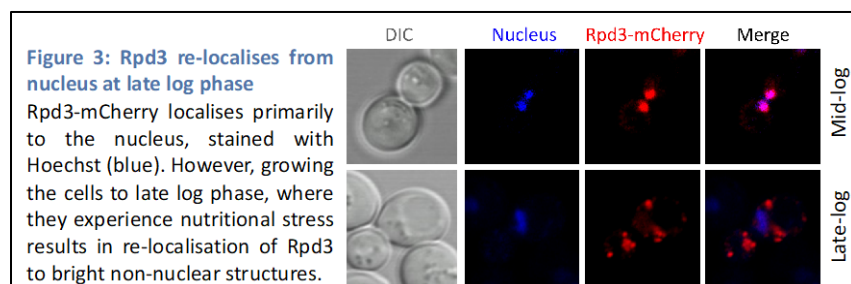
To localise Rpd3 in yeast we used a Gibson assembly cloning strategy to insert the *RPD3* gene into an inducible (using the copper sensitive *CUP1* promoter) yeast expression plasmid to create versions of Rpd3 tagged with the red



fluorescent protein, mCherry (Figure 2). This approach was

successful and tagging Rpd3 at the N- and C- termini expressed fusion proteins that localise to the nucleus and cytoplasm. Furthermore, these tagged versions were functional, which was confirmed by their ability to complement the recycling defect of *rpd3Δ* cells.

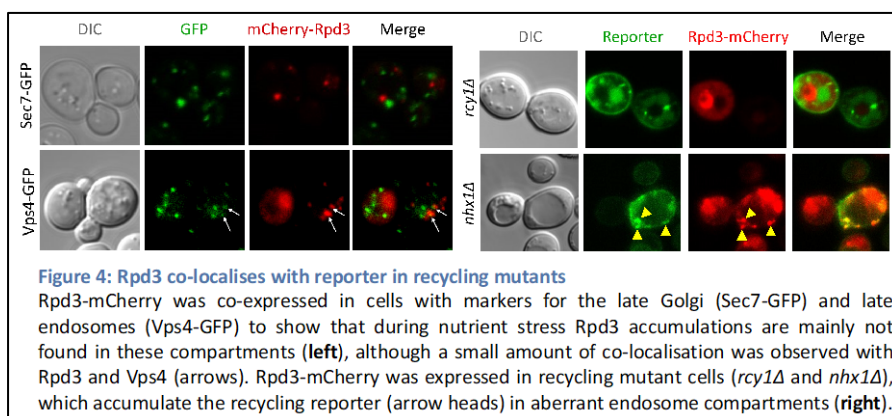
Rpd3 localisation is dependent on growth conditions



We found that when cells are grown to nutrient limiting late log phase, Rpd3 does not localise to the nucleus and instead accumulates in bright structures within the cytoplasm (Figure 3). This effect is unique to Rpd3 as Pho23 and Ume1 are retained in the nucleus when cells are grown to late log phase (data not shown).

Rpd3 localises to recycling endosomes

To determine the identity of the bright non-nuclear structures identified in late log phase cells, Rpd3-mCherry was co-expressed in cells with markers for the late Golgi (Sec7-GFP) and late endosomes (Vps4-GFP). During nutrient stress Rpd3 accumulations are mainly not found in these compartments, although a small amount of co-localisation was observed with Rpd3 and Vps4 (Figure 4). To test if these structures were recycling endosomes, the early and late acting recycling factors, Rcy1 and Nhx1, respectively, were deleted and aberrant recycling intermediate compartments marked with our specific GFP tagged reporter. We found deletion of the late acting recycling factor Nhx1 did reveal that Rpd3 localises to recycling endosome structures (Figure 4).



Future directions of work

The contribution of each Rpd3-complex member to the recycling pathway could be further dissected using the reagents generated here, these could also be used in defining the compartments that Rpd3 localises to in recycling defective mutants. In order to investigate the role of Rpd3-complex as a HDAC complex bioinformatic analysis of existing gene expression profiles for null mutants of the Rpd3-complex could be performed and cross-reference with known trafficking machinery that may regulate recycling at the transcription level. Due to time constraints I could not start to explore whether the Rpd3 complex has an indirect role in the recycling pathway, as well as definitively identifying what compartments Rpd3 localises to.

Value of the studentship to the student

Having such an incredible opportunity has been immensely valuable in several ways. I have developed my ability to plan and carry out experiments from cutting and purifying DNA from a gel to super resolution microscopy. This studentship has allowed me to apply theory I learnt in my degree in a practical setting as well as improving my skills in the lab and in presenting data (e.g. at lab meeting and as a conference poster). I found it rewarding to be able to work independently in a lab environment and as a result I feel prepared to take on future projects with confidence. This studentship has given me an insight into what a career in research would involve and has convinced me that I want to do a PhD, and I am now actively searching for opportunities after my degree.

Value of the studentship to the host lab

This internship was a complete success! Josephine integrated with the lab really well and was an asset to the team. Josephine learned all the required skills quickly and was able to generate a bunch of cool data. Josephine presented this story as a poster at a conference in Manchester and got an honourable mention during the judging announcement (I'm fairly certain she was the only undergraduate to present). I am delighted Josephine now intends to pursue a PhD; she will be great and I would highly recommended her to any lab.

References

1. Maxfield, F. R. & McGraw. **Nat. Rev. Mol. Cell Biol.** 5, 121–132 (2004).
2. Hsu, V. W., Bai, M. & Li, J. **Nat. Rev. Mol. Cell Biol.** 13, 323–328 (2012).
3. MacDonald, C. & Piper, R. C. J. **Cell Biol.** 216, 3275–3290 (2017).
4. Rundlett, S. E. et al. **Proc. Natl. Acad. Sci. U. S. A.** 93, 14503–14508 (1996).